Hamburger Beiträge
zur Angewandten Mathematik

Asymptotic Expansions and Numerical Methods in Computational Fluid Dynamics

A. Meister

Reihe F
Computational Fluid Dynamics and Data Analysis 17
December 2001

Hamburger Beiträge zur Angewandten Mathematik

Reihe A	Preprints
Reihe B	Berichte
Reihe C	Mathematische Modelle und Simulation
Reihe D	Elektrische Netzwerke und Bauelemente
Reihe E	Scientific Computing
Reihe F	Computational Fluid Dynamics and Data Analysis

Asymptotic Expansions and Numerical Methods in Computational Fluid Dynamics

A. Meister*

1 Introduction

In this Chapter we give an introduction concerning the efficiency of asymptotic expansions as well as their applicability and limitations with respect to the investigation of partial differential equations. Nevertheless, the fundamental results presented in Section 2 are of general importance and can be applied to different tasks like integral equations and related problems.
A wide variety of problems in industry and research are modeled by hyperbolic partial differential equations, e. g. traffic flow problems, acoustics, radiation transfer, crystal growth, etc. We focus our attention on the Euler equations of gas dynamics which are a typical and well-known representative of this class of equations. The Euler equations describe the conservation of mass, momentum and energy of an inviscid flow of an ideal gas and are therefore often used in the field of computational fluid dynamics. Since the extension to viscous flow fields incorporates the Euler equations, the following analysis and investigation is also of fundamental interest in the context of the Navier-Stokes equations.

2 Asymptotic Expansions

In the mathematical literature the common expression of an asymptotic expansion was firstly mentioned by Poincaré and Stieltjes in 1886 [59, 73]. Up to now asymptotic expansions are widely used by mathematicians, physicists and engineers. Examples of applications are the analysis of explicitly given functions [33, 53] and the investigation of ordinary as well as partial differential equations [29, 53, 33, 65, 32, 37]. The main idea is to extract the fundamental properties of the underlying problem by means of a formal single or multiple scale asymptotic expansion without ascertain the solution of the whole problem explicitly. Thereby, it has to be noticed that the choice of the asymptotic expansion determines the function space in which the solution is sought.

*Department of Mathematics, Center for Differential Equations und Dynamical Systems, University of Hamburg, Germany

Consequently, the advantage or disadvantage of an asymptotic analysis is significantly influenced by the type and form of the expansion used such that the choice of the incorporated asymptotic sequence as well as the scales considered become of general importance.
The objective of this Section is the analysis of inviscid fluid flow governed by the Euler equations of gas dynamics in the limit of a vanishing Mach number. The results of a single and multiple length scale, single time scale analysis are afterwards employed to extend the validity of numerical methods from the compressible to the low Mach number regime.
In advance we focus our view to the consideration of the basic ingredients of asymptotic expansions. Thereby, we emphasize the general procedure of an asymptotic analysis, their possibilities and limitations by means of very simple model problems.
In this Section $\mathbf{G}$ and $\mathcal{I}$ are subsets of $\mathbb{R}^d$ and $\mathbb{R}$, respectively. In order to introduce an asymptotic expansion the definition of an asymptotic sequence is necessary.

Definition 2.1 *Let $\epsilon_0 \in \overline{\mathcal{I}}$. A sequence of functions $\{\phi_n\}_{n\in\mathbb{N}_0}$ with $\phi_n : \mathcal{I} \setminus \{\epsilon_0\} \to \mathbb{R}$ is called asymptotic sequence (with respect to ϵ_0) if*

$$\phi_{n+1}(\epsilon) = o\left(\phi_n(\epsilon)\right), \quad \epsilon \to \epsilon_0, \tag{2.1}$$

holds for all $n \in \mathbb{N}_0$.

Note, that the equation (2.1) can be written as

$$\lim_{\substack{\epsilon\to\epsilon_0 \\ \epsilon\in\mathcal{I}\setminus\{\epsilon_0\}}} \frac{\phi_{n+1}(\epsilon)}{\phi_n(\epsilon)} = 0.$$

Analogously, we use $f(\mathbf{x};\epsilon) = o\left(\phi(\epsilon)\right)$, $\epsilon \to \epsilon_0$, in the meaning of

$$\lim_{\substack{\epsilon\to\epsilon_0 \\ \epsilon\in\mathcal{I}\setminus\{\epsilon_0\}}} \frac{f(\mathbf{x};\epsilon)}{\phi_n(\epsilon)} = 0$$

and we write $f(\mathbf{x};\epsilon) = O\left(\phi(\epsilon)\right)$, $\epsilon \to \epsilon_0$, in the case that

$$\lim_{\substack{\epsilon\to\epsilon_0 \\ \epsilon\in\mathcal{I}\setminus\{\epsilon_0\}}} \frac{f(\mathbf{x};\epsilon)}{\phi_n(\epsilon)} = h(\mathbf{x}).$$

The simplest example of an asymptotic sequence is given by $\phi_n(\epsilon) = (\epsilon - \epsilon_0)^n$. However, one can define more complicated asymptotic sequences like

$$\phi_0(\epsilon) = \log(\epsilon - \epsilon_0),\ \phi_1(\epsilon) = 1,\ \phi_2(\epsilon) = (\epsilon - \epsilon_0)\log(\epsilon - \epsilon_0),\ \phi_3(\epsilon) = (\epsilon - \epsilon_0),$$
$$\phi_4(\epsilon) = (\epsilon - \epsilon_0)^2\log^2(\epsilon - \epsilon_0),\ \phi_5(\epsilon) = (\epsilon - \epsilon_0)^2\log(\epsilon - \epsilon_0),\ \phi_6(\epsilon) = (\epsilon - \epsilon_0)^2,$$
$$\phi_7(\epsilon) = (\epsilon - \epsilon_0)^3\log^3(\epsilon - \epsilon_0),\ \phi_8(\epsilon) = (\epsilon - \epsilon_0)^3\log^2(\epsilon - \epsilon_0), \ldots$$

The proof that this sequence satisfies the condition (2.1) is left as an exercise[1].
Once the asymptotic sequence is specified, we are able to define an asymptotic single scale expansion with respect to an arbitrary know or unknown function f.

[1] A comprehensive proof for $\epsilon_0 = 0$ is given in [53].

Definition 2.2 *For a given asymptotic sequence* $\{\phi_n\}_{n\in\mathbb{N}_0}$, $\phi_n : \mathcal{I}\setminus\{\epsilon_0\}\to\mathbb{R}$, *and a function* $f : \mathbf{G}\times\mathcal{I}\setminus\{\epsilon_0\}\to\mathbb{R}$, $(\mathbf{x};\epsilon)\overset{f}{\mapsto} f(\mathbf{x};\epsilon)$, *the sum*

$$\sum_{n=0}^{N}\phi_n(\epsilon)f^{(n)}(\mathbf{x}) \tag{2.2}$$

including the asymptotic function sequence $\left\{f^{(n)}\right\}_{n\in\mathbb{N}_0}$ *with* $f^{(n)} : \mathbf{G}\to\mathbb{R}$ *is called an asymptotic single scale expansion to* $N+1$ *terms of* f *as* $\epsilon\to\epsilon_0$ *if*

$$f(\mathbf{x};\epsilon)-\sum_{n=0}^{N}\phi_n(\epsilon)f^{(n)}(\mathbf{x}) = o\left(\phi_N(\epsilon)\right), \quad \epsilon\to\epsilon_0, \tag{2.3}$$

holds in $\mathbf{G}$. *The asymptotic expansion* (2.2) *is called uniformly valid in* $\mathbf{G}'\subset\mathbf{G}$ *if* (2.2) *satisfies* (2.3) *uniformly in* $\mathbf{G}'$.

In advance to the consideration of different model problems we now prove some fundamental properties of asymptotic expansions

Lemma 2.3 *Let* $\sum_{n=0}^{N}\phi_n(\epsilon)f^{(n)}(\mathbf{x})$ *be an asymptotic single scale expansion to* $N+1$ *terms of* f *as* $\epsilon\to\epsilon_0$. *Then*

$$f(\mathbf{x};\epsilon)-\sum_{n=0}^{k}\phi_n(\epsilon)f^{(n)}(\mathbf{x}) = o\left(\phi_k(\epsilon)\right), \quad \epsilon\to\epsilon_0,$$

for $k=0,\dots,N$.

Proof:
Using the decay property of the asymptotic expansion one gets

$$\begin{aligned} f(\mathbf{x};\epsilon)-\sum_{n=0}^{N-1}\phi_n(\epsilon)f^{(n)}(\mathbf{x}) &= f(\mathbf{x};\epsilon)-\sum_{n=0}^{N}\phi_n(\epsilon)f^{(n)}(\mathbf{x})+\phi_N(\epsilon)f^{(N)}(\mathbf{x}) \\ &= o\left(\phi_N(\epsilon)\right)+O\left(\phi_N(\epsilon)\right)=O\left(\phi_N(\epsilon)\right)=o\left(\phi_{N-1}(\epsilon)\right) \end{aligned}$$

as $\epsilon\to\epsilon_0$. Successive reduction of the upper index of the sum completes the proof. □
In addition to the choice of the asymptotic sequence a statement concerning the determination of the asymptotic functions $f^{(n)}$, $n=0,\dots,N$, is necessary to derive the asymptotic expansion for a given function f. We close this gap by means of the following

Lemma 2.4 *Let* $\{\phi_n(\epsilon)\}_{n\in\mathbb{N}_0}$ *be an asymptotic sequence as* ϵ *tends to* ϵ_0. *Then*

$$\sum_{n=0}^{N}\phi_n(\epsilon)f^{(n)}(\mathbf{x})$$

represents an asymptotic single scale expansion to $N+1$ *terms of* $f : \mathbf{G} \times \mathcal{I} \setminus \{\epsilon_0\} \to \mathbb{R}$ *with respect to* ϵ_0 *if and only if*

$$f^{(n)}(\mathbf{x}) = \lim_{\epsilon \to \epsilon_0} \left(\frac{f(\mathbf{x};\epsilon) - \sum\limits_{k=0}^{n-1} \phi_k(\epsilon) f^{(k)}(\mathbf{x})}{\phi_n(\epsilon)} \right) \tag{2.4}$$

holds for all $\mathbf{x} \in \mathbf{G}$ *and* $n \in \{0, \ldots, N\}$.

Proof:
From Lemma 2.3 it follows that each asymptotic single scale expansion to $N+1$ terms represents also an asymptotic single scale expansion to $k+1$ terms for $k = 0, \ldots, N-1$. With respect to this fact it is sufficient to prove the statement of Lemma 2.4 exclusively for $n = N$. In this case we obtain the equivalence directly from

$$\lim_{\epsilon \to \epsilon_0} \left(\frac{f(\mathbf{x};\epsilon) - \sum\limits_{k=0}^{N} \phi_k(\epsilon) f^{(k)}(\mathbf{x})}{\phi_N(\epsilon)} \right) = \lim_{\epsilon \to \epsilon_0} \left(\frac{f(\mathbf{x};\epsilon) - \sum\limits_{k=0}^{N-1} \phi_k(\epsilon) f^{(k)}(\mathbf{x})}{\phi_N(\epsilon)} \right) - f^{(N)}(\mathbf{x}).$$

□

Unfortunately, the calculation of the asymptotic functions $f^{(n)}$ by means of equation (2.4) requires the explicit incorporation of the function f. Thus, it is impossible to employ equation (2.4) for a huge class of problems from natural sciences where the solution f is sought and usually at most implicitly given by some governing conditions like ordinary or partial differential equations. Nevertheless, Lemma 2.4 is of general importance concerning the investigation of different properties of asymptotic expansions. As a first conclusion of Lemma 2.4 we obviously get the uniqueness of a single scale asymptotic expansion with respect to a function f in the case of a fixed asymptotic sequence. Moreover, the statement of equation (2.4) can be used to emphasize the influence of the definition of the asymptotic sequence on the success of the whole analysis. Obviously, the asymptotic sequence determines the function space in which the solution is sought. If an asymptotic sequence is introduced which is to coarse with respect to the underlying problem, then the function space does not contain the solution and consequently one can only obtain an approximation of the function sought. As an example, we consider the function

$$f(x;\epsilon) = \left(x + \sqrt{\epsilon}\right)^2 \tag{2.5}$$

in the limit of a vanishing parameter ϵ. In the context of the asymptotic sequence $\{\phi_n(\epsilon) = \epsilon^n\}_{n \in \mathbb{N}_0}$ Lemma 2.4 yields

$$f^{(0)}(x) = \lim_{\epsilon \to 0} \frac{f(x;\epsilon)}{\epsilon^0} = x^2$$

and

$$f^{(1)}(x) = \lim_{\epsilon \to 0} \frac{f(x;\epsilon) - x^2}{\epsilon^1} = \infty.$$

Thus, the best approximation with respect to this sequence is $f(x;\epsilon) = x^2 + o(1)$, $\epsilon \to 0$. On the other hand, a very fine asymptotic sequence leads to an increased number of terms within the asymptotic expansion whereby the asymptotic functions will vanish identically for each unnecessary element of the asymptotic sequence. However, the function sparse is large enough to contain the solution f. Using the sequence $\left\{\phi_n(\epsilon) = \epsilon^{\frac{n}{4}}\right\}_{n \in \mathbb{N}_0}$ with respect to function (2.5) yields $f^{(0)}(x) = x^2$, $f^{(1)}(x) = 0$, $f^{(2)}(x) = 2x$, $f^{(3)}(x) = 0$, $f^{(4)}(x) = 1$, $f^{(n)}(x) = 0$, $n \geq 5$, and $f(x;\epsilon) = \sum\limits_{n=0}^{4} \phi_n(\epsilon) f^{(n)}(x)$.

The procedure of an asymptotic analysis in the context of ordinary and partial differential equations distinguishes from the above mentioned algorithm. Thereby, one usually proceeds as follows:

- Assume that the solution f of the underlying differential equation can be expressed in the form of an asymptotic expansion.
- Introduce the asymptotic expansion into the governing equations.
- Derive a system of perturbation equations by identifying terms multiplied by corresponding function $\Psi(\epsilon)$ with respect to the decay properties in the limit of interest.
- Investigate the perturbation equations to extract the main features of the solution or the solution itself.

This strategy is based on the following result.

Lemma 2.5 *Let $\{\phi_n(\epsilon)\}_{n \in \mathbb{N}_0}$, be an asymptotic sequence and L_n, $n = 0, \ldots, N$ arbitrary terms which are independent of ϵ. Then the statement*

$$\sum_{n=0}^{N} \phi_n(\epsilon) L_n = o\left(\phi_N(\epsilon)\right), \ \epsilon \to \epsilon_0 \tag{2.6}$$

holds if and only if $L_n = 0$, $n = 0, \ldots, N$.

Proof:

Let us assume the existence of terms $L_0, \ldots, L_N$ with $\max\limits_{n=0,\ldots,N} |L_n| > 0$ for which the equation (2.6) holds and let $m = \min\limits_{n=0,\ldots,N; L_n \neq 0} n$. Using (2.1), which is supposed to hold, we obtain, for $m \leq N$:

$$\sum_{n=0}^{m} \phi_n(\epsilon) L_n = o\left(\phi_N(\epsilon)\right) - \sum_{n=m+1}^{N} \phi_n(\epsilon) L_n = o\left(\phi_m(\epsilon)\right), \quad \epsilon \to \epsilon_0.$$

The last equation is a consequence of (2.6). Dividing by $\phi_m(\epsilon)$ and taking the limit $\epsilon \to \epsilon_0$ one gets

$$L_m = \lim_{\epsilon \to \epsilon_0} \frac{\sum_{n=0}^{m} \phi_n(\epsilon) L_n}{\phi_m(\epsilon)} = \lim_{\epsilon \to \epsilon_0} \frac{o\left(\phi_m(\epsilon)\right)}{\phi_m(\epsilon)} = 0$$

in contradiction to the definition of m. The opposite direction is trivial. $\square$

Note, that one starts with the assumption concerning the representation of the function f. Due to this fact the asymptotic analysis is called formal and the perturbation equations do not lead to a rigorous proof concerning the behavior of the function f except the solution can be derived explicitly.

Let us now consider the analysis of the following initial value problem.

Investigate the solution $f \in C^1(\mathbb{R}^+) \cap C^0(\mathbb{R}_0^+)$ *of*

$$f(x;\epsilon) + \epsilon f'(x;\epsilon) = x + 2\epsilon \quad for \quad x \in \mathbb{R}^+ \tag{2.7}$$

and

$$f(0;\epsilon) = \epsilon \tag{2.8}$$

for $\epsilon \in (0, \widetilde{\epsilon})$, $1 \gg \widetilde{\epsilon} > 0$.

It is mentionable that throughout the Chapter each derivation is at no time applied with respect to the perturbation parameter.

Due to the occurence of the perturbation parameter in the form of ϵ it seems to be natural to determine the asymptotic expansion in the form $\{\phi_n(\epsilon) = \epsilon^n\}_{n \in \mathbb{N}_0}$. Thus, we assume that the solution f can be expressed as

$$f(x;\epsilon) = \sum_{n=0}^{N} \epsilon^n f^{(n)}(x) + o\left(\epsilon^N\right), \quad \epsilon \to 0. \tag{2.9}$$

Introducing the asymptotic expansion (2.9) into the ordinary differential equation (2.7) leads to the equation

$$f^{(0)}(x) + \sum_{n=1}^{N} \epsilon^n \left(f^{(n)}(x) + \left(f^{(n-1)}\right)'(x) \right) + \epsilon^{N+1} \left(f^{(N)}\right)'(x) = x + 2\epsilon + o\left(\epsilon^N\right), \quad \epsilon \to 0. \tag{2.10}$$

Identifying terms multiplied by the same power of ϵ yields the following system of perturbation equations in $\mathbb{R}^+$

$$O(1) \quad : \quad f^{(0)}(x) = x, \tag{2.11}$$

$$O(\epsilon) \quad : \quad f^{(1)}(x) + \left(f^{(0)}\right)'(x) = 2, \tag{2.12}$$

$$O(\epsilon^n) \quad : \quad f^{(n)}(x) + \left(f^{(n-1)}\right)'(x) = 0 \ \text{ for } \ n = 2, \ldots, N. \tag{2.13}$$

From (2.11) we get

$$\left(f^{(0)}\right)'(x) = 1$$

and thus equation (2.12) becomes

$$f^{(1)}(x) = 2 - 1 = 1,$$

which if used in conjunction with (2.13) gives

$$f^{(2)}(x) = 0.$$

A successive application of equation (2.13) with increasing order shows

$$f^{(n)}(x) = 0 \text{ for } n = 2, \ldots, N,$$

such that

$$f(x;\epsilon) = x + \epsilon + o\left(\epsilon^N\right), \quad \epsilon \to 0.$$

As N is arbitrary it follows that the result takes the form

$$f(x;\epsilon) = x + \epsilon$$

and satisfies the initial value problem. Obviously, the initial condition has not been used within the derivation of the solution and therefore their fullfilment is purely coincidence. Such initial value problems are called regular perturbed.

We have seen that the calculation of an appropriate asymptotic single scale expansion requires the definition of a well suited asymptotic sequence. Nevertheless, the behaviour of solutions for a large number of problems arising in practical applications show phenomena on different scales which cann't be resolved by an asymptotic single scale expansion independent of the asymptotic sequence used. An example is given by the following model problem.

Find a function $f \in C^2\left(\mathbb{R}^+\right) \cap C\left(\mathbb{R}_0^+\right)$ *that fullfills the ordinary differential equation*

$$\epsilon^2 f''(x;\epsilon) + f(x;\epsilon) = (1-\epsilon^2)\sin x \tag{2.14}$$

for $x \in \mathbb{R}^+$ *as well as the intial conditions*

$$f(0;\epsilon) = \epsilon \tag{2.15}$$

and

$$f'(0;\epsilon) = 1 \tag{2.16}$$

where $\epsilon \in (0, \widetilde{\epsilon})$, $1 \gg \widetilde{\epsilon} > 0$.

Assuming that the solution can be expressed in the form of the well-known asymptotic expansion

$$f(x;\epsilon)=\sum_{n=0}^{N}\epsilon^n f^{(n)}(x)+o\left(\epsilon^N\right),\quad \epsilon\to 0 \tag{2.17}$$

and introducing the expression into the differential equation yields the system of perturbation equations in $\mathbb{R}^+$

$$\begin{aligned}
O(1) &: \ f^{(0)}(x)=\sin x,\\
O(\epsilon) &: \ f^{(1)}(x)=0,\\
O(\epsilon^2) &: \ \left(f^{(0)}\right)''(x)+f^{(2)}(x)=-\sin x,\\
O(\epsilon^n) &: \ \left(f^{(n)}\right)''(x)+f^{(n+2)}(x)=0 \ \text{ for } \ n=1,\dots,N-2.
\end{aligned}$$

Obviously, the asymptotic expansion reads

$$f(x;\epsilon)=\sin x+o\left(\epsilon^N\right),\quad \epsilon\to 0, \tag{2.18}$$

for arbitrary large N. Although, we obtain $f'(0;\epsilon)=1$, the second initial condition is violated since $f(0;\epsilon)=0\neq\epsilon$. Here we speak of a singular perturbation problem which require the consideration of multiple scales. Motivated by this result we introduce an extended formulation of an asymptotic expansion which takes account of multiple scales.

Definition 2.6 *Let* $\{\phi_n\}_{n\in\mathbb{N}_0}$, $\phi_n : \mathcal{I}\setminus\{\epsilon_0\}\to\mathbb{R}$ *be an asymptotic sequence,* f : $\mathbf{G}\times\mathcal{I}\setminus\{\epsilon_0\}\to\mathbb{R}$, $(\mathbf{x};\epsilon)\overset{f}{\mapsto} f(\mathbf{x};\epsilon)$ *and* $\mathbf{g}:\mathbf{G}\times\mathcal{I}\setminus\{\epsilon_0\}\to\widetilde{\mathbf{G}}$. *The sum*

$$\sum_{n=0}^{N}\phi_n(\epsilon)\left(f^{(n)}\circ\mathbf{g}\right)(\mathbf{x};\epsilon) \tag{2.19}$$

including the asymptotic function sequence $\left\{f^{(n)}\right\}_{n\in\mathbb{N}_0}$ *with* $f^{(n)}:\widetilde{\mathbf{G}}\to\mathbb{R}$ *is called an asymptotic multiple scale expansion to* $N+1$ *terms of* f *as* $\epsilon\to\epsilon_0$ *if*

$$f(\mathbf{x};\epsilon)-\sum_{n=0}^{N}\phi_n(\epsilon)\left(f^{(n)}\circ\mathbf{g}\right)(\mathbf{x};\epsilon)=o\left(\phi_N(\epsilon)\right),\quad \epsilon\to\epsilon_0, \tag{2.20}$$

holds in $\mathbf{G}$. *The asymptotic expansion* (2.19) *is called uniformly valid in* $\mathbf{G}'\subset\mathbf{G}$ *if* (2.19) *satisfies* (2.20) *uniformly in* $\mathbf{G}'$.

The advantage of multiple scale expansions lies in the inclusion of the space $\widetilde{\mathbf{G}}$ which is of higher dimension compared to $\mathbf{G}$. Although, the asymptotic functions $f^{(n)}$ are independent of the perturbation parameter we are able to resolve phenomena on scales depending on ϵ by means of the mapping $\mathbf{g}$. Taking $\mathbf{g}(\mathbf{x};\epsilon)=\mathbf{x}$ shows that the set of single scale expansions is completely included in the set of multiple scale expansions. Let us now review problem (2.14) using the mapping

$$\begin{array}{rcl}\mathbf{g}:\mathbb{R}^+\times(0,\widetilde{\epsilon}) & \rightarrow & \mathbb{R}^+\times\mathbb{R}^+\\ (x;\epsilon) & \overset{\mathbf{g}}{\mapsto} & (x,x/\epsilon)\end{array}$$

and sufficiently smooth functions

$$\begin{array}{rcl}f^{(n)}:\mathbb{R}^+\times\mathbb{R}^+ & \rightarrow & \mathbb{R}\\ (\eta,\xi) & \overset{f^{(n)}}{\mapsto} & f^{(n)}(\eta,\xi).\end{array}$$

Concerning the derivatives we obtain

$$\left(f^{(n)}\circ\mathbf{g}\right)'(x;\epsilon)=\partial_\eta f^{(n)}\left(\mathbf{g}(x;\epsilon)\right)+\frac{1}{\epsilon}\partial_\xi f^{(n)}\left(\mathbf{g}(x;\epsilon)\right). \tag{2.21}$$

and

$$\left(f^{(n)}\circ\mathbf{g}\right)''(x;\epsilon)=\partial_\eta^2 f^{(n)}\left(\mathbf{g}(x;\epsilon)\right)+\frac{2}{\epsilon}\partial_\xi\partial_\eta f^{(n)}\left(\mathbf{g}(x;\epsilon)\right)+\frac{1}{\epsilon^2}\partial_\xi^2 f^{(n)}\left(\mathbf{g}(x;\epsilon)\right). \tag{2.22}$$

Similar to the single scale case it is assumed that the solution f of the initial value problem (2.14)-(2.16) possess the form

$$f(x;\epsilon)=\sum_{n=0}^{N}\epsilon^n\left(f^{(n)}\circ\mathbf{g}\right)(x;\epsilon)+o\left(\epsilon^N\right),\quad\epsilon\rightarrow 0.$$

Using (2.22) the ordinary differential equation can be written in terms of the asymptotic functions as

$$\begin{aligned}&(1-\epsilon^2)\sin\eta\\ &\quad=\left(\partial_\xi^2 f^{(0)}+f^{(0)}\right)(\eta,\xi)+\epsilon\left(2\partial_\xi\partial_\eta f^{(0)}+\partial_\xi^2 f^{(1)}+f^{(1)}\right)(\eta,\xi)\\ &\qquad+\sum_{n=2}^{N}\epsilon^n\left(\partial_\eta^2 f^{(n-2)}+2\partial_\xi\partial_\eta f^{(n-1)}+\partial_\xi^2 f^{(n)}+f^{(n)}\right)(\eta,\xi)+o\left(\epsilon^N\right),\ \epsilon\rightarrow 0,\end{aligned} \tag{2.23}$$

for $(\eta,\xi)\in\widetilde{\mathbf{G}}=\widetilde{\mathbf{G}}(\epsilon)=\{(\eta,\xi)\in\mathbb{R}^+\times\mathbb{R}^+|(\eta,\xi)=\mathbf{g}(x;\epsilon),x\in\mathbf{G}=\mathbb{R}^+\}$.
In contrast to the single scale expansion the manifold $\widetilde{\mathbf{G}}$ depends on the reference parameter ϵ and therefore we are, unfortunately, not able to decompose the equation (2.23) by means of Lemma 2.5 in the same manner as done in the context of the single scale case. In order to overcome this difficulty it is convenient to introduce the space

$$\hat{\mathbf{G}}=\left\{(\eta,\xi)\in\mathbb{R}^+\times\mathbb{R}^+|\xi<\eta/\widetilde{\epsilon}\right\}$$

and to require that the asymptotic functions $f^{(n)}$ used within the asymptotic expansion satisfy the equation (2.23) in $\hat{\mathbf{G}}$. Due to this extended assumption we obtain the simplified equations

$$O(1) : \left(\partial_\xi^2 f^{(0)} + f^{(0)}\right)(\eta, \xi) = \sin\eta, \tag{2.24}$$

$$O(\epsilon) : \left(2\partial_\xi\partial_\eta f^{(0)} + \partial_\xi^2 f^{(1)} + f^{(1)}\right)(\eta, \xi) = 0, \tag{2.25}$$

$$O(\epsilon^2) : \left(\partial_\eta^2 f^{(0)} + 2\partial_\xi\partial_\eta f^{(1)} + \partial_\xi^2 f^{(2)} + f^{(2)}\right)(\eta, \xi) = -\sin\eta, \tag{2.26}$$

$$O(\epsilon^n) : \left(\partial_\eta^2 f^{(n-2)} + 2\partial_\xi\partial_\eta f^{(n-1)} + \partial_\xi^2 f^{(n)} + f^{(n)}\right)(\eta, \xi) = 0 \text{ for } n = 3, \ldots, N. \tag{2.27}$$

in $\hat{\mathbf{G}}$ as well as the perturbation equations arising from the initial conditions in the form

$$O(1/\epsilon) \quad : \quad \partial_\xi f^{(0)}(0,0) = 0, \tag{2.28}$$

$$O(1) \quad : \quad \left(\partial_\eta f^{(0)} + \partial_\xi f^{(1)}\right)(0,0) = 1, \tag{2.29}$$

$$O(1) \quad : \quad f^{(0)}(0,0) = 0, \tag{2.30}$$

$$O(\epsilon) \quad : \quad \left(\partial_\eta f^{(1)} + \partial_\xi f^{(2)}\right)(0,0) = 0, \tag{2.31}$$

$$O(\epsilon) \quad : \quad f^{(1)}(0,0) = 1, \tag{2.32}$$

$$O(\epsilon^n) \quad : \quad \left(\partial_\eta f^{(n)} + \partial_\xi f^{(n+1)}\right)(0,0) = 0 \;\text{ for }\; n = 2, \ldots, N-1, \tag{2.33}$$

$$O(\epsilon^n) \quad : \quad f^{(n)}(0,0) = 1 \;\text{ for }\; n = 2, \ldots, N. \tag{2.34}$$

In order to determine the leading order asymptotic function $f^{(0)}$ we consider the initial value problem built by the partial differential equation (2.24) and the initial conditions (2.28) and (2.30). The solution takes the form

$$f^{(0)}(\eta, \xi) = \gamma_1(\eta)\sin\xi + \gamma_2(\eta)\cos\xi + \sin\eta$$

with $\gamma_1(0) = \gamma_2(0) = 0$. Using

$$f^{(0)}(\eta, \xi) = \sin\eta \tag{2.35}$$

the perturbation equation (2.25) becomes

$$\left(\partial_\xi^2 f^{(1)} + f^{(1)}\right)(\eta, \xi) = 0. \tag{2.36}$$

Moreover the initial condition (2.29) can be written as

$$\partial_\xi f^{(1)}(0,0) = 1 - \cos 0 = 0. \tag{2.37}$$

With respect to the partial differential equation (2.36) and the initial conditions (2.32) and (2.37) the asymptotic function $f^{(1)}$ can be identified in the form

$$f^{(1)}(\eta, \xi) = \gamma_1(\eta)\sin\xi + \gamma_2(\eta)\cos\xi$$

with $\gamma_1(0) = 0$ and $\gamma_2(0) = 1$. The ansatz

$$f^{(1)}(\eta, \xi) = \cos \xi$$

in conjunction with (2.26) yields

$$\left(\partial_\xi^2 f^{(2)} + f^{(2)}\right)(\eta, \xi) = 0.$$

Thus, $f^{(2)}(\eta, \xi) = 0$ represents a suitable solution. A successive repetition using the equations (2.27), (2.33) and (2.34) leads to the possible setting

$$f^{(n)}(\eta, \xi) = 0, \quad n = 3, \dots, N-1.$$

Consequently, the asymptotic expansion reads

$$f(x; \epsilon) = \sin x + \epsilon \cos \frac{x}{\epsilon} + o(\epsilon^{N-1}), \quad \epsilon \to 0.$$

It is easily seen by straightforward calculations that

$$f(x; \epsilon) = \sin x + \epsilon \cos \frac{x}{\epsilon} \tag{2.38}$$

represents indeed the solution of the original initial value problem. By means of this result we are now able to prove that $f(x; \epsilon) = \sin x$ is the best approximation of (2.38) which can be obtain by a single scale asymptotic expansion

$$f(x; \epsilon) = \sum_{n=0}^{N} \phi_n(\epsilon) f^{(n)}(x) + o\left(\phi_N(\epsilon)\right) \tag{2.39}$$

independent of the asymptotic sequence used.

Lemma 2.7 *Suppose $f(x; \epsilon) = \sin x + \epsilon \cos \frac{x}{\epsilon}$. Then, there exists no single scale expansion* (2.39) *which satisfies*

$$f(x; \epsilon) = \sum_{n=0}^{N} \phi_n(\epsilon) f^{(n)}(x) + o\left(\epsilon\right), \quad \epsilon \to 0.$$

Proof:
Consider an asymptotic sequence with $1 = o\left(\phi_0(\epsilon)\right)$, $\epsilon \to 0$. Hence, we have

$$\lim_{\epsilon \to 0} \frac{f(x; \epsilon)}{\phi_0(\epsilon)} = 0 \tag{2.40}$$

which means that all parts of the asymptotic sequence which are associated with an element of the asymptotic sequence satisfying $1 = o\left(\phi_k(\epsilon)\right)$, $\epsilon \to 0$ can be neglected.

On the other hand the limit (2.40) does not exist if $\phi_0(\epsilon) = o(1)$, $\epsilon \to 0$. Thus, a sensible asymptotic sequence has to satisfy

$$\lim_{\epsilon \to 0} \phi_0(\epsilon) = c \in \mathbb{R} \setminus \{0\}.$$

Without loss of generality we define $\phi_0(\epsilon) = 1$. Now, Lemma 2.4 yields

$$\lim_{\epsilon \to 0} \frac{f(x;\epsilon)}{\phi_0(\epsilon)} = \sin x.$$

It turns out that

$$\lim_{\epsilon \to 0} \frac{f(x;\epsilon) - \phi_0(\epsilon) f^{(0)}(x)}{\phi_1(\epsilon)} = \lim_{\epsilon \to 0} \frac{\epsilon \cos \frac{x}{\epsilon}}{\phi_1(\epsilon)} = 0, \tag{2.41}$$

if $\epsilon = o(\phi_1(\epsilon))$, $\epsilon \to 0$. Thus, in order to improve the asymptotic expoansion we have to introduce ϕ_1 such that both $\phi_1(\epsilon) = o(1)$ and $\epsilon = O(\phi_1(\epsilon))$ hold in the limit of a vanishing parameter ϵ. Unfortunately, in the context of such requirements either the limit (2.41) which is necessary to define the asymptotic functions $\phi^{(1)}$ is infinite or it does not exist. This fact shows that one cann't get rid of the term $\epsilon \cos \frac{x}{\epsilon}$. Obviously, this property completes the proof. $\square$

The combination of both initial value problems emphasize that the success of an asymptotic analysis depends on the asymptotic sequence used as well as the scales considered.

3 Governing Equations

In the present study, we investigate the time-dependent Euler equations in conservative form. These are a system of non-linear conservation laws which results naturally from the fundamental laws of conservation of mass, momentum and energy. Using the domain $\hat{\mathbf{G}} \subset \mathbb{R}^d$, $d = 1, 2, 3$, which is assumed to be polygonal bounded, i.e. $\partial\hat{\mathbf{G}} = \cup_{k=1}^{n} \partial\hat{\mathbf{G}}_k$, the dimensional form of the governing equations can be expressed as

$$\partial_{\hat{t}} \hat{\mathbf{u}} + \sum_{j=1}^{d} \partial_{\hat{x}_j} \mathbf{f}_j(\hat{\mathbf{u}}) = \mathbf{0} \text{ in } \hat{\mathbf{G}} \times \mathbb{R}_0^+, \tag{3.1}$$

where $\hat{\mathbf{u}} = \left(\hat{\rho}, \hat{m}_1, \ldots, \hat{m}_d, \hat{\rho}\hat{E}\right)^T$ denotes the vector of conserved variables. Furthermore, $\mathbf{f}_j$ are the convective fluxes which are given by

$$\mathbf{f}_j(\hat{\mathbf{u}}) = \begin{pmatrix} \hat{m}_j \\ \hat{m}_j \hat{v}_1 + \delta_{1j}\hat{p} \\ \vdots \\ \hat{m}_j \hat{v}_d + \delta_{dj}\hat{p} \\ \hat{H}\hat{m}_j \end{pmatrix}, \; j = 1, \ldots, d, \tag{3.2}$$

where δ_{ij} denotes the Kronecker symbol. The dimensional quantities $\hat{\rho}$, $\hat{v}_j$, $\hat{m}_j = \hat{\rho}\hat{v}_j$, $\hat{E}$, $\hat{H} = \hat{E} + \hat{p}/\hat{\rho}$ describe the density, velocity and momentum in $\hat{x}_j$-direction, total energy, and enthalphy of the fluid. The pressure is defined by the equation of state

$$\hat{p} = (\gamma - 1)\hat{\rho}\left(\hat{E} - \frac{1}{2}|\hat{\mathbf{v}}|^2\right), \tag{3.3}$$

where γ denotes the ratio of specific heats, which is constant with $\gamma = 1.4$ throughout the Chapter. As an additional assumption which is sensible from a mathematical as well as physical point of view, we require that each physical quantity $\hat{\varphi}$ is bounded in the sense that for each $\hat{t} \in \mathbb{R}_0^+$ there exists an upper bound $\hat{c}_{\hat{\varphi}}(t) \in \mathbb{R}$ such that

$$|\hat{\varphi}(\hat{\mathbf{x}}, \hat{t})| \leq \hat{c}_{\hat{\varphi}}(t) \tag{3.4}$$

for all $\hat{\mathbf{x}} \in \hat{\mathbf{G}}$. The system of Euler equations is to be solved under initial conditions

$$\hat{\mathbf{u}}(\hat{\mathbf{x}}, \hat{0}) = \hat{\mathbf{u}}_0(\hat{\mathbf{x}}), \;\; \hat{\mathbf{x}} \in \overline{\hat{\mathbf{G}}},$$

as well as under boundary conditions

$$\hat{\mathbf{u}}(\hat{\mathbf{x}}, \hat{t}) = \hat{\mathbf{u}}_{\partial\hat{\mathbf{G}}_k}(\hat{t}), \;\; \hat{t} \in \mathbb{R}^+, \;\; \hat{\mathbf{x}} \in \partial\hat{\mathbf{G}}_k, \;\; k = 1 \ldots, n.$$

If we denote by $\hat{\mathbf{F}}_j(\hat{\mathbf{u}})$ the Jacobian matrices of $\mathbf{f}_j(\hat{\mathbf{u}})$ with respect to the conserved quantities the Euler equations can be recasted in their quasilinear form

$$\partial_{\hat{t}}\hat{\mathbf{u}} + \sum_{j=1}^{d} \hat{\mathbf{F}}_j(\hat{\mathbf{u}})\partial_{\hat{x}_j}\hat{\mathbf{u}} = \hat{0}.$$

A system (3.1) consisting of n equations ($n = d+2$ for the system of Euler's equations) is called hyperbolic (in time direction), if the matrix

$$\hat{\mathbf{F}}(\hat{\mathbf{u}}, \mathbf{n}) := \sum_{j=1}^{d} \hat{\mathbf{F}}_j(\hat{\mathbf{u}})\mathbf{n}_j \in \mathbb{R}^{n \times n}$$

has exactly n real eigenvalues for all $\hat{\mathbf{u}} \in \mathcal{S} \subset \mathbb{R}^n$ and all $\mathbf{n} \in \mathbb{R}^d$, where $\mathcal{S}$ denotes the state space of the conserved variables. It is an easy exercise to check that the Euler equations are indeed hyperbolic. Hyperbolic systems describe transport processes.

Although the following properties of the Euler equations can be found in many textbooks (see [23], [24], for example), we list them for easy reference. In the context of the two-dimensional case the Jacobian matrices are given by

$$\hat{\mathbf{F}}_1(\hat{\mathbf{u}}) = \begin{bmatrix} \hat{0} & \hat{1} & \hat{0} & \hat{0} \\ \frac{\gamma-3}{2}\hat{v}_1^2 + \frac{\gamma-1}{2}\hat{v}_2^2 & (3-\gamma)\hat{v}_1 & (1-\gamma)\hat{v}_2 & \gamma - 1 \\ -\hat{v}_1\hat{v}_2 & \hat{v}_2 & \hat{v}_1 & \hat{0} \\ (\gamma-1)\hat{v}_1|\hat{\mathbf{v}}|^2 - \gamma\hat{v}_1\hat{E} & \gamma\hat{E} - \frac{\gamma-1}{2}(\hat{v}_2^2 + 3\hat{v}_1^2) & (1-\gamma)\hat{v}_1\hat{v}_2 & \gamma\hat{v}_1 \end{bmatrix}$$

and

$$\hat{\mathbf{F}}_2(\hat{\mathbf{u}}) = \begin{bmatrix} \hat{0} & \hat{0} & \hat{1} & \hat{0} \\ -\hat{v}_1\hat{v}_2 & \hat{v}_2 & \hat{v}_1 & \hat{0} \\ \frac{\gamma-3}{2}\hat{v}_2^2 + \frac{\gamma-1}{2}\hat{v}_1^2 & (1-\gamma)\hat{v}_1 & (3-\gamma)\hat{v}_2 & \gamma - 1 \\ (\gamma-1)\hat{v}_2|\hat{\mathbf{v}}|^2 - \gamma\hat{v}_2\hat{E} & (1-\gamma)\hat{v}_1\hat{v}_2 & \gamma\hat{E} - \frac{\gamma-1}{2}(\hat{v}_1^2 + 3\hat{v}_2^2) & \gamma\hat{v}_2 \end{bmatrix}.$$

The matrix $\hat{\mathbf{F}}(\hat{\mathbf{u}}, \mathbf{n})$ is diagonalisable by the product

$$\left(\hat{\mathbf{R}}(\hat{\mathbf{u}}, \mathbf{n})\right)^{-1} \hat{\mathbf{F}}(\hat{\mathbf{u}}, \mathbf{n})\hat{\mathbf{R}}(\hat{\mathbf{u}}, \mathbf{n})$$

with a regular matrix $\hat{\mathbf{R}}(\hat{\mathbf{u}}, \mathbf{n}) \in \mathbb{R}^{4\times 4}$ and their eigenvalues are given by $\hat{\mathbf{v}} \cdot \mathbf{n}$ (occuring twice), $\hat{\mathbf{v}} \cdot \mathbf{n} - \hat{c}|\mathbf{n}|$ and $\hat{\mathbf{v}} \cdot \mathbf{n} + \hat{c}|\mathbf{n}|$, where $\hat{c} := \sqrt{\gamma\frac{\hat{p}}{\hat{\rho}}}$ denotes the speed of sound. Obviously, $\hat{\mathbf{R}}(\hat{\mathbf{u}}, \mathbf{n})$ represents the matrix consisting of the four linear independent eigenvectors of $\hat{\mathbf{F}}(\hat{\mathbf{u}}, \mathbf{n})$.
In the context of compressible flow fields the non-dimensionalization of the Euler equations is usually performed by means of the reference values for length $\hat{x}_{ref}$, density $\hat{\rho}_{ref}$ and fluid velocity $\hat{v}_{ref}$ which are taken from the underlying physical flow field. The remaining reference values are determined via functional relationships like $\hat{p}_{ref} = \hat{\rho}_{ref}\hat{v}_{ref}^2$, $\hat{E}_{ref} = \hat{p}_{ref}/\hat{\rho}_{ref}$ and $\hat{t}_{ref} = \hat{v}_{ref}/\hat{x}_{ref}$. Introducing the expression

$$\hat{\varphi} = \varphi \cdot \hat{\varphi}_{ref}$$

for each physical quantity $\hat{\varphi}$ into the governing equations yields a non-dimensional formulation of the Euler equations which is identical to (3.1). Even the equation of state (3.3) remains unchanged.
In the case of a small velocity reference the definition of the pressure reference is no longer appropriate since it does not represent a sensible measure of the physical pressure field. In order to meet this fact we employ an independent pressure reference and hence the dimensionless form of the Euler equations and the equation of state become

$$\begin{aligned} \partial_t \rho &+ \nabla_{\mathbf{x}} \cdot \mathbf{m} &= 0 \\ \partial_t \mathbf{m} &+ \nabla_{\mathbf{x}} \cdot (\mathbf{m} \otimes \mathbf{v}) + \frac{1}{\mathbf{M}^2}\nabla_{\mathbf{x}} p &= \mathbf{0} \\ \partial_t (\rho E) &+ \nabla_{\mathbf{x}} \cdot (H\mathbf{m}) &= 0 \end{aligned} \tag{3.5}$$

and

$$p = (\gamma - 1)\,\rho\left(E - \frac{\mathbf{M}^2}{2}|\mathbf{v}|^2\right). \tag{3.6}$$

The non-dimensional characteristic number $\mathbf{M}$ appearing within (3.5) and (3.6) is called the Mach number which is defined as

$$\mathbf{M} = \frac{\hat{v}_{ref}}{\hat{c}_{ref}} \tag{3.7}$$

where $\hat{c}_{ref} = \sqrt{\hat{p}_{ref}/\hat{\rho}_{ref}}$ denotes the reference value for the speed of sound $\hat{c}$. Note that the nondimensional solution depends on the reference values and therefore we take into account this fact by writing $\varphi(\mathbf{x}, t; \mathbf{M})$.

3.1 Asymptotic Analysis of the Euler Equations

Based on the characteristic number $\mathbf{M}$ we are now able to investigate the behaviour of the physical quantities in the low Mach number limit by means of a formal asymptotic analysis. This proceeding was firstly suggested by Klainerman and Majda [34, 35]. In their study the fluid was assumed to be barotropic and a single scale asymptotic expansion was used. Hence, as we will see later on, acoustic effects were neglected in their investigation. Asano [2] and Ukai [77] improved the results in the sense that weaker assumptions on the initial conditions are considered. In particular, the divergence free condition of the initial data was removed. In [36, 48] a single time scale, multiple length scale asymptotic analysis of the compressible Euler equations is employed in order to investigate the behaviour of the fluid flow in the low Mach number regime. Thereby the conservative formulation of the Euler equations is considered and the results are used to extend the validity of a numerical method from the compressible to the low Mach number regime by the introduction of multiple pressure variables, whereby acoustic effects as well as variable density distributions are taken into account [36].
Following [48] we are now investigating the Euler equations by means of an asymptotic single and multiple scale expansion whereby the choice of the scales depends on the flow domain considered. Moreover, we assume throughout the Chapter that the non-dimensional formulation of the governing equations (3.5) consists exclusively of physical quantities φ satisfying $\varphi = O(1)$ if the Mach number tends to zero. The success of an asymptotic analysis depends crucially on the choice of the incorporated asymptotic sequence $\{\phi_n(\mathbf{M})\}_{n\in\mathbb{N}_0}$ which in our case has to satisfy the assumption $\phi_n(\mathbf{M}) = o\left(\phi_{n-1}(\mathbf{M})\right)$, $\mathbf{M} \to 0$. The perturbation parameter within the governing equations (3.5) is the reciprocal value of the square of the Mach number. This seems to be the reason why many asymptotic expansions in the literature are based on the asymptotic sequence $\phi_n(\mathbf{M}) = \mathbf{M}^{2n}$. We employ the asymptotic sequence

$$\phi_n(\mathbf{M}) = \mathbf{M}^n, \quad n \in \mathbb{N}_0, \tag{3.8}$$

which is actually not obvious but several explanations concerning this choice will be given below. As we have learned from Section 2 the use of (2.7) instead of $\phi_n(\mathbf{M}) = \mathbf{M}^{2n}$ will lead at most to some vanishing asymptotic functions. Nevertheless, the function space associated with (2.7) completely contains the function space build by $\phi_n(\mathbf{M}) = \mathbf{M}^{2n}$ and consequently we can ensure that no informations will get lost.
First, we focus our view on a domain $\mathbf{G} \times \mathbb{R}_0^+$ with a bounded spatial part $\mathbf{G} \subset \mathbb{R}^d$. Consequently, there exists always a lower bound $\mathbf{M}_l > 0$ such that for each $\mathbf{M} \in (0, \mathbf{M}_l)$ no phenomena on a scale $\xi = \mathbf{M}\mathbf{x}$ are present in the distribution of the solution vector $\mathbf{u} = (\rho, m_1, \dots, m_d, \rho E)^T$. Hence, we define the asymptotic solution space $\mathcal{U}_s$ as the

set of all functions $\mathbf{u} : \mathbf{G} \times \mathbb{R}_0^+ \times (0, \widetilde{\mathbf{M}}) \to \mathbb{R}^d$, $\widetilde{\mathbf{M}} > 0$ satisfying the Euler equations (3.5), whereby each physical quantity φ can be expressed by an asymptotic expansion

$$\varphi(\mathbf{x}, t; \mathbf{M}) = \sum_{i=0}^{j} \mathbf{M}^i \varphi^{(i)}(\mathbf{x}, t) + o(\mathbf{M}^j), \ j = 0, 1, 2, \ \mathbf{M} \to 0,$$

which is uniformly valid in $\mathbf{G} \times \mathbb{R}_0^+$.
In order to study the properties of the asymptotic functions $\varphi^{(i)}$, $i = 0, 1, 2$ we introduce the asymptotic expansion into the Euler equations. Due to the fact that the asymptotic functions are independent of the reference parameter Lemma 2.5 gives us the justification to identify terms multiplied by the same power of $\mathbf{M}$. This procedure leads directly to the system of pertubation equations

$$\begin{aligned}
\partial_t \rho^{(i)} + \nabla_{\mathbf{x}} \cdot \mathbf{m}^{(i)} &= 0, \quad i = 0, 1, 2, && (3.9)\\
\nabla_{\mathbf{x}} p^{(0)} &= \mathbf{0} && (3.10)\\
\nabla_{\mathbf{x}} p^{(1)} &= \mathbf{0} && (3.11)\\
\partial_t \mathbf{m}^{(0)} + \nabla_{\mathbf{x}} \cdot \left(\mathbf{m}^{(0)} \otimes \mathbf{v}^{(0)}\right) + \nabla_{\mathbf{x}} p^{(2)} &= \mathbf{0} && (3.12)\\
\partial_t \left(\rho E\right)^{(i)} + \nabla_{\mathbf{x}} \cdot \left(\rho H \mathbf{v}\right)^{(i)} &= 0, \quad i = 0, 1, 2, && (3.13)
\end{aligned}$$

in $\mathbf{G} \times \mathbb{R}_0^+$. The following important result follows immediately from (3.10) and (3.11).

Theorem 3.1 *Given $\mathbf{u} \in \mathcal{U}_s$ there hold*

$$p^{(0)} = p^{(0)}(t) \quad \textit{and} \quad p^{(1)} = p^{(1)}(t). \tag{3.14}$$

Thereom 3.1 implies that the maximum influence of spatial fluctuations inside the pressure distribution are of order $O(\mathbf{M}^2)$ whereas $O(1)$-variations can only appear in the temporal evolution uniformly in $\mathbf{G}$. Therefore, the investigation of the time-dependent change of the leading order pressure $p^{(0)}$ represents a significant part in order to gain informations concerning the dominant pressure features.

Theorem 3.2 *Given $\mathbf{u} \in \mathcal{U}_s$ there holds*

$$\frac{1}{\gamma} \frac{d \ln p^{(0)}}{dt} = -\frac{1}{|\mathbf{G}|} \int_{\partial \mathbf{G}} \mathbf{v}^{(0)} \cdot \mathbf{n} \, ds,$$

where $\partial \mathbf{G}$ and $\mathbf{n}$ denote the boundary of the domain $\mathbf{G}$ and the unit outer normal vector on $\partial \mathbf{G}$, respectively.

Proof:
Introducing the asymptotic expansion into the equation of state yields

$$p^{(0)} = (\gamma - 1)(\rho E)^{(0)}. \tag{3.15}$$

Hence, the leading order total enthalphy per unit volume can be expressed as

$$(\rho H)^{(0)} = (\rho E)^{(0)} + p^{(0)} = \frac{\gamma}{\gamma - 1} p^{(0)}. \tag{3.16}$$

Consequently, equation (3.10) yields

$$\nabla_{\mathbf{x}} (\rho H)^{(0)} = \mathbf{0}. \tag{3.17}$$

Taking into account the leading order energy equation (3.13) it follows

$$\begin{aligned} 0 &= \partial_t (\rho E)^{(0)} + (\rho H)^{(0)} \nabla_{\mathbf{x}} \cdot \mathbf{v}^{(0)} + \mathbf{v}^{(0)} \cdot \nabla_{\mathbf{x}} (\rho H)^{(0)} \\ &= \frac{1}{\gamma - 1} \frac{dp^{(0)}}{dt} + \frac{\gamma}{\gamma - 1} p^{(0)} \nabla_{\mathbf{x}} \cdot \mathbf{v}^{(0)} \end{aligned} \tag{3.18}$$

by the use of the equations (3.15) – (3.17) and the fact that $(H\mathbf{m})^{(0)} = (\rho H)^{(0)} \mathbf{v}^{(0)}$. Integrating over the domain $\mathbf{G}$ and applying Gauss' divergence Theorem give

$$\frac{1}{\gamma} \frac{d \ln p^{(0)}}{dt} = \frac{1}{\gamma p^{(0)}} \frac{dp^{(0)}}{dt} = -\frac{1}{|\mathbf{G}|} \int_{\mathbf{G}} \nabla_{\mathbf{x}} \cdot \mathbf{v}^{(0)} \, d\mathbf{x} = -\frac{1}{|\mathbf{G}|} \int_{\partial \mathbf{G}} \mathbf{v}^{(0)} \cdot \mathbf{n} \, ds.$$

□

Theorem 3.2 describes the connection between the leading order pressure and velocity and shows that the global rise of the spatially homogeneous pressure term is due to compression from the boundary $\partial\mathbf{G}$ or expansion of the reacting gas itself. Furthermore, equation (3.18) proves that the divergence of the leading order velocity field is spatially constant and its temporal evolution depends on the velocity distribution along the boundary of the computational domain. The statement of Theorem 3.2 is important with regard to the pressure decomposition in a numerical method for low Mach number flow. Due to this result one can define the leading order pressure term as an average over all of the computational domain. As a further consequence of the single scale expansion it is not necessary to consider a first order term seperately. Therefore in a numerical frameworkone, which is based on the results of a single scale asymptotic analysis one can decompose the pressure in the form $p = p^{(0)} + \mathbf{M}^2 p^{(2)}$. The following Theorem substantiates that the leading order density $\rho^{(0)}$ and pressure $p^{(0)}$ satisfy the equation for quasi-static adiabatic compression of mass elements along particle paths according to the velocity $\mathbf{v}^{(0)}$.

Theorem 3.3 *Let $\mathbf{u} \in \mathcal{U}_s$. Then the leading order pressure term $p^{(0)}$ and density $\rho^{(0)}$ satisfy*

$$\frac{D \ln \rho^{(0)}}{Dt} = \frac{1}{\gamma} \frac{d \ln p^{(0)}}{dt}$$

with $\frac{D}{Dt} = \partial_t + \mathbf{v}^{(0)} \cdot \nabla_{\mathbf{x}}$.

Proof:
The proof is given by a simple combination of the leading order continuity equation in the form

$$\frac{D\rho^{(0)}}{Dt} = -\rho^{(0)} \nabla_{\mathbf{x}} \cdot \mathbf{v}^{(0)}$$

with equation (3.18). $\square$

Introducing the entropy $s := \frac{p^{(0)}}{\rho^{(0)\gamma}}$ we obtain

$$\frac{1}{s}\frac{Ds}{Dt} = \frac{D}{Dt}\left(\ln \frac{p^{(0)}}{\rho^{(0)\gamma}}\right) = \frac{D \ln p^{(0)}}{Dt} - \gamma \frac{D \ln \rho^{(0)}}{Dt} = 0. \tag{3.19}$$

Furthermore, we can write the continuity equation in the form

$$\frac{D\rho^{(0)}}{Dt} = \frac{\rho^{(0)}}{\gamma p^{(0)}} \frac{dp^{(0)}}{dt} = -\frac{\rho^{(0)}}{|\mathbf{G}|} \int_{\partial \mathbf{G}} \mathbf{v}^{(0)} \cdot \mathbf{n} \, ds. \tag{3.20}$$

By the use of equation (3.19), the continuity equation describes the isentropic advection of mass elements along its particle path where the compression or expansion is due to a global variation of the spatially homogeneous leading order pressure or to the distribution of the leading order velocity along the boundary of the computational domain, respectively. Note that a vanishing right hand side of equation (3.20) implies a constant pressure term $p^{(0)}$, a divergence free velocity field $\mathbf{v}^{(0)}$ as well as

$$\int_{\Gamma} \mathbf{v}^{(0)} \cdot \mathbf{n} \, ds = 0$$

for all pathes Γ in $\mathbf{G}$. Therefore, in a numerical method the boundary conditions should directly determine the temporal rise of the spatially homogeneous pressure $p^{(0)}$ and hence the simulation of this effect is very simple. An example is given by a cylinder-piston-system where the moving piston yields a negative velocity distribution $\mathbf{v}^{(0)} \cdot \mathbf{n}$ along the inflow boundary which leads to a global increase of the pressure.
In contrast to the previous analysis we now consider a spatial domain $\mathbf{G} \subset \mathbb{R}^d$ which satisfies

$$(d_{\min}(\mathbf{G}))^{-1} = o\left(\frac{\mathbf{M}}{\hat{l}_{ref}}\right), \mathbf{M} \to 0, \tag{3.21}$$

with

$$d_{\min}(\mathbf{G}) := \sup_{\mathbf{x},\mathbf{y} \in \mathbf{G}} \min_{k=1,\dots,d} |x_k - y_k|.$$

This means that the domain $\mathbf{G}$ is always large enough so that long wave phenomena on a scale $\xi = \mathbf{M}\mathbf{x}$ can appear. Note that this assumption implies that $\mathbf{G} = \mathbb{R}^d$ or $\mathbf{G}$ depends on $\mathbf{M}$. Furthermore, there exists always a positive real number $\mathbf{M}'$ such that

$$\mathbf{B}_{\mathbf{x}}\left(\frac{1}{\mathbf{M}}\right) := \left\{ \mathbf{x} \in \mathbb{R}^d \,\middle|\, |\mathbf{x}| \leq \frac{1}{\mathbf{M}} \right\} \subset \mathbf{G}$$

for all $\mathbf{M} \leq \mathbf{M}'$.
In order to take into account a single time scale and multiple space scales we introduce the mapping

$$\begin{array}{rccc} \mathbf{g}: & \mathbb{R}^d \times \mathbb{R}_0^+ \times (0, \widetilde{\mathbf{M}}) & \rightarrow & \mathbb{R}^{2d} \times \mathbb{R}_0^+ \\ & (\mathbf{x}, t; \mathbf{M}) & \stackrel{\mathbf{g}}{\longmapsto} & (\mathbf{x}, \mathbf{M}\mathbf{x}, t)\,. \end{array} \tag{3.22}$$

In correspondance to the single length scale case we define $\widetilde{\mathcal{U}}_m$ as the space consisting of vector functions $\mathbf{u}$ satisfying the Euler equations where each physical quantity w can be expressed by an uniformly valid multiple scale asymptotic expansion

$$\varphi\left(\mathbf{x}, t; \mathbf{M}\right) = \sum_{i=0}^{j} \mathbf{M}^i \, \varphi^{(i)}\left(\mathbf{g}(\mathbf{x}, t; \mathbf{M})\right) + o\left(\mathbf{M}^j\right), \; \mathbf{M} \rightarrow 0, \; j = 0, 1, 2$$

with the asymptotic functions

$$\begin{array}{rccc} \varphi^{(i)}: & \mathbb{R}^d \times \mathbb{R}^d \times \mathbb{R}_0^+ & \rightarrow & \mathbb{R}, \; i = 0, 1, 2 \\ & (\eta, \xi, t) & \stackrel{\varphi^{(i)}}{\longmapsto} & \varphi^{(i)}\left(\eta, \xi, t\right). \end{array}$$

First, we consider the so-called sublinear growth condition of the asymptotic functions which represents a basic tool insight the following analysis.

Lemma 3.4
Let $w : \mathbb{R}^d \times \mathbb{R}_0^+ \times (0, \widetilde{\mathbf{M}}) \rightarrow \mathbb{R}$ be uniformly bounded with respect to $\mathbf{x}$ and $\mathbf{M}$ and let the asymptotic multiple scale expansion

$$w\left(\mathbf{x}, t; \mathbf{M}\right) = \sum_{i=0}^{j} \mathbf{M}^i \, \varphi^{(i)}\left(\mathbf{g}(\mathbf{x}, t; \mathbf{M})\right) + o\left(\mathbf{M}^j\right), \; \mathbf{M} \rightarrow 0$$

be uniformly valid in $\mathbb{R}^d \times \mathbb{R}_0^+$ for each $j = 0, 1, 2$. Then for the leading order asymptotic function $\varphi^{(0)}$ there holds

$$\varphi^{(0)}\left(\mathbf{g}(\mathbf{x}, t; \mathbf{M})\right) = o\left(|\mathbf{x}|^\alpha\right), \; \mathbf{x} \in \partial B_{\mathbf{x}}\left(\frac{1}{\mathbf{M}}\right), \; \mathbf{M} \rightarrow 0 \tag{3.23}$$

for all $\alpha > 0$. Furthermore, the first order and second order asymptotic function satisfy

$$\varphi^{(i)}\left(\mathbf{g}(\mathbf{x}, t; \mathbf{M})\right) = o\left(|\mathbf{x}|\right), \; \mathbf{x} \in \partial B_{\mathbf{x}}\left(\frac{1}{\mathbf{M}}\right), \; \mathbf{M} \rightarrow 0, \; i = 1, 2, \tag{3.24}$$

respectively.

Proof:
From the uniform validity of the asymptotic expansion we have

$$\varphi^{(i)}\left(\mathbf{g}(\mathbf{x},t;\mathbf{M})\right) = o\left(\mathbf{M}^{-1}\right),\ \mathbf{M}\to 0 \tag{3.25}$$

uniformly in $\mathbf{G}\times\mathbb{R}_0^+$ for $i=1,2$. Given a null sequence $\{\mathbf{M}_n\}_{n\in\mathbb{N}}$ we define an arbitrary vector sequence $\{\mathbf{x}_n\}_{n\in\mathbb{N}}$ with $\mathbf{x}_n\in\partial B_{\mathbf{x}}\left(\frac{1}{\mathbf{M}_n}\right)$. Using the uniform validity of (3.25) we obtain

$$0=\lim_{n\to\infty}\frac{\varphi^{(i)}\left(\mathbf{g}(\mathbf{x}_n,t;\mathbf{M}_n)\right)}{\mathbf{M}_n^{-1}}=\lim_{n\to\infty}\frac{\varphi^{(i)}\left(\mathbf{g}(\mathbf{x}_n,t;\mathbf{M}_n)\right)}{|\mathbf{x}_n|}$$

which proves statement (3.24). In order to derive the equation (3.23) we employ the uniform boundeness of the function w which gives

$$\varphi(\mathbf{x},t;\mathbf{M})=o(r^\alpha),\ \mathbf{x}\in\partial B_{\mathbf{x}}(r),\ r\to\infty \tag{3.26}$$

for all $\alpha>0$. Using the asymptotic expansion we obtain

$$\varphi(\mathbf{x},t;\mathbf{M})=\varphi^{(0)}\left(\mathbf{g}(\mathbf{x},t;\mathbf{M})\right)+o(1),\ \mathbf{M}\to 0 \tag{3.27}$$

uniformly in $\mathbf{G}\times\mathbb{R}_0^+$. A simple combination of the equations (3.26) and (3.27) leads to

$$\begin{aligned}\varphi^{(0)}\left(\mathbf{g}(\mathbf{x},t;\mathbf{M})\right) &= \varphi(\mathbf{x},t;\mathbf{M})+o(1)\\ &= o\left(\mathbf{M}^{-\alpha}\right)+o(1)=o\left(|\mathbf{x}|^\alpha\right),\end{aligned}$$

where $\mathbf{x}\in\partial B_{\mathbf{x}}\left(\frac{1}{\mathbf{M}}\right)$ and $\mathbf{M}\to 0$. □

Note that the statement of Theorem 3.4 does not depend on the special form of the mapping $\mathbf{g}$ and therefore the sublinear growth condition is also valid in the case of a single scale expansion if an unbounded domain is considered. The assumption that the physical quantity w is uniformly bounded is motivated by the property (3.4) and guarentees that we have chosen the reference values in a propper manner.
By using the derivatives

$$\partial_t(\varphi^{(i)}\circ\mathbf{g})(\mathbf{x},t;\mathbf{M})=\partial_t\varphi^{(i)}(\mathbf{g}(\mathbf{x},t;\mathbf{M})) \tag{3.28}$$

and

$$\partial_{x_j}(\varphi^{(i)}\circ\mathbf{g})(\mathbf{x},t;\mathbf{M})=\partial_{\eta_j}\varphi^{(i)}(\mathbf{g}(\mathbf{x},t;\mathbf{M}))+\mathbf{M}\partial_{\xi_j}\varphi^{(i)}(\mathbf{g}(\mathbf{x},t;\mathbf{M})),\ j=1,\dots,d \tag{3.29}$$

and introducing the asymptotic expansion into the Euler equations we obtain

$$\begin{aligned}&\partial_t\rho^{(0)}+\nabla_\eta\rho^{(0)}\\ &+\ \mathbf{M}\left(\partial_t\rho^{(1)}+\nabla_\eta\rho^{(1)}+\nabla_\xi\rho^{(0)}\right)+\mathbf{M}^2\left(\partial_t\rho^{(2)}+\nabla_\eta\rho^{(2)}+\nabla_\xi\rho^{(1)}\right)\\ &=\ o\left(\mathbf{M}^2\right),\ \mathbf{M}\to 0 \text{ in } \widetilde{\mathcal{D}},\end{aligned} \tag{3.30}$$

$$
\begin{aligned}
&\mathbf{M}^{-2}\nabla_\eta p^{(0)} + \mathbf{M}^{-1}\left(\nabla_\eta p^{(1)} + \nabla_\xi p^{(0)}\right) \\
&\quad + \quad \left(\partial_t \mathbf{m}^{(0)} + \nabla_\eta \cdot \left(\mathbf{m}^{(0)} \otimes \mathbf{v}^{(0)}\right) + \nabla_\eta p^{(2)} + \nabla_\xi p^{(1)}\right) \\
&\quad = \quad o\left(1\right), \ \mathbf{M} \to 0 \text{ in } \widetilde{\mathcal{D}},
\end{aligned} \tag{3.31}
$$

$$
\begin{aligned}
&\partial_t(\rho E)^{(0)} + \nabla_\eta \cdot (H\mathbf{m})^{(0)} \\
&\quad + \quad \mathbf{M}\left(\partial_t(\rho E)^{(1)} + \nabla_\eta \cdot (H\mathbf{m})^{(1)} + \nabla_\xi \cdot (H\mathbf{m})^{(0)}\right) \\
&\quad + \quad \mathbf{M}^2\left(\partial_t(\rho E)^{(2)} + \nabla_\eta \cdot (H\mathbf{m})^{(2)} + \nabla_\xi \cdot (H\mathbf{m})^{(1)}\right) \\
&\quad = \quad o\left(\mathbf{M}^2\right), \ \mathbf{M} \to 0 \text{ in } \widetilde{\mathcal{D}},
\end{aligned} \tag{3.32}
$$

where the manifold $\widetilde{\mathcal{D}}$ is defined to be

$$
\widetilde{\mathcal{D}} := \left\{(\eta,\xi,t) \in \mathbb{R}^{2d} \times \mathbb{R}_0^+ \,\middle|\, (\eta,\xi,t) = \mathbf{g}(\mathbf{x},t;\mathbf{M}),\ (\mathbf{x},t) \in \mathbf{G} \times \mathbb{R}_0^+ \right\}.
$$

As mentioned in Section 2 we have to increase the assumption concerning the asymptotic functions to enable the decomposition of the above system (3.30) – (3.32) in the same manner as proceeded in the context of a single scale expansion. Therefore, we introduce the space $\mathcal{U}_m \subset \widetilde{\mathcal{U}}_m$ by the assumptions that the asymptotic functions $\varphi^{(0)}$, $\varphi^{(1)}$ $\varphi^{(2)}$ which are related to the physical quantity w given by a function $\mathbf{u} \in \mathcal{U}_m$ satisfy the equations (3.30) – (3.32) in

$$
\mathcal{D} := \left\{(\eta,\xi,t) \in \mathbb{R}^{2d} \times \mathbb{R}_0^+ \,\middle|\, \xi_j < \widetilde{\mathbf{M}}\eta_j, j = 1,\dots,d\right\}
$$

and fulfill the sublinear growth condition in the generalized sense

$$
\varphi^{(0)}\left(\eta,\xi,t\right) = o\left(|\eta|^\alpha\right),\ \eta \in \partial B_\eta\left(\frac{1}{\mathbf{M}}\right),\ \mathbf{M} \to 0
$$

for all $\alpha > 0$ and

$$
\varphi^{(i)}\left(\eta,\xi,t\right) = o\left(|\eta|\right),\ \eta \in \partial B_\eta\left(\frac{1}{\mathbf{M}}\right),\ \mathbf{M} \to 0,\ i = 1,2.
$$

Analogously to the single scale case we can express the equations (3.30) – (3.32) in the form

$$
\begin{aligned}
\partial_t \rho^{(0)} + \nabla_\eta \cdot \mathbf{m}^{(0)} &= 0 && (3.33)\\
\partial_t \rho^{(1)} + \nabla_\eta \cdot \mathbf{m}^{(1)} &= -\nabla_\xi \cdot \mathbf{m}^{(0)} && (3.34)\\
\partial_t \rho^{(2)} + \nabla_\eta \cdot \mathbf{m}^{(2)} &= -\nabla_\xi \cdot \mathbf{m}^{(1)} && (3.35)\\
\nabla_\eta p^{(0)} &= \mathbf{0} && (3.36)\\
\nabla_\eta p^{(1)} &= -\nabla_\xi p^{(0)} && (3.37)\\
\partial_t \mathbf{m}^{(0)} + \nabla_\eta \cdot \left(\mathbf{m}^{(0)} \otimes \mathbf{v}^{(0)}\right) + \nabla_\eta p^{(2)} &= -\nabla_\xi p^{(1)} && (3.38)\\
\partial_t \left(\rho E\right)^{(0)} + \nabla_\eta \cdot \left(\rho H \mathbf{v}\right)^{(0)} &= 0 && (3.39)\\
\partial_t \left(\rho E\right)^{(1)} + \nabla_\eta \cdot \left(\rho H \mathbf{v}\right)^{(1)} &= -\nabla_\xi \cdot \left(\rho H \mathbf{v}\right)^{(0)} && (3.40)\\
\partial_t \left(\rho E\right)^{(2)} + \nabla_\eta \cdot \left(\rho H \mathbf{v}\right)^{(2)} &= -\nabla_\xi \cdot \left(\rho H \mathbf{v}\right)^{(1)} && (3.41)
\end{aligned}
$$

in $\mathcal{D}$.
In the following we derive some properties of the asymptotic functions which are fundamental in order to get a deeper insight into the limit behaviour of a flow field which is governed by the d-dimensional Euler equations.

Theorem 3.5 *Let $\mathbf{u} \in \mathcal{U}_m$. Then there hold*

$$p^{(0)} = p^{(0)}(t) \quad \textit{and} \quad p^{(1)} = p^{(1)}(\xi, t). \tag{3.42}$$

Proof:
Equation (3.36) directly gives $p^{(0)} = p^{(0)}(\xi, t)$. The property (3.21) in connection with the mapping $\mathbf{g}$ used enables the integration of equation (3.37) over the open ball $B_\eta\left(\frac{1}{\mathbf{M}}\right)$. Using the sublinear growth condition leads to

$$
\begin{aligned}
\nabla_\xi p^{(0)} &= -\frac{1}{|B_\eta\left(\frac{1}{\mathbf{M}}\right)|} \int_{B_\eta\left(\frac{1}{\mathbf{M}}\right)} \nabla_\eta p^{(1)} \, d\eta = -\frac{1}{|B_\eta\left(\frac{1}{\mathbf{M}}\right)|} \int_{\partial B_\eta\left(\frac{1}{\mathbf{M}}\right)} p^{(1)} \cdot \mathbf{n} \, ds \\
&= O(\mathbf{M}^d) \, O(\mathbf{M}^{1-d}) \, o(\mathbf{M}^{-1}) = o(1), \ \mathbf{M} \to 0.
\end{aligned}
$$

Hence, we obtain $p^{(0)} = p^{(0)}(t)$ and the first order momentum equation (3.37) gives $p^{(1)} = p^{(1)}(\xi, t)$. □

Theorem 3.5 shows that even in the multiple scale expansion the leading order pressure is at most varying with respect to time whereas the pressure term $p^{(1)}$ carries acoustic phenomena. Hence, the first order pressure should be used to involve these important effects and one can not subadd this pressure term into $p^{(0)}$. The pressure reads

$$p(\mathbf{x}, t; \mathbf{M}) = p^{(0)}(t) + \mathbf{M} p^{(1)}(\xi, t) + \mathbf{M}^2 p^{(2)}(\eta, \xi, t) + o\left(\mathbf{M}^2\right), \quad \mathbf{M} \to 0. \tag{3.43}$$

The following Theorems are devoted to derive the divergence free condition of the velocity field in the limit of a vanishing Mach number where the domain $\mathbf{G}$ is unbounded in the sense of equation (3.21). The proof of the next Theorem is identical to the derivation of equation (3.18).

Theorem 3.6 *Let* $\mathbf{u} \in \mathcal{U}_m$. *Then there holds*

$$\nabla_\eta \cdot \mathbf{v}^{(0)} = -\frac{1}{\gamma p^{(0)}} \frac{dp^{(0)}}{dt}. \tag{3.44}$$

Theorem 3.7 *Let* $\mathbf{u} \in \mathcal{U}_m$. *Then there hold*

$$\lim_{\mathbf{M} \to 0} \nabla_{\mathbf{x}} \cdot \mathbf{v}(\mathbf{x}, t; \mathbf{M}) = 0 \tag{3.45}$$

and

$$p^{(0)} = const. \tag{3.46}$$

Proof:
With regard the fact that the leading order pressure is spatially homogeneous one obtains

$$\begin{aligned} \frac{1}{\gamma p^{(0)}} \frac{dp^{(0)}}{dt} &= -\frac{1}{|B_\eta\left(\frac{1}{\mathbf{M}}\right)|} \int_{B_\eta\left(\frac{1}{\mathbf{M}}\right)} \nabla_\eta \cdot \mathbf{v}^{(0)} \, d\eta \\ &= -\frac{1}{|B_\eta\left(\frac{1}{\mathbf{M}}\right)|} \int_{\partial B_\eta\left(\frac{1}{\mathbf{M}}\right)} \mathbf{v}^{(0)} \cdot \mathbf{n} \, ds. \end{aligned}$$

Using the sublinear growth condition of the leading order velocity field gives

$$\frac{1}{\gamma p^{(0)}} \frac{dp^{(0)}}{dt} = o(\mathbf{M}^{1-\alpha}), \ \mathbf{M} \to 0$$

for all $\alpha > 0$. Hence, the choice $\alpha = \frac{1}{2}$ in combination with the positivity of the pressure term leads to

$$\frac{dp^{(0)}}{dt} = 0.$$

Then (3.44) yields

$$\nabla_\eta \cdot \mathbf{v}^{(0)} = 0$$

and by the use of equation (3.29) it follows

$$\nabla_{\mathbf{x}} \cdot \mathbf{v} = \nabla_\eta \cdot \mathbf{v}^{(0)} + o(1) = o(1), \ \mathbf{M} \to 0$$

which completes the proof. $\square$

With regard to the validity of the sublinear growth condition in the case of a single scale expansion as mentioned we would like to emphasize that the divergence free condition as well as the statement (3.46) also hold for each function $\mathbf{u} \in \mathcal{U}_s$ if an unbounded domain $\mathbf{G}$ is considered. The essence of Theorem 3.7 lies in the fact that the leading order pressure term acts as a constant background pressure. Thus, spatial fluctuations as well as time-dependent influences of the pressure distribution are at most of order $o(1)$. Due to the lack of compression from the boundary we obtain a time-independent pressure distribution in the limit of a vanishing Mach number. Furthermore, high frequency variations are only introduced by the second order pressure $p^{(2)}$ and hence their maximum effect is of order $o(\mathbf{M})$. It seems to be remarkable that despide of the above mentioned properties it is important to take into account both pressure terms $p^{(1)}$ and $p^{(2)}$ even in the case of a small reference parameter. This fact is based on a simple consideration of the second order momentum equation which shows the influences of the gradients $\nabla_\xi p^{(1)}$ and $\nabla_\eta p^{(2)}$ on the leading order momentum.
Obviously, the usual way to develop a numrical method which resolves possible long wave phenomena should be based on an asymptotic multiple length scale expansion. Unfortunately, this fact leads into the delimma that many flow problems of interest are connected with confined domains (e.g. the flow in a piston) and hence one can not use the sublinear growth condition. As a consequence of this circumstance we get

$$\nabla_\xi p^{(0)} = -\frac{1}{|\mathbf{G}|} \int_{\partial \mathbf{G}} p^{(1)} \mathbf{n} \, ds. \tag{3.47}$$

In the case of periodic boundary conditions we obtain $p^{(0)} = p^{(0)}(t)$ and $p^{(1)} = p^{(1)}(\xi, t)$. However, the integral in (3.47) is not vanishing in general and therefore a numerical method should reflect this situation in the sense that the average process which is usually used to define the distinguish pressure terms has to produce a spatially varying leading order pressure. Furthermore, if the Mach number becomes sufficiently small so that the influence of the acoustic phenomena vanish than in correspondence with the results of the asymptotic single scale analysis the first order pressure should vanish identically and the leading order pressure should become spatially homogeneous.
In order to investigate the first order pressure $p^{(1)}$ it is convenient to introduce the average operator

$$\overline{w}(\xi, t) := \lim_{\mathbf{M} \to 0} \frac{1}{\left|B_\eta\left(\frac{1}{\mathbf{M}}\right)\right|} \int\limits_{B_\eta\left(\frac{1}{\mathbf{M}}\right)} \varphi(\eta, \xi, t) \, d\eta. \tag{3.48}$$

Using this notation we get the following two statements.

Theorem 3.8 *Let $\mathbf{u} \in \mathcal{U}_m$. Then there hold*

$$\overline{\partial_t \mathbf{m}^{(0)}} + \nabla_\xi p^{(1)} = \mathbf{0} \tag{3.49}$$

and

$$\partial_t p^{(1)} + \gamma p^{(0)} \overline{\nabla_\xi \mathbf{v}^{(0)}} = 0. \tag{3.50}$$

Proof:
The sublinear growth condition yields

$$\frac{1}{\left|B_\eta\left(\frac{1}{\mathbf{M}}\right)\right|}\int\limits_{B_\eta\left(\frac{1}{\mathbf{M}}\right)} \nabla_\eta p^{(2)} + \nabla_\eta\cdot\left(\mathbf{m}^{(0)}\otimes\mathbf{v}^{(0)}\right)\ d\eta = o(1),\ \mathbf{M}\to 0,$$

and from Theorem 3.5 one obtains $p^{(1)} = \overline{p^{(1)}}$. Thus, averaging the momentum equation (3.38) leads to

$$\begin{aligned}
\mathbf{0} &= \lim_{\mathbf{M}\to 0}\frac{1}{\left|B_\eta\left(\frac{1}{\mathbf{M}}\right)\right|}\int\limits_{B_\eta\left(\frac{1}{\mathbf{M}}\right)} \left(\partial_t\mathbf{m}^{(0)} + \nabla_\eta\cdot\left(\mathbf{m}^{(0)}\otimes\mathbf{v}^{(0)}\right) + \nabla_\eta p^{(2)} + \nabla_\xi p^{(1)}\right)\ d\eta \\
&= \lim_{\mathbf{M}\to 0}\frac{1}{\left|B_\eta\left(\frac{1}{\mathbf{M}}\right)\right|}\int\limits_{B_\eta\left(\frac{1}{\mathbf{M}}\right)} \partial_t\mathbf{m}^{(0)}\ d\eta + \nabla_\xi p^{(1)} \\
&= \overline{\partial_t\mathbf{m}^{(0)}} + \nabla_\xi p^{(1)}
\end{aligned}$$

which proves the first statement. Concerning the equation of state we get the relationships

$$(\rho E)^{(1)} = \frac{1}{\gamma-1}p^{(1)}$$

and

$$(\rho H)^{(0)} = \frac{\gamma}{\gamma-1}p^{(0)}.$$

Using the equation (3.42) and (3.46) inside the averaged first order energy equation in combination with the sublinear growth condition leads to

$$\begin{aligned}
0 &= (\gamma-1)\left(\overline{\partial_t\left(\rho E\right)^{(1)}} + \underbrace{\overline{\nabla_\eta\left(\rho H\mathbf{v}\right)^{(1)}}}_{=0} + \overline{\nabla_\xi\left(\rho H\mathbf{v}\right)^{(0)}}\right) \\
&= \partial_t p^{(1)} + (\gamma-1)\overline{\mathbf{v}^{(0)}\underbrace{\nabla_\xi\left(\rho H\right)^{(0)}}_{=0} + \left(\rho H\right)^{(0)}\nabla_\xi\mathbf{v}^{(0)}} \\
&= \partial_t p^{(1)} + \gamma p^{(0)}\overline{\nabla_\xi\mathbf{v}^{(0)}}.
\end{aligned}$$

□

The equations (3.49) and (3.50) describe the propagation of acoustic waves. In order to close this system we assume that the leading order density distribution carries non-trivial spatially informations only on the acoustic scale. In this case the average momentum equation (3.49) can be modified in the following way.

Theorem 3.9 *Let* $\mathbf{u} \in \mathcal{U}_m$ *and*

$$\rho^{(0)} = \rho^{(0)}\left(\xi, t\right). \tag{3.51}$$

Then there hold

$$\rho^{(0)} = \rho^{(0)}\left(\xi\right)$$

and

$$\overline{\partial_t \mathbf{v}^{(0)}} + \frac{1}{\rho^{(0)}} \nabla_\xi p^{(1)} = \mathbf{0}. \tag{3.52}$$

Proof:
The first statement is directly given by

$$\partial_t \rho^{(0)} = \overline{\partial_t \rho^{(0)}} = -\overline{\nabla_\eta \mathbf{m}^{(0)}} = 0.$$

This property yields

$$\overline{\partial_t \mathbf{m}^{(0)}} = \overline{\mathbf{v}^{(0)} \partial_t \rho^{(0)}} + \overline{\rho^{(0)} \partial_t \mathbf{v}^{(0)}} = \rho^{(0)} \overline{\partial_t \mathbf{v}^{(0)}}$$

and therefore Theorem 3.8 completes the proof. □

In order to derive a physical meaning of the first order pressure term we assume that each asymptotic function is sufficiently smooth in the sense that each neccessary change between two limit processes is allowed. Thus, we can write equation (3.52) in the form

$$\partial_t \overline{\mathbf{v}^{(0)}} + \frac{1}{\rho^{(0)}} \nabla_\xi p^{(1)} = \mathbf{0} \tag{3.53}$$

and finally we obtain the wave equation

$$\partial_t^2 p^{(1)} - \nabla_\xi \left(c \nabla_\xi p^{(1)} \right) = 0$$

where c is defined to be

$$c = \frac{\gamma p^{(0)}}{\rho^{(0)}}.$$

Hence, the pressure $p^{(1)}$ shows wave character and the evolution of this acoustic term can numerically be calculated by a simple discretization of the acoustic system which consists of the equations (3.50) and (3.53).

In order to supply a measure concerning the comparison between the analytical and numerical pressure distribution we introduce the indicator

$$\mathrm{Ind}(p) = \begin{cases} \dfrac{p_{\max} - p_{\min}}{p_{\max}\, \Delta \mathbf{x}_p} & \text{if } \; p_{\max} \neq p_{\min}, \\ 0 & \text{otherwise,} \end{cases} \tag{3.54}$$

where $p_{\max}$, $p_{\min}$, $\Delta\mathbf{x}_p$ denote the maximal and minimal pressure value and the minimal spatial distance between $p_{\max}$ and $p_{\min}$ with respect to the Euclidean norm, respectively. In the context of the single length scale asymptotic analysis the expression (3.14) directly proves

$$\operatorname{Ind}(p) = O\left(\mathbf{M}^2\right), \quad \mathbf{M} \to 0. \tag{3.55}$$

With respect to the multiple length scale expansion we distinguish two different cases. If the first order pressure field is spatially constant then the expansion (3.43) degenerates to the single scale expression

$$p(\mathbf{x}, t; \mathbf{M}) = p^{(0)}(t) + \mathbf{M}p^{(1)}(t) + \mathbf{M}^2 p^{(2)}(\mathbf{x}, t) + o\left(\mathbf{M}^2\right), \quad \mathbf{M} \to 0,$$

and consequently $\operatorname{Ind}(p) = O\left(\mathbf{M}^2\right)$, $\mathbf{M} \to 0$, follows. In the case of a spatially varying first order pressure field $p^{(1)}$ we conclude $p_{\max} - p_{\min} = O\left(\mathbf{M}\right)$, $\mathbf{M} \to 0$. Due to the fact that spatial variations within $p^{(1)}$ are associated with the length scale ξ we obtain $\frac{1}{\Delta\mathbf{x}_p} = O\left(\mathbf{M}\right)$, $\mathbf{M} \to 0$, which proves

$$\operatorname{Ind}(p) = O\left(\mathbf{M}^2\right), \quad \mathbf{M} \to 0, \tag{3.56}$$

also in the multiple length scale case.

4 Numerical Methods

Flow fields in fluid mechanics are subdivided into compressible and incompressible flows. The decomposition is usually based on the Mach number representing the quotient of the flow velocity and the speed of sound. Compressible inviscid fluid flow of an ideal gas is modeled by the Euler equations of gas dynamics as mentioned in Section 3, (see equation (3.1)). Thereby, the incorporated pressure is determined by an algebraic equation of state (3.3). On the other hand, within the incompressible Euler equations the pressure takes the role of a Lagrangian multiplier such that the velocity field satisfies an elliptic divergence constraint.

Although the equations are of different type there is no exact dividing line between the compressible and incompressible regime. For example, the flow in a nozzle often shows large compressible as well as incompressible regions. Furthermore, a laminar combustion with a Mach number between 10^{-4} and 10^{-3} can be accelerated by external or self-induced forces in such a way that a fast transition from deflagration to detonation takes place and drives the flow field towards a complete compressible regime where the Mach number grows to values between 5 and 10.

Obviously, current flow solvers which are based on the equations of either compressible or incompressible fluid flow are usually not suitable to simulate flow fields of varying type except when the transition between both regimes is handled in a physical senseful manner. Briley et. al. [5] and Merkle et. al. [56] reported of performance and accuracy problems in the case that standard compressible methods are used for the simulation of

low Mach number flows. Sesterhenn [66] investigated this phenomenon with the view on rounding errors, Volpe [80] described the influence of mesh adaption and Hauke et. al. [20] studied the effects of using different sets of variables. All these and several further research activities show that the extension of a compressible solver to the incompressible regime and vice versa requires an appropriate mathematical analysis of the governing equations in order to extract the main features of the physical quantities in the limit of interest.
Let us start with the description of a state of the art finite volume scheme developed and presented in a series of publications [19, 45, 69, 22, 44, 47, 46, 54, 52, 51, 55, 57, 11]. Concerning the extension of this standard compressible flow solver to the low Mach number regime we distinguish two different strategies, a preconditioning technique and a flux correction approach. Both algorithms will be extensively explained in the following.
In order to rewrite the Euler equations in a convenient manner for standard compressible flow solvers we define the auxiliary variables

$$\widetilde{p} = \frac{p}{\mathbf{M}^2}, \quad \widetilde{c} = \frac{c}{\mathbf{M}}, \quad \widetilde{E} = \frac{E}{\mathbf{M}^2} \quad \text{and} \quad \widetilde{H} = \frac{H}{\mathbf{M}^2}. \tag{4.1}$$

Thus the system (3.1) becomes

$$\partial_t \widetilde{\mathbf{u}} + \sum_{\ell=1}^{2} \partial_{x_\ell} \widetilde{\mathbf{f}}_\ell(\widetilde{\mathbf{u}}) = \mathbf{0} \ \text{ in } \ \mathbf{G} \times \mathbb{R}^+, \tag{4.2}$$

where $\widetilde{\mathbf{u}} = (\rho, \rho v_1, \rho v_2, \rho \widetilde{E})^T$, $\widetilde{\mathbf{f}}_\ell(\widetilde{\mathbf{u}}) = (\rho v_\ell, \ \rho v_\ell v_1 + \delta_1^\ell \widetilde{p}, \ \rho v_\ell v_2 + \delta_2^\ell \widetilde{p}, \ \rho \widetilde{H} v_\ell)^T$ and $\widetilde{p} = (\gamma - 1)\rho \left(\widetilde{E} - \frac{|\mathbf{v}|^2}{2} \right)$.
Smooth solutions of the system of the Euler equations exist in general only for short time and well-known phenomena like shock waves and contact discontinuities develop naturally. Hence we introduce the concept of weak solutions. A bounded set $\sigma \subset \mathbb{R}^2$ is said to be a control volume if Gauss' integral theorem is applicable to functions defined on σ. The mapping $\widetilde{\mathbf{u}}$ is called a weak solution of the system (4.2) if

$$\frac{d}{dt} \int_\sigma \widetilde{\mathbf{u}} \, d\mathbf{x} + \sum_{\ell=1}^{2} \int_{\partial\sigma} \widetilde{\mathbf{f}}_\ell(\widetilde{\mathbf{u}}) n_\ell \, ds = \mathbf{0} \tag{4.3}$$

is valid on every control volume $\sigma \subset \mathbf{G}$ with outer unit normal vector $\mathbf{n} = (n_1, n_2)^T$. Note that this formula can be derived from the system (4.2) by integrating over a control volume and applying Gauss' integral theorem. The solution class considered can be described by the function space $BV(\mathbb{R}_0^+; L^1 \cap L^\infty(\mathbb{R}^2; \mathbb{R}^4))$, i.e. the mapping $t \mapsto \widetilde{\mathbf{u}}(\cdot, t)$ is of bounded variation and the image is an integrable function of the space variables which is bounded almost everywhere.
With respect to the numerical solution of equation (4.2) the space part $\mathbf{G}$ and the time part $\mathbb{R}^+$ have to be discretized. We are starting from an arbitrary conforming

triangulation $\mathcal{T}_h$ which is usually called the primary mesh [21] and which consists of triangles $\mathcal{T}$. Furthermore, $\mathcal{N}_h$ denotes the index set of all nodes of the triangulation $\mathcal{T}_h$ and is subdivided by $\mathcal{N}_h = \mathcal{N}_{h,\mathbf{G}} \cup \mathcal{N}_{h,\partial\mathbf{G}}$, where $\mathcal{N}_{h,\mathbf{G}}$ is associated with the inner points and $\mathcal{N}_{h,\partial\mathbf{G}}$ includes the indices of the boundary points. Although a triangle itself can be used as a control volume, we consider boxes σ_i which are defined as the open set including the node $\mathbf{x}_i = (x_{i1}, x_{i2})^T$ (see Figure 1 (left)) and which are bounded by the straight lines l_{ij}^k, $k = 1, 2$, connecting the midpoint of the corresponding edge with the point $\mathbf{x}_s = (x_{s1}, x_{s2})^T$ (see Figure 1 (right)). Here $\mathbf{x}_s$ is defined by

$$\mathbf{x}_s = \sum_{m\in\{i,j,k\}} \alpha_m^s \mathbf{x}_m \quad \text{with} \quad \alpha_m^s = \frac{1}{2\left(|l_i| + |l_j| + |l_k|\right)} \sum_{\substack{\overline{m}\in\{i,j,k\} \\ \overline{m}\neq m}} |l_{\overline{m}}|.$$

The union of these boxes σ_i, $i \in \mathcal{N}_h$, is called the secondary mesh.

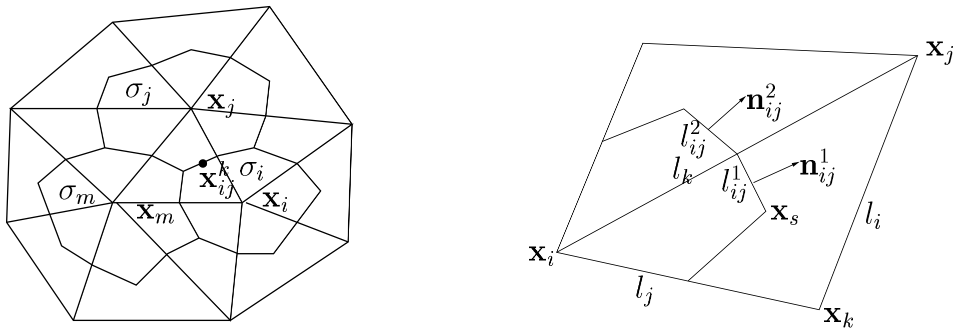

Figure 1: General form of a control volume of the triangulation $\mathcal{T}_h$ (left) and its boundary (right)

Introducing the cell average

$$\widetilde{\mathbf{u}}_i(t) = \frac{1}{|\sigma_i|} \int_{\sigma_i} \widetilde{\mathbf{u}}(\mathbf{x}, t)\, d\mathbf{x},$$

the integral form (4.3) with respect to an inner box σ_i can be written as

$$\frac{d}{dt}\widetilde{\mathbf{u}}_i(t) = -\frac{1}{|\sigma_i|} \sum_{j\in N(i)} \sum_{k=1}^{2} \int_{l_{ij}^k} \sum_{\ell=1}^{2} \widetilde{\mathbf{f}}_\ell(\widetilde{\mathbf{u}}(\mathbf{x}, t)) n_\ell \, ds, \tag{4.4}$$

where $N(i)$ denotes the index set of all neighbouring boxes of the control volume σ_i. Note that in the case of a boundary box σ_i, $i \in \mathcal{N}_{h,\partial\mathbf{G}}$, the boundary conditions have to be considered additionally. Concerning the initial conditions the freestream values $(\rho_\infty, v_{1,\infty}, v_{2,\infty}, \widetilde{p}_\infty)^T$ are used to define the constant initial distribution via $\widetilde{\mathbf{u}}_0(\mathbf{x}) = \left(\rho_\infty, \rho_\infty v_{1,\infty}, \rho_\infty v_{2,\infty}, \dfrac{\widetilde{p}_\infty}{\gamma - 1} + \dfrac{\rho_\infty |\mathbf{v}_\infty|^2}{2}\right)^T$.

Straightforward calculations prove the rotational invariance of the Euler equations such that (4.4) can be rewritten as

$$\frac{d}{dt}\widetilde{\mathbf{u}}_i(t) = -\frac{1}{|\sigma_i|} \sum_{j \in N(i)} \sum_{k=1}^{2} \int_{l_{ij}^k} \mathbf{T}^{-1}(\mathbf{n})\, \widetilde{\mathbf{f}}_1(\mathbf{T}(\mathbf{n})\, \widetilde{\mathbf{u}}(\mathbf{x},t))\, ds, \tag{4.5}$$

where the rotational matrix is given by

$$\mathbf{T}(\mathbf{n}) = \begin{pmatrix} 1 & 0 & 0 & 0 \\ 0 & n_1 & n_2 & 0 \\ 0 & -n_2 & n_1 & 0 \\ 0 & 0 & 0 & 1 \end{pmatrix}.$$

Note that in the case of a boundary box σ_i there exist two adjacent cells σ_j, $j \in \mathcal{N}_{h,\partial\mathbf{G}}$, such that $\partial\sigma_i \cap \partial\sigma_j$ consists of one line segment l_{ij}^k only. In order to achieve a unique representation we interpret the lacking line segment as having the length zero. Obviously, the evaluation of the line integrals leads into trouble when $\widetilde{\mathbf{u}}$ is discontinuous across $\partial\sigma_i$. For the solution of these Riemann problems we introduce the concept of a numerical flux function which is often called a Riemann solver. During the past more than forty years a huge variety of numerical flux functions has been developed showing different advantages as well as failings [13, 72, 79, 17, 16, 62, 58, 31, 60]. Such schemes can be found in various well-written text books [75, 39, 23, 24, 12, 42].
In 1991 Liou and Steffen [43] proposed a new flux splitting scheme called AUSM (Advection Upstream Splitting Method) which successfully combines the accuracy of the flux difference splitting schemes with the simplicity of the flux vector splitting methods. Thus, the method is able to capture a stationary contact discontinuity without numerical diffusion and avoids the carbuncle phenomenon. Unfortunately it suffers from some difficulties like oscillations in the pressure distribution behind a moving shock. Three years later Liou and Wada [81] presented an improved AUSM which they called AUSMDV. This method combines the so-called AUSMD, AUSMV and Hänel's scheme including an additional numerical dissipation to remove the glitches at the sonic point within rarefaction waves. "D" and "V" means that the corresponding scheme is flux difference or flux vector splitting based, respectively. The method has desirable properties like no numerical dissipation on stationary and moving contact discontinuities as well as preserving enthalpy in steady flows, high resolution for shock waves and the scheme avoids pressure oscillations observed in the AUSM scheme. Furthermore, the resulting numerical flux function is continuously differentiable and can be extended to simulate chemically reacting [81, 18] as well as turbulent flow fields [51, 52] and was modified for unsteady flow fields on moving grids [45]. With regard to these favourable properties we employ the AUSMDV scheme in the current numerical framework. Thus, we approximate the boundary integral from (4.5) by means of

$$\int_{l_{ij}^k} \mathbf{T}^{-1}(\mathbf{n})\, \widetilde{\mathbf{f}}_1(\mathbf{T}(\mathbf{n})\, \widetilde{\mathbf{u}}(\mathbf{x},t))\, ds = \left|l_{ij}^k\right| \mathbf{H}^{AUSMDV}\left(\widetilde{\mathbf{z}}_i, \widetilde{\mathbf{z}}_j; \mathbf{n}_{ij}^k\right). \tag{4.6}$$

Herein, $\widetilde{\mathbf{z}}_i$ and $\widetilde{\mathbf{z}}_j$ represent an approximation of the conserved variables at the left and right hand side of the midpoint $\mathbf{x}_{ij}^k$ corresponding to the line segment l_{ij}^k. Using the cell averages , i. e. $\widetilde{\mathbf{z}}_i = \widetilde{\mathbf{u}}_i$ and $\widetilde{\mathbf{z}}_j = \widetilde{\mathbf{u}}_j$, leads to a spatially first-order accurate scheme. The central approach for the construction of higher-order finite volume methods is based on the recovery of improved approximations $\widetilde{\mathbf{z}}_i$, $\widetilde{\mathbf{z}}_j$ from the given cell averages. A detailed introduction and mathematical analysis of different reconstruction technique is presented in [68]. Within this study we concentrate on the recovery based on linear polynomials. We employ two different approaches, namely a Total Variation Diminishing (TVD) like ansatz including the slope limiter of Barth and Jespersen [4] which is proposed in [47, 52] and a Weighted Essentially Non-Oscillatory (WENO) reconstruction technique following the work of Friedrich [9].
In the present study we distinguish three different types of boundary conditions: Fixed wall, inflow and outflow boundary. Therefore we subdivide the boundary of the triangulation into three parts $\partial\mathcal{T}_h = \partial\mathcal{T}_{h,w} \cup \partial\mathcal{T}_{h,in} \cup \partial\mathcal{T}_{h,out}$, where $\partial\mathcal{T}_{h,w}$, $\partial\mathcal{T}_{h,in}$, $\partial\mathcal{T}_{h,out}$ denote fixed wall, inflow and outflow parts, respectively. First, we require that no fluid particle can pass a solid wall. Thus we assume $v_{\mathbf{n}}(\mathbf{x},t) = \mathbf{v}(\mathbf{x},t) \cdot \mathbf{n}(\mathbf{x}) = 0$ for all $\mathbf{x} \in \partial\mathcal{T}_{h,w}$ and $t \in \mathbb{R}_0^+$. Consequently, the mass flux as well as the energy flux through this boundary vanish and we obtain

$$\int\limits_{\partial\sigma_i \cap \partial\mathcal{T}_{h,w}} \mathbf{T}^{-1}(\mathbf{n})\,\widetilde{\mathbf{f}}_1(\mathbf{T}(\mathbf{n})\,\widetilde{\mathbf{u}}(\mathbf{x},t))\,ds = \sum_{l_{\sigma_i} \subset \partial\mathcal{T}_{h,w}} |l_{\sigma_i}| \begin{pmatrix} 0 \\ \widetilde{p}(\mathbf{x}_i^m, t) \cdot \mathbf{n}_{\sigma_i} \\ 0 \end{pmatrix}, \tag{4.7}$$

where $\mathbf{x}_i^m$ represents the midpoint of the line segment l_{σ_i} (see Figure 2). Note that the pressure $\widetilde{p}$ is defined by means of the constant or linear distribution $\widetilde{\mathbf{z}}_i$ and no evaluation of a numerical flux function is necessary. Furthermore, the fluxes through the inflow and outflow parts are approximated by

$$\int\limits_{\partial\sigma_i \cap \partial\mathcal{T}_{h,in}} \mathbf{T}^{-1}(\mathbf{n})\,\widetilde{\mathbf{f}}_1(\mathbf{T}(\mathbf{n})\,\widetilde{\mathbf{u}}(\mathbf{x},t))\,ds = \sum_{l_{\sigma_i} \subset \partial\mathcal{T}_{h,in}} |l_{\sigma_i}|\,\mathbf{H}^{AUSMDV}(\widetilde{\mathbf{z}}_i, \widetilde{\mathbf{z}}_\infty; \mathbf{n}_{\sigma_i}) \tag{4.8}$$

and

$$\int\limits_{\partial\sigma_i \cap \partial\mathcal{T}_{h,out}} \mathbf{T}^{-1}(\mathbf{n})\,\widetilde{\mathbf{f}}_1(\mathbf{T}(\mathbf{n})\,\widetilde{\mathbf{u}}(\mathbf{x},t))\,ds = \sum_{l_{\sigma_i} \subset \partial\mathcal{T}_{h,out}} |l_{\sigma_i}|\,\mathbf{H}^{AUSMDV}(\widetilde{\mathbf{z}}_i, \widetilde{\mathbf{z}}_i; \mathbf{n}_{\sigma_i}), \tag{4.9}$$

respectively. It is mentionable that the consistency of the numerical flux function yields $\mathbf{H}^{AUSMDV}(\widetilde{\mathbf{z}}_i, \widetilde{\mathbf{z}}_i; \mathbf{n}_{\sigma_i}) = \mathbf{T}^{-1}(\mathbf{n}_{\sigma_i})\,\widetilde{\mathbf{f}}_1(\mathbf{T}(\mathbf{n}_{\sigma_i})\,\widetilde{\mathbf{z}}_i)$.
With respect to the asymptotic analysis of the numerical method it is necessary to explicitly point out the numerical flux function employed. First, we introduce the AUSMD-type scheme. Here the numerical flux is defined by

$$\mathbf{H}^{AUSMD}(\widetilde{\mathbf{z}}_L, \widetilde{\mathbf{z}}_R; \mathbf{n}) = \frac{1}{2}\left((\rho v_{\mathbf{n}})_{1/2}(\Phi_L + \Phi_R) + |(\rho v_{\mathbf{n}})_{1/2}|(\Phi_L - \Phi_R)\right) + \Psi_{1/2}, \tag{4.10}$$

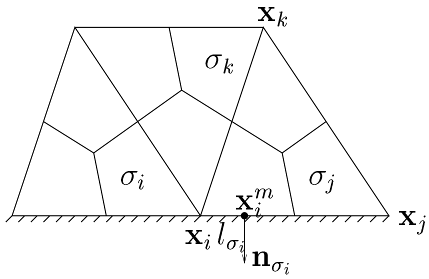

Figure 2: Boundary control volume

where $\Phi = \left(1, v_{\mathbf{n}}, v_{\mathbf{t}}, \widetilde{H}\right)^T$, $\Psi_{1/2} = \left(0, \widetilde{p}_{1/2}, 0, 0\right)^T$ and the indices $\mathbf{n}$ and $\mathbf{t}$ denote the velocity components perpendicular and parallel to the edge, respectively. In order to capture steady as well as moving contact discontinuities, we define the coefficients $\alpha_L = \frac{2(\widetilde{p}/\rho)_L}{(\widetilde{p}/\rho)_L+(\widetilde{p}/\rho)_R}$, $\alpha_R = \frac{2(\widetilde{p}/\rho)_R}{(\widetilde{p}/\rho)_L+(\widetilde{p}/\rho)_R}$ and $\widetilde{c}_m = \max\{\widetilde{c}_L, \widetilde{c}_R\}$. If $\widetilde{\mathrm{Ma}}_{\mathbf{n},L/R} := \frac{v_{\mathbf{n},L/R}}{\widetilde{c}_m}$, then the pressure flux is given by

$$\widetilde{p}_{1/2} = \widetilde{p}_L^+ + \widetilde{p}_R^- \tag{4.11}$$

where

$$\widetilde{p}_{L/R}^{\pm} = \begin{cases} \frac{1}{4}\,\widetilde{p}_{L/R}\,\left(\widetilde{\mathrm{Ma}}_{\mathbf{n},L/R} \pm 1\right)^2\left(2 \mp \widetilde{\mathrm{Ma}}_{\mathbf{n},L/R}\right), & \text{if } \left|\widetilde{\mathrm{Ma}}_{\mathbf{n},L/R}\right| \le 1 \\ \frac{1}{2}\,\widetilde{p}_{L/R}\,\frac{v_{\mathbf{n},L/R} \pm |v_{\mathbf{n},L/R}|}{v_{\mathbf{n},L/R}}, & \text{otherwise.} \end{cases} \tag{4.12}$$

The velocity splitting reads

$$v_{\mathbf{n},L/R}^{\pm} = \begin{cases} \alpha_{L/R}\left\{\pm\frac{\left(v_{\mathbf{n},L/R} \pm \widetilde{c}_m\right)^2}{4\,\widetilde{c}_m} - \frac{v_{\mathbf{n},L/R} \pm |v_{\mathbf{n},L/R}|}{2}\right\} + \frac{v_{\mathbf{n},L/R} \pm |v_{\mathbf{n},L/R}|}{2}, & \text{if } \left|\widetilde{\mathrm{Ma}}_{\mathbf{n},L/R}\right| \le 1 \\ \frac{v_{\mathbf{n},L/R} \pm |v_{\mathbf{n},L/R}|}{2}, & \text{otherwise.} \end{cases} \tag{4.13}$$

Thus, the mass flux splitting $(\rho v_{\mathbf{n}})_{1/2} = v_{\mathbf{n},L}^+\,\rho_L + v_{\mathbf{n},R}^-\,\rho_R$ is well-defined. Secondly, we consider the AUSMV-type scheme. This scheme differs from the AUSMD-type scheme only in the first momentum flux, which is given by

$$\mathbf{H}_{m_1}^{AUSMV}(\widetilde{\mathbf{z}}_L, \widetilde{\mathbf{z}}_R; \mathbf{n}) = v_{\mathbf{n},L}^+\,(\rho v_{\mathbf{n}})_L + v_{\mathbf{n},R}^-\,(\rho v_{\mathbf{n}})_R + \widetilde{p}_{1/2}.$$

Liou and Wada observed in numerical investigations, that the AUSMV has a higher shock capturing capability than the AUSMD but produces oscillations in the velocity field behind moving contact discontinuities [81]. According to these properties a mixed numerical flux in the form

$$\begin{aligned} &\mathbf{H}^{AUSMD+V}(\widetilde{\mathbf{z}}_L, \widetilde{\mathbf{z}}_R; \mathbf{n}) \\ &= \left(\frac{1}{2} + s\right)\mathbf{H}^{AUSMV}(\widetilde{\mathbf{z}}_L, \widetilde{\mathbf{z}}_R; \mathbf{n}) + \left(\frac{1}{2} - s\right)\mathbf{H}^{AUSMD}(\widetilde{\mathbf{z}}_L, \widetilde{\mathbf{z}}_R; \mathbf{n}) \end{aligned} \tag{4.14}$$

is used, where $s := \frac{1}{2}\min\left(1, K\frac{|\widetilde{p}_R-\widetilde{p}_L|}{\min\{\widetilde{p}_R,\widetilde{p}_L\}}\right)$. Analogously to [81] a parameter $K = 10$ is employed. Two problems of this scheme have to be overcome. First, there are glitches at an expansive sonic point. In this case an additional numerical dissipation is used. We detect the sonic point within a rarefaction wave with the help of $A := ((v_{\mathbf{n},L} - \widetilde{c}_L) < 0) \,\&\, ((v_{\mathbf{n},R} - \widetilde{c}_R) > 0)$ and $B := ((v_{\mathbf{n},L} + \widetilde{c}_L) < 0) \,\&\, ((v_{\mathbf{n},R} + \widetilde{c}_R) > 0)$ and we define the dissipation function in the form

$$\mathbf{H}^{DIFF}(\widetilde{\mathbf{z}}_L, \widetilde{\mathbf{z}}_R; \mathbf{n}) = \begin{cases} C\left[(v_{\mathbf{n},L} - \widetilde{c}_L) - (v_{\mathbf{n},R} - \widetilde{c}_R)\right]\left[(\rho\Phi)_L - (\rho\Phi)_R\right], & \text{if } A \,\&\, \neg B \\ C\left[(v_{\mathbf{n},L} + \widetilde{c}_L) - (v_{\mathbf{n},R} + \widetilde{c}_R)\right]\left[(\rho\Phi)_L - (\rho\Phi)_R\right], & \text{if } \neg A \,\&\, B \\ \mathbf{0}, & \text{otherwise} \end{cases} \tag{4.15}$$

with the constant $C = 0.125$. Second, we are faced with the so called carbuncle phenomenon. This phenomenon represents a numerical instability which probably comes from the interaction of unphysical values of the flow variables inside of discrete shock waves calculated by a one-dimensional scheme in a multi-dimensional flow. Analogously to the numerical flux function of Roe [62] and Osher [58], the scheme (4.14) described above suffers from this oscillation problem. Hence a more dissipative scheme is required in this case to stabilize the shock wave. Liou and Wada employed Hänel's scheme [16] where the numerical flux is given by

$$\mathbf{H}^{H\ddot{a}nel}(\widetilde{\mathbf{z}}_L, \widetilde{\mathbf{z}}_R; \mathbf{n}) := v^+_{\mathbf{n},L}\rho_L\Phi_L + v^-_{\mathbf{n},R}\rho_R\Phi_R + \Psi_{1/2}. \tag{4.16}$$

Here the velocity splitting and the interface pressure are defined by equation (4.13) and equations (4.11), (4.12) with the modification $\alpha_L = \alpha_R = 1$ and $\widetilde{c}_m = \widetilde{c}_L$ or $\widetilde{c}_R$, respectively. For the localization of the shock wave we use

$$S_i := \begin{cases} 1, & \text{if } \exists\, j \in N(i) \text{ with } (v_{\mathbf{n},i} - \widetilde{c}_i) > 0 \,\&\, (v_{\mathbf{n},j} - \widetilde{c}_j) < 0 \\ & \qquad\qquad\qquad \text{or } (v_{\mathbf{n},i} + \widetilde{c}_i) > 0 \,\&\, (v_{\mathbf{n},j} + \widetilde{c}_j) < 0 \\ 0, & \text{otherwise.} \end{cases} \tag{4.17}$$

With application of (4.14) we finally obtain our numerical flux function in the form

$$\begin{aligned} &\mathbf{H}^{AUSMDV}(\widetilde{\mathbf{z}}_L, \widetilde{\mathbf{z}}_R; \mathbf{n}) \\ &= \mathbf{T}^{-1}(\mathbf{n})\Bigg\{\delta_2^{(S_L+S_R)}\mathbf{H}^{H\ddot{a}nel}(\widetilde{\mathbf{z}}_L, \widetilde{\mathbf{z}}_R; \mathbf{n}) \\ &\quad + \left(1 - \delta_2^{(S_L+S_R)}\right)\left(\mathbf{H}^{AUSMD+V}(\widetilde{\mathbf{z}}_L, \widetilde{\mathbf{z}}_R; \mathbf{n}) + \mathbf{H}^{DIFF}(\widetilde{\mathbf{z}}_L, \widetilde{\mathbf{z}}_R; \mathbf{n})\right)\Bigg\}. \end{aligned} \tag{4.18}$$

The equation (4.5) in conjunction with (4.6) exhibits that now the conservation laws have been transformed into a system of ordinary differential equations. Concerning the time discretization we take advantage of the fact that we restrict ourself to the consideration of steady flow fields. Thus we utilize very simple first order time stepping techniques, namely the so called forward and backward Euler differences. Hence the complete numerical method reads as

$$\mathbf{u}_i^{n+1} = \mathbf{u}_i^n - \frac{\Delta t}{|\sigma_i|} \sum_{j \in N(i)} \sum_{k=1}^{2} \left| l_{ij}^k \right| \mathbf{H}^{AUSMDV} \left(\widetilde{\mathbf{z}}_i^m, \widetilde{\mathbf{z}}_j^m; \mathbf{n}_{ij}^k \right), \tag{4.19}$$

where $m \in \{n, n+1\}$, $\mathbf{u}_i^n = \mathbf{u}_i(t^n)$, and $t^{n+1} = t^n + \Delta t$. In the case of an implicit approach, i.e. $m = n+1$, a linearization of the numerical flux function is performed which leads to a linear system of equations including a large, sparse and usually unsymmetric matrix. The performance of an implicit method decisively depends on the properties of the incorporated solver for the linear system of equations. Based on a systematic investigation and comparison of Krylov subspace methods [47] we decided to apply the BiCGSTAB algorithm developed by van der Vorst [78] but in a preconditioned formulation, see [55]. For a comprehensive derivation and analysis of different Krylov subspace methods we refer to [3, 63, 15, 49] and the literature therein.
In advance to the investigation of the numerical method with respect to low Mach number fluid flow we have to ensure the validity of the described scheme in the trans-, super- and hypersonic regime. Therefore we have chosen several well-known test cases from computational fluid dynamics which are consolidated in Table 1.

Configuration	$\widetilde{\mathrm{Ma}}_\infty = \frac{\lvert\mathbf{v}_\infty\rvert}{\widetilde{c}_\infty}$	Angle of attack	Recovery technique	References
SKF 1.1 airfoil	0.65	3°	WENO	[71]
RAE2822 airfoil	0.75	3°	WENO	[61]
NACA0012 airfoil	0.8	1.25°	WENO	[38]
Combustion chamber	2.0	0°	TVD	[82]
Cylinder	10.0	0°	WENO	

Table 1: Trans-, super-, and hypersonic inviscid test cases

The first test case shows the transsonic flow about the SKF 1.1 two element airfoil [71] at $\widetilde{\mathrm{Ma}}_\infty = 0.65$ and an angle of attack $\alpha = 3°$ (see Figure 3). In order to validate our numerical method by the experimental data, it must be corrected for wall interferences [70]. To overcome the high value of the lift coefficient, we use $\alpha = -0.25°$ for our scheme. From the comparison (Figure 4) between the computed and the experimental C_p-values, it is obvious that our numerical data gives a good approximation of the real physical phenomenon.

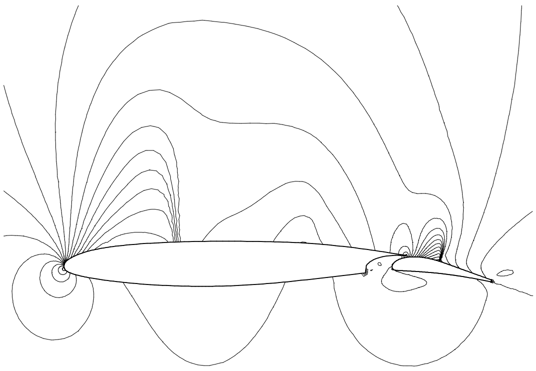

Figure 3: Isolines of the density distribution in the vicinity of the airfoil

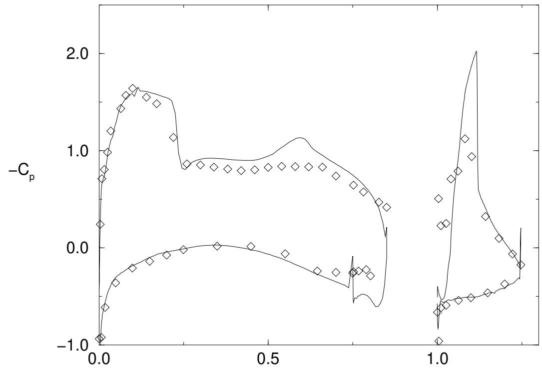

Figure 4: Comparison of the C_p-distribution, – Finite-volume scheme, ⋄ Reference data [71]

The second transsonic test case represents a steady state flow past the RAE2822 airfoil at a freestream Mach number $\widetilde{\mathrm{Ma}}_\infty = 0.75$ and $\alpha = 3°$. The density distribution obtained is shown in Figure 5. From Figure 6 we can learn about the good correspondence between the computed C_p-distribution and the results presented during a GAMM workshop [61].

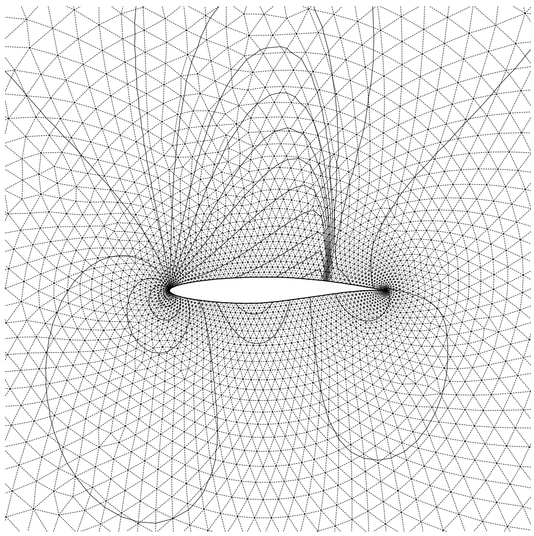

Figure 5: Isolines of the density distribution in the vicinity of the airfoil

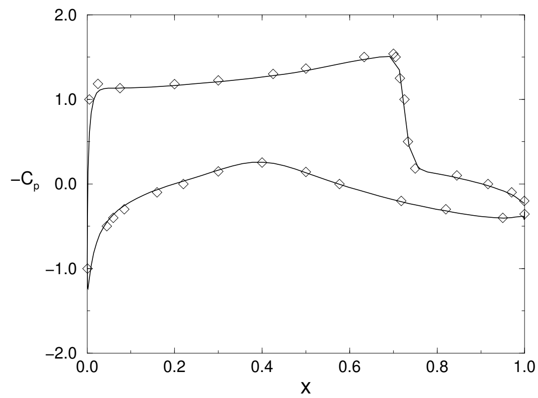

Figure 6: Comparison of the C_p-distribution, – Finite volume scheme, ⋄ Reference data [61]

Concerning the transsonic regime we finally regard the flow about the NACA0012 airfoil at $\widetilde{\mathrm{Ma}}_\infty = 0.8$ and $\alpha = 1.25°$. The isolines of the density distributions are depicted in Figure 7 and Figure 8 shows a comparison of our computed C_p-distribution with the results obtained by Thomas [74] on a structured grid with a dicretization method similar to Jameson's [31].

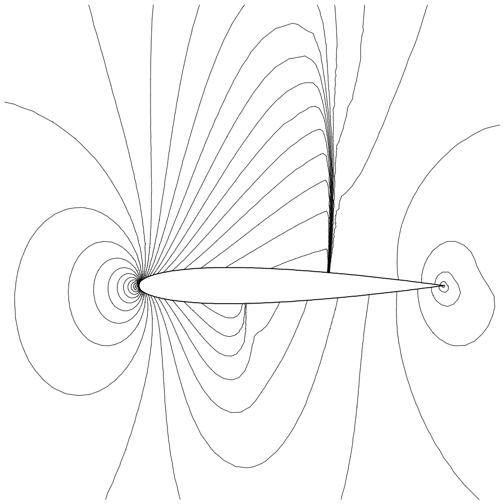

Figure 7: Isolines of the density distribution in the vicinity of the airfoil

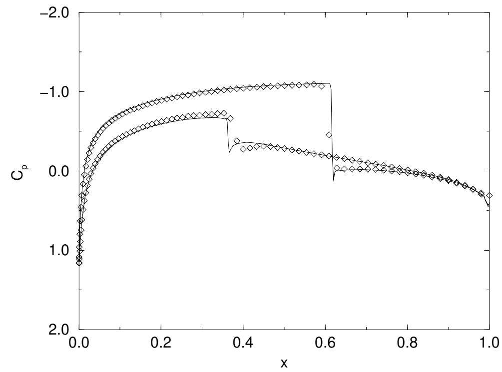

Figure 8: C_p distribution, – Finite volume scheme, $\diamond$ Reference data [74]

In order to indicate the accuracy and performance of the presented finite volume scheme in the context of supersonic flow fields we consider the remaining two test cases. The first test case is concerned with the simulation of a supersonic steady state flow through a combustion chamber. The flow field features a complicated pattern of shock and rarefaction waves as well as contact discontinuities. As one can see from Figures 9 - 12 all these features mentioned are resolved sharply by means of an adapted triangulation.

We finish the evaluation of the described numerical scheme by means of a hypersonic

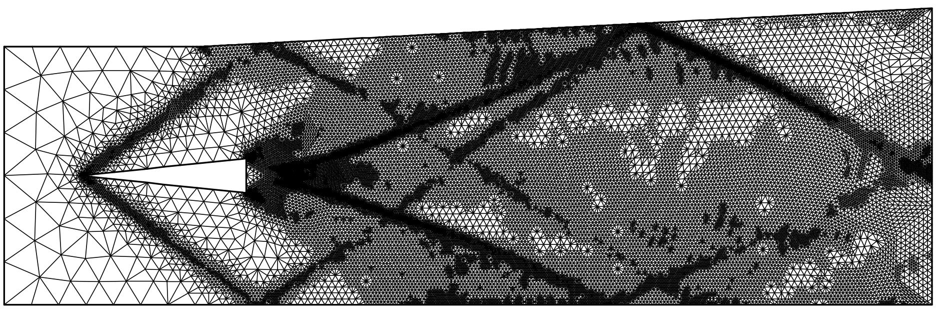

Figure 9: Triangulation of the combustion chamber

flow past a cylinder at $\widetilde{\mathrm{Ma}}_\infty = 10.0$. In Figure 13 we present the computed pressure and

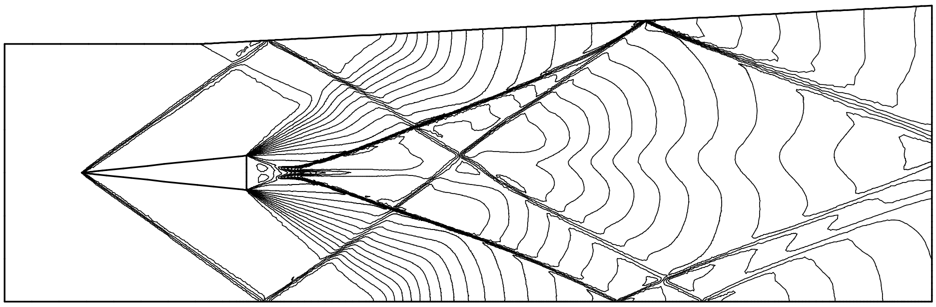

Figure 10: Isolines of the density

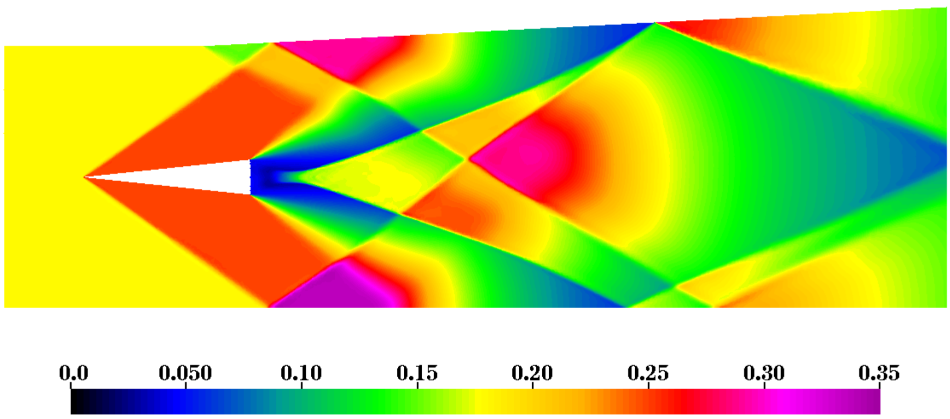

Figure 11: Pressure distribution

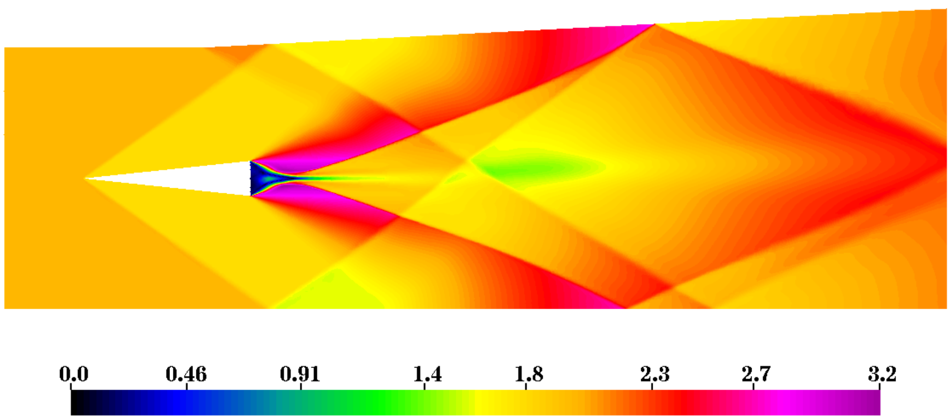

Figure 12: Local Mach number distribution $\widetilde{\mathrm{Ma}} = |\mathbf{v}|/\widetilde{c}$

density distribution. For the validation of our results, we also show the Mach number distribution along the stagnation point line, see Figure 14. The shock location is in excellent accordance with the analytic value (represented as the dashed line in Figure 14) obtained from [1].

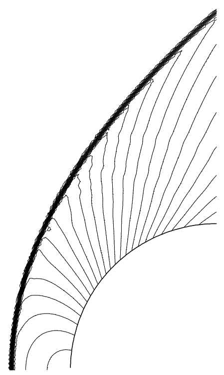

Figure 13: Isolines of pressure

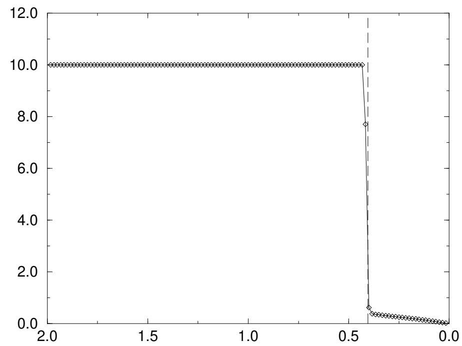

Figure 14: Mach number distribution along the stagnation point line

The union of all these test cases emphasize the validity, stability and high resolution properties of the finite volume approximation in the field of trans-, super-, and hypersonic inviscid fluid flow.

4.1 Asymptotic Analysis of the Finite Volume Scheme

The objective of this section is the theoretical investigation of the finite volume scheme in the low Mach number limit. For the sake of simplicity we consider the first order accurate approximation, i.e. $\widetilde{\mathbf{z}}_i = \widetilde{\mathbf{u}}_i$, $\widetilde{\mathbf{z}}_j = \widetilde{\mathbf{u}}_j$, in an explicit formulation.
The transition between subsonic and supersonic parts of the flow field represents a feature of transsonic fluid flow and does not occur in the low Mach number regime. As a consequence we obtain from (4.17) the statement $S_i = 0$ for all $i \in \mathcal{N}_h$, and thus the influence of the dissipative numerical flux function $\mathbf{H}^{H\ddot{a}nel}$ vanishes within the AUSMDV scheme, see equation (4.18). Furthermore, the Boolean numbers A, B used for the definition of $\mathbf{H}^{DIFF}$ are always zero, so that we can disregard the impact of this function in the low Mach number regime and the AUSMDV scheme (4.18) finally takes the form

$$\mathbf{H}^{AUSMDV}(\widetilde{\mathbf{z}}_L, \widetilde{\mathbf{z}}_R; \mathbf{n}) = \mathbf{T}^{-1}(\mathbf{n})\mathbf{H}^{AUSMD+V}(\widetilde{\mathbf{z}}_L, \widetilde{\mathbf{z}}_R; \mathbf{n}). \tag{4.20}$$

Although the numerical flux function is significantly easier to investigate in the absence of sonic points, several quiet different ingredients still remain within the AUSMDV scheme. Due to that fact we proceed as follows: First we introduce the abbreviation

$$\Delta_{ij}\varphi = \varphi_i - \varphi_j,$$

second we successively analyze some important parts of the flux function to achieve statements concerning their proportion and third we merge these facts and prove statements concerning the behaviour of the whole finite volume method in the low Mach number limit.

Using a simple retransformation of the auxiliary variables defined by (4.1) into the corresponding physical quantities yields the following order relation for $\widetilde{\mathrm{Ma}}_{\mathbf{n},i/j}$ in the form

$$\widetilde{\mathrm{Ma}}_{\mathbf{n},i/j} = \frac{|v_{\mathbf{n},i/j}|}{\widetilde{c}_m} = \mathbf{M} \underbrace{\frac{|v_{\mathbf{n},i/j}|}{c_m}}_{=\mathrm{Ma}_{\mathbf{n},i/j}=O(1)} = O(\mathbf{M}), \quad \mathbf{M} \to 0. \tag{4.21}$$

Furthermore the auxiliary pressure variable $\widetilde{p}^{\pm}_{i/j}$ (see (4.12)) satisfies

$$\widetilde{p}^{\pm}_{i/j} = \frac{1}{4} p_{i/j} \left(\frac{2}{\mathbf{M}^2} \pm \frac{3\mathrm{Ma}_{\mathbf{n},i/j}}{\mathbf{M}} \mp \mathbf{M}\mathrm{Ma}^3_{\mathbf{n},i/j} \right) \tag{4.22}$$

and the velocity component in normal direction (4.13) can be written as

$$v^{\pm}_{\mathbf{n},i/j} = \pm \frac{1}{\mathbf{M}} \frac{\alpha_{i/j} c_m}{4} + \left(1 - \alpha_{i/j}\right) \frac{v_{\mathbf{n},i/j} \pm \left|v_{\mathbf{n},i/j}\right|}{2} + \frac{\alpha_{i/j} v_{\mathbf{n},i/j}}{2} \pm \mathbf{M} \frac{\alpha_{i/j} v_{\mathbf{n},i/j}}{c_m} \tag{4.23}$$

by means of the coefficients $\alpha_{i/j} = \frac{2(p/\rho)_{i/j}}{(p/\rho)_i + (p/\rho)_j}$. The equation (4.23) yields a first hint concerning a potential failure of the scheme in the low Mach number regime since it is currently obvious that the numerical velocity component in normal direction and its physical counterpart are of different orders with respect to a vanishing Mach number. Composing the statements outlined above, the mass flux provided by the AUSMDV scheme takes the form

$$\begin{aligned} &\mathbf{H}^{AUSMDV}_{\rho}(\widetilde{\mathbf{u}}_i, \widetilde{\mathbf{u}}_j; \mathbf{n}) \\ &= \frac{1}{2\mathbf{M}} \frac{c_m}{(p/\rho)_i + (p/\rho)_j} \Delta_{ij} p + (1 - \alpha_i) \rho_i \frac{v_{\mathbf{n},i} + |v_{\mathbf{n},i}|}{2} \\ &\quad + (1 - \alpha_j) \rho_j \frac{v_{\mathbf{n},j} - |v_{\mathbf{n},j}|}{2} + \frac{\Delta_{ij}(p v_{\mathbf{n}})}{(p/\rho)_i + (p/\rho)_j} + O(\mathbf{M}), \quad \mathbf{M} \to 0. \end{aligned} \tag{4.24}$$

In contrast to the continuity equation the momentum fluxes of the AUSMD and AUSMV method are different and have to be considered separately. In the case of the AUSMD scheme we state

$$\begin{aligned} &\frac{1}{2} \left\{ (\rho v_{\mathbf{n}})_{1/2} (v_{\mathbf{n},i} + v_{\mathbf{n},j}) + |\, (\rho v_{\mathbf{n}})_{1/2} \,| \, (v_{\mathbf{n},i} - v_{\mathbf{n},j}) \right\} \\ &= \frac{1}{4\mathbf{M}} \frac{c_m}{(p/\rho)_i + (p/\rho)_j} \Big((v_{\mathbf{n},i} + v_{\mathbf{n},j}) \Delta_{ij} p + \Delta_{ij} v_{\mathbf{n}} |\Delta_{ij} p| \Big) + O(1), \quad \mathbf{M} \to 0 \end{aligned} \tag{4.25}$$

whereas the AUSMV method includes the term

$$v^{+}_{\mathbf{n},i} (\rho v_{\mathbf{n}})_i + v^{-}_{\mathbf{n},j} (\rho v_{\mathbf{n}})_j = \frac{1}{2\mathbf{M}} \frac{c_m}{(p/\rho)_i + (p/\rho)_j} \Delta_{ij} (p v_{\mathbf{n}}) + O(1), \quad \mathbf{M} \to 0. \tag{4.26}$$

It is easily seen that the weight factor s fulfills $s = O(1)$, $\mathbf{M} \to 0$, so that (4.25) and (4.26) lead to the expression for the components of the numerical momentum flux in x_1-direction in the form

$$
\begin{aligned}
&\mathbf{H}_{m_1}^{AUSMDV}(\widetilde{\mathbf{u}}_i, \widetilde{\mathbf{u}}_j; \mathbf{n}) \\
&= \frac{1}{\mathbf{M}^2}\frac{p_i + p_j}{2} n_1 + \frac{1}{\mathbf{M}}\frac{3}{4c_m}\Delta_{ij}\left(p v_{\mathbf{n}}\right) n_1 \\
&\quad + \frac{1}{4\mathbf{M}}\frac{c_m}{(p/\rho)_i + (p/\rho)_j}\left(\frac{\Delta_{ij}p}{2}(v_{\mathbf{n},i} + v_{\mathbf{n},j}) n_1 + \frac{|\Delta_{ij}p|}{2}(v_{\mathbf{n},i} - v_{\mathbf{n},j}) n_1 + \Delta_{ij}\left(p v_{\mathbf{n}}\right) n_1\right. \\
&\qquad\qquad \left. - \frac{\Delta_{ij}p}{2}(v_{\mathbf{t},i} + v_{\mathbf{t},j}) n_2 - \frac{|\Delta_{ij}p|}{2}(v_{\mathbf{t},i} - v_{\mathbf{t},j}) n_2\right) \\
&\quad + \frac{s}{4\mathbf{M}}\frac{c_m}{(p/\rho)_i + (p/\rho)_j}\left(\Delta_{ij}p(v_{\mathbf{n},i} + v_{\mathbf{n},j}) n_2 + |\Delta_{ij}p|(v_{\mathbf{n},i} - v_{\mathbf{n},j}) n_2 + 2\Delta_{ij}\left(p v_{\mathbf{n}}\right) n_2\right) \\
&\quad + O(1), \quad \mathbf{M} \to 0.
\end{aligned} \tag{4.27}
$$

Analogously, we can rewrite the numerical energy flux of the finite volume approximation as

$$
\begin{aligned}
\mathbf{H}_{(\rho\widetilde{E})}^{AUSMDV}(\widetilde{\mathbf{u}}_i, \widetilde{\mathbf{u}}_j; \mathbf{n}) &= \frac{1}{4\mathbf{M}^3}\frac{c_m}{(p/\rho)_i + (p/\rho)_j}\Big(\Delta_{ij}p(H_i + H_j) + |\Delta_{ij}p|(H_i - H_j)\Big) \\
&\quad + O\left(\frac{1}{\mathbf{M}^2}\right), \quad \mathbf{M} \to 0.
\end{aligned} \tag{4.28}
$$

In accordance to the continuous asymptotic analysis we introduce a discrete asymptotic expansion originally proposed by Viozat and Guillard [14]. Similar to (3.1) we assume that each physical cell average $\varphi_i \in \{\rho_i, v_{1,i}, v_{2,i}, p_i, E_i\}$ with respect to the box σ_i, $i \in \mathcal{N}_h$, can be expressed in the form of an asymptotic single scale expansion

$$
\varphi_i(t; \mathbf{M}) = \sum_{m=0}^{j} \mathbf{M}^m \varphi_i^{(m)}(t) + o\left(\mathbf{M}^j\right), \quad \mathbf{M} \to 0, \quad j = 0, 1, 2. \tag{4.29}
$$

Introducing the expansion (4.29) into the finite volume method leads to the following version of the semidiscrete mass and energy equations with respect to an inner control volume σ_i, $i \in \mathcal{N}_{h,G}$:

$$
\begin{aligned}
\frac{d}{dt}\rho_i &= -\frac{1}{\mathbf{M}}\frac{1}{|\sigma_i|}\sum_{j \in N(i)}\sum_{k=1}^{2}\frac{\eta_{ij}}{2}\Delta_{ij}p\left|l_{ij}^k\right| + O(1), \quad \mathbf{M} \to 0, &(4.30)\\
\frac{d}{dt}(\rho E)_i &= -\frac{1}{\mathbf{M}}\frac{1}{|\sigma_i|}\sum_{j \in N(i)}\sum_{k=1}^{2}\frac{\eta_{ij}}{4}\Big(\Delta_{ij}p(H_i + H_j) + |\Delta_{ij}p|\left(H_i - H_j\right)\Big)\left|l_{ij}^k\right| \\
&\quad + O(1), \quad \mathbf{M} \to 0, &(4.31)
\end{aligned}
$$

whereby $\eta_{ij} = \frac{c_m}{(p/\rho)_i + (p/\rho)_j}$.

Theorem 4.1 *The discrete leading order pressure field satisfies*

$$p_i^{(0)} = p_j^{(0)}$$

for all $i, j \in \mathcal{N}_h$.

Proof:
Identifying terms multiplied by the same power of $\mathbf{M}$ enables the exploration of the discrete asymptotic leading as well as of the first order pressure term in the low Mach number regime. First we obtain from (4.30) and (4.31) the so called perturbation equations

$$0 = \sum_{j \in N(i)} \sum_{k=1}^{2} \frac{\eta_{ij}^{(0)}}{2} \Delta_{ij} p^{(0)} \left| l_{ij}^k \right| \tag{4.32}$$

and

$$0 = \sum_{j \in N(i)} \sum_{k=1}^{2} \frac{\eta_{ij}^{(0)}}{4} \left(\Delta_{ij} p^{(0)} (H_i^{(0)} + H_j^{(0)}) + \left| \Delta_{ij} p^{(0)} \right| (H_i^{(0)} - H_j^{(0)}) \right) \left| l_{ij}^k \right|, \tag{4.33}$$

respectively. Taking into account $\eta_{ij}^{(0)} = \frac{c_m^{(0)}}{(p^{(0)}/\rho^{(0)})_i + (p^{(0)}/\rho^{(0)})_j} > 0$, we can directly conclude from (4.32) that the minimum as well as the maximum leading order pressure value has to be located within a boundary control volume σ_k, $k \in \mathcal{N}_{h,\partial G}$. In order to obtain also statements with respect to the pressure cell average p_i within boundary control volumes, we have to explore the numerical boundary fluxes (4.7), (4.8) and (4.9) additionally. The boundary condition for an impermeable wall prohibits mass flux and energy flux through such boundary parts. Consequently, both equations (4.32) and (4.33) are unaffected by the flux through line segments $l_{\sigma_i} \subset \partial\mathcal{T}_{h,w}$. Let us now focus our attention to the inflow boundaries. Utilizing $\widetilde{\mathbf{z}}_j = \widetilde{\mathbf{z}}_i$ we obtain $\Delta_{ij} p^{(0)} = \Delta_{ii} p^{(0)} = 0$, and as a consequence

$$\mathbf{H}_\rho(\widetilde{\mathbf{z}}_i, \widetilde{\mathbf{z}}_j, \mathbf{n}) = O(1), \quad \mathbf{M} \to 0,$$

holds which implies that there will not appear an additional term within equation (4.32) with respect to the approximation of inflow parts. Exclusively, the outflow boundary affects the perturbation equation (4.32). Thus we can extend the validity of equation (4.32) from $i \in \mathcal{N}_{h,G}$ to $i \in \mathcal{N}_h$ by writing

$$0 = \vartheta_i \frac{\eta_{i\infty}^{(0)}}{2} \Delta_{i\infty} p^{(0)} \left| l_{\sigma_i} \right| + \sum_{j \in N(i)} \sum_{k=1}^{2} \frac{\eta_{ij}^{(0)}}{2} \Delta_{ij} p^{(0)} \left| l_{ij}^k \right|, \tag{4.34}$$

where ϑ_i represents the number of line segments $l_{\sigma_i} \subset \partial\sigma_i$ satisfying $l_{\sigma_i} \subset \partial\mathcal{T}_{h,out}$. As mentioned above there always exists an index $i \in \mathcal{N}_{h,\partial G}$ such that $p_i^{(0)} = \max_{k\in\mathcal{N}_h} p_k^{(0)}$. Introducing this property into (4.34) yields

$$\underbrace{\vartheta_i \frac{\eta_{i\infty}^{(0)}}{2}}_{>0} \Delta_{i\infty}p^{(0)} \underbrace{|l_{\sigma_i}|}_{>0} = -\sum_{j\in N(i)} \sum_{k=1}^{2} \underbrace{\frac{\eta_{ij}^{(0)}}{2}}_{>0} \underbrace{\Delta_{ij}p^{(0)}}_{\geq 0} \underbrace{|l_{ij}^k|}_{>0} \leq 0. \tag{4.35}$$

Obviously, we directly obtain $p_i^{(0)} = p_j^{(0)}$ for all $j \in N(i)$ if $\vartheta_i = 0$. On the other hand, we can conclude $p_i^{(0)} - p_\infty^{(0)} \leq 0$ if $\vartheta_i > 0$ which immediately proves the statement

$$p_\infty^{(0)} = \max_{k\in\mathcal{N}_h} p_k^{(0)}$$

with regard to the initial conditions. Similarly, we obtain $p_\infty^{(0)} = \min_{k\in\mathcal{N}_h} p_k^{(0)}$. Assembling both results shows that the discrete leading order pressure term is spatially constant in accordance to the behaviour in the continuous case. □

Note that we can likewise prove the same property by means of the energy equation instead of the mass conservation law.

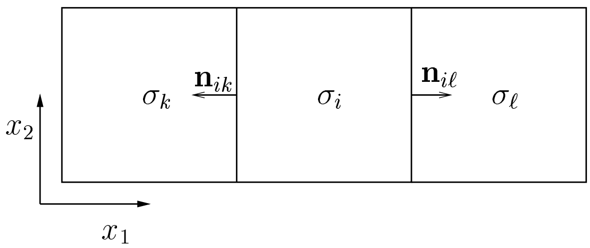

Figure 15: Notation used in the structured mesh

To derive statements concerning the discrete first order pressure distribution $p_i^{(1)}$, $i \in \mathcal{N}_h$, we consider a structured mesh depicted in Figure 15. We will now present an evidence of variations within the first order pressure field which are in contradiction to the results of the continuous asymptotic analysis.

Theorem 4.2 *Let*

$$i \in \mathcal{N}_{h,G} \tag{4.36}$$

and

$$\rho_i^{(0)} = \rho_j^{(0)} \ \text{ for all } \ j \in N(i). \tag{4.37}$$

Furthermore, we assume

$$v_{k,1}^{(0)} - v_{i,1}^{(0)} = v_{i,1}^{(0)} - v_{\ell,1}^{(0)} \neq 0, \tag{4.38}$$

where the indices are taken in conjunction with Figure 15. Then there holds

$$p_k^{(1)} \neq p_\ell^{(1)}.$$

Proof:
Due to the fact that the leading order pressure term is spatially constant we obtain from the assumption (4.37) the expression

$$c_m^{(0)} = \max\{c_i^{(0)}, c_j^{(0)}\} = c_i^{(0)} =: c^{(0)}$$

for all $j \in N(i)$. Furthermore, the order relation with respect to the weight factor s can be aggravated to

$$s = \frac{1}{2}\min\left(1, K\frac{|p_j - p_i|}{\min\{p_j, p_i\}}\right) = \frac{1}{2}\min\left(1, \mathbf{M}K\frac{\left|p_j^{(1)} - p_i^{(1)}\right|}{\min\{p_j, p_i\}}\right) = O(\mathbf{M}), \quad \mathbf{M} \to 0.$$

Thus introducing the asymptotic expansion into the numerical momentum flux (4.27) and taking account of $\Delta_{ij} p^{(0)} = 0$ yields

$$\begin{aligned}
&\mathbf{H}_{m_1}^{AUSMDV}(\widetilde{\mathbf{z}}_i, \widetilde{\mathbf{z}}_j, \mathbf{n}) \\
&\quad = \frac{1}{\mathbf{M}^2} p^{(0)} n_1 + \frac{1}{\mathbf{M}}\left(\frac{p_i^{(1)} + p_j^{(1)}}{2} + \left(\frac{3p^{(0)}}{4c^{(0)}} + \eta_{ij}^{(0)} p^{(0)}\right)\Delta_{ij} v_{\mathbf{n}}^{(0)}\right) n_1 + O(1), \quad \mathbf{M} \to 0,
\end{aligned}$$

where $p^{(0)} = p_i^{(0)} = p_j^{(0)}$. We are now able to write the semidiscrete formulation of the momentum equation with respect to the x_1-direction as

$$\begin{aligned}
\frac{d}{dt}(\rho v_1)_i &= -\frac{1}{\mathbf{M}^2} p^{(0)} \underbrace{\sum_{j\in N(i)} \sum_{k=1}^{2} n_{ij,1}^k \left|l_{ij}^k\right|}_{=0} \\
&\quad -\frac{1}{\mathbf{M}} \sum_{j\in N(i)} \sum_{k=1}^{2} \left(\frac{p_i^{(1)} + p_j^{(1)}}{2} + \left(\frac{3p^{(0)}}{4c^{(0)}} + \eta_{ij}^{(0)} p^{(0)}\right)\Delta_{ij} v_{\mathbf{n}_{ij}^k}^{(0)}\right) n_{ij,1}^k \left|l_{ij}^k\right| \\
&\quad + O(1), \quad \mathbf{M} \to 0.
\end{aligned}$$

Now we are able to explore the first order pressure distribution by means of the perturbation equation of order $O\left(\mathbf{M}^{-1}\right)$, $\mathbf{M} \to 0$. With respect to the underlying discretization (see Figure 15) we get

$$p_k^{(1)} - p_\ell^{(1)} = \left(\frac{3p^{(0)}}{2c^{(0)}} + 2\eta_{i\ell}^{(0)} p^{(0)}\right)\Delta_{i\ell} v_1^{(0)} + \left(\frac{3p^{(0)}}{2c^{(0)}} + 2\eta_{ik}^{(0)} p^{(0)}\right)\Delta_{ik} v_1^{(0)}.$$

Due to the assumption (4.37) we obtain $0 < \eta_{i\ell}^{(0)} = \eta_{ik}^{(0)} =: \eta^{(0)}$ and consequently (4.38) yields

$$p_k^{(1)} - p_\ell^{(1)} = \underbrace{\left(\frac{3p^{(0)}}{2c^{(0)}} + 2\eta^{(0)}p^{(0)}\right)}_{>0} \underbrace{\left(v_{i,1}^{(0)} - v_{\ell,1}^{(0)} - v_{i,1}^{(0)} + v_{k,1}^{(0)}\right)}_{\neq 0} \neq 0. \tag{4.39}$$

□

This Theorem emphasizes that variations within the leading order velocity field can cause variations within the first order pressure distribution. These fluctuations are associated with the mesh size instead of the Mach number and thus we can state that this property contradicts the results of the continuous single as well as multiple length scale asymptotic analysis.
Note that the failure of the scheme due to variations within the first order pressure field can not be detected by such a kind of an asymptotic analysis which is based on the asymptotic sequence $\phi_n(\mathbf{M}) = \mathbf{M}^{2n}$.
It is remarkable that we didn't require any assumptions concerning the leading order velocity component $v_2^{(0)}$. Thus one can easily define a velocity distribution $\mathbf{v}$ such that the velocity field is divergence free in a discrete manner and satisfies the equation (4.38).
The statement concerning the spatial variations of the first order pressure distribution is based on a structured mesh and some quite theoretical assumptions (4.36), (4.37) and (4.38). Nevertheless, the results encourage the investigation of realistic flow fields to recognize these or somewhat related properties also within numerical simulations. Therefore, we consider the inviscid flow past the RAE2822 airfoil at varying freestream Mach numbers Ma_∞ between 10^{-6} and 0.1. From the isolines of the pressure distribution depicted in Figure 16 we suppose the unreliable and unphysical behaviour of the numerical method in the low Mach number regime. However, we have to point out the existence of the mentioned pressure fluctuations analytically. We close this gap by means of the indicator $\mathrm{Ind}(p)$ defined by equation (3.54). Thereby, the pressure p_i is considered to be located at the barycentre of the associated control volume σ_i and the indicator is evaluated in the obvious corresponding discrete manner.
The solid line within diagram 17 represents $\mathrm{Ind}(p) = \mathbf{M}$. A comparison of the solid line with the results of the implicit as well as explicit finite volume scheme shows the unphysical behaviour

$$\mathrm{Ind}(p) = O(\mathbf{M}), \quad \mathbf{M} \to 0.$$

4.2 Preconditioning for two-dimensional flow

Preconditioning the governing equations was originally proposed by Chorin [7] and afterwards extended and systematically investigated by Turkel [76]. Chorin derived the preconditioned incompressible Navier-Stokes equations by adding a time-derivative of

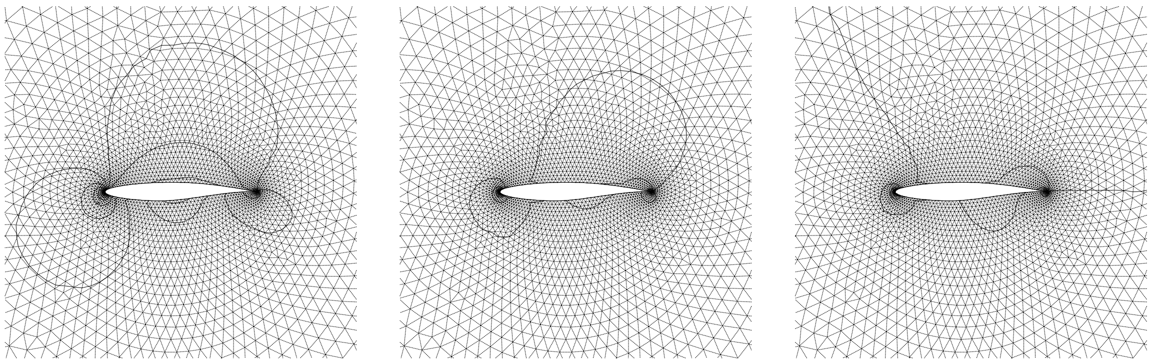

Figure 16: Isolines of the pressure distribution for varying freestream Mach numbers (10^{-1} (left), 10^{-2} (middle), 10^{-5} (right)) for the AUSMDV method

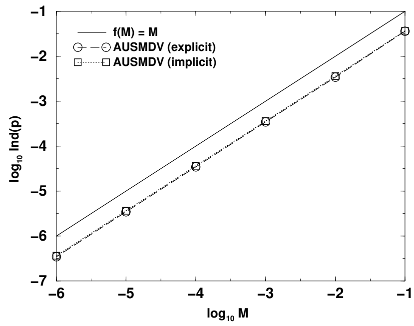

Figure 17: Pressure fluctuation $\mathrm{Ind}(p) = \dfrac{p_{\max} - p_{\min}}{p_{\max}\, \Delta \mathbf{x}_p}$ versus the Mach number for the AUSMDV scheme

an arbitrary density function ρ to the divergence constraint and by simultaneously replacing the pressure inside the momentum equation by a likewise arbitrary equation of state $p = \rho/\delta$ with $\delta > 0$. Chorin mainly considered numerical aspects of the preconditioning technique by means of a finite difference method while Turkel described the influence of different preconditioners with respect to the characteristic propagation speeds of the system. Turkel suggested a quite simple preconditioner in the context of the compressible Euler equations formulated in terms of the entropy variables $\widetilde{\mathbf{w}} = (\widetilde{p}, v_1, v_2, \widetilde{s})^T$, whereby $\widetilde{s}$ denotes the entropy determined as $\widetilde{s} = \ln \frac{\widetilde{p}}{\rho^\gamma}$.
Our purpose is now to carry over the preconditioning strategy into the current numerical framework. Therefore, we recast the governing equations (4.2) in their quasilinear form

$$\partial_t \widetilde{\mathbf{u}} + \sum_{\ell=1}^{2} \widetilde{\mathbf{F}}_\ell\left(\widetilde{\mathbf{u}}\right) \partial_{x_\ell} \widetilde{\mathbf{u}} = \mathbf{0}, \tag{4.40}$$

where $\widetilde{\mathbf{F}}_\ell\left(\widetilde{\mathbf{u}}\right)$, $\ell = 1, 2$, denote the Jacobian matrices of $\widetilde{\mathbf{f}}_\ell\left(\widetilde{\mathbf{u}}\right)$, $\ell = 1, 2$, with respect to the conserved variables, i. e. $\widetilde{\mathbf{F}}_\ell\left(\widetilde{\mathbf{u}}\right) = \frac{\partial \widetilde{\mathbf{f}}_\ell}{\partial \widetilde{\mathbf{u}}}\left(\widetilde{\mathbf{u}}\right)$.

Concerning the transformation of the governing equations we consider the matrices

$$\widetilde{\mathbf{W}}\left(\widetilde{\mathbf{u}}\right) = \frac{\partial \widetilde{\mathbf{w}}}{\partial \widetilde{\mathbf{u}}} \quad \text{and} \quad \widetilde{\mathbf{U}}\left(\widetilde{\mathbf{w}}\right) = \frac{\partial \widetilde{\mathbf{u}}}{\partial \widetilde{\mathbf{w}}}$$

which satisfy $\widetilde{\mathbf{U}}\left(\widetilde{\mathbf{w}}\right)\widetilde{\mathbf{W}}\left(\widetilde{\mathbf{u}}\right) = \mathbf{I}$. Multiplying (4.40) with $\widetilde{\mathbf{W}}\left(\widetilde{\mathbf{u}}\right)$ yields

$$\mathbf{0} = \partial_t \widetilde{\mathbf{w}} + \sum_{\ell=1}^{2} \widetilde{\mathbf{G}}_\ell\left(\widetilde{\mathbf{w}}\right) \partial_{x_\ell} \widetilde{\mathbf{w}}, \tag{4.41}$$

where

$$\widetilde{\mathbf{G}}_1\left(\widetilde{\mathbf{w}}\right) = \widetilde{\mathbf{W}}\left(\widetilde{\mathbf{u}}\right)\widetilde{\mathbf{F}}_1\left(\widetilde{\mathbf{u}}\right)\widetilde{\mathbf{U}}\left(\widetilde{\mathbf{w}}\right) = \begin{pmatrix} v_1 & \rho\widetilde{c}^2 & 0 & 0 \\ \frac{1}{\rho} & v_1 & 0 & 0 \\ 0 & 0 & v_1 & 0 \\ 0 & 0 & 0 & v_1 \end{pmatrix} \tag{4.42}$$

and

$$\widetilde{\mathbf{G}}_2\left(\widetilde{\mathbf{w}}\right) = \widetilde{\mathbf{W}}\left(\widetilde{\mathbf{u}}\right)\widetilde{\mathbf{F}}_2\left(\widetilde{\mathbf{u}}\right)\widetilde{\mathbf{U}}\left(\widetilde{\mathbf{w}}\right) = \begin{pmatrix} v_2 & 0 & \rho\widetilde{c}^2 & 0 \\ 0 & v_2 & 0 & 0 \\ \frac{1}{\rho} & 0 & v_2 & 0 \\ 0 & 0 & 0 & v_2 \end{pmatrix} \tag{4.43}$$

hold. The matrices $\widetilde{\mathbf{G}}_\ell$, $\ell = 1, 2$, reveal the weak coupling of the entropy equation with the velocity equations and the pressure equation. Due to that fact Turkel suggested to modify the velocity equations and the pressure equation whereas the entropy equation still remains unchanged. In a general formulation, the preconditioning can be written as

$$\mathbf{P}^{-1}\left(\widetilde{\mathbf{w}}\right) \partial_t \widetilde{\mathbf{w}} + \sum_{\ell=1}^{2} \widetilde{\mathbf{G}}_\ell\left(\widetilde{\mathbf{w}}\right) \partial_{x_\ell} \widetilde{\mathbf{w}} = \mathbf{0}, \tag{4.44}$$

where

$$\mathbf{P}^{-1}\left(\widetilde{\mathbf{w}}\right) = \begin{pmatrix} \frac{\widetilde{c}^2}{\zeta \mathbf{M}_\epsilon^2} & 0 & 0 & \delta \\ \frac{\alpha v_1}{\rho \zeta \mathbf{M}_\epsilon^2} & 1 & 0 & \delta \\ \frac{\alpha v_2}{\rho \zeta \mathbf{M}_\epsilon^2} & 0 & 1 & \delta \\ 0 & 0 & 0 & 1 \end{pmatrix}$$

with $\mathbf{M}_\epsilon^2$ chosen to be

$$\mathbf{M}_\epsilon^2 = \begin{cases} \epsilon^2 & , \quad \mathbf{M} < \epsilon \\ \mathbf{M}^2 & , \quad \epsilon \le \mathbf{M} < 1 \\ 1 & , \quad \mathbf{M} \ge 1 \end{cases}$$

to ensure that the preconditioning matrix is always nonsingular. In this context the choice $\delta = 0$ leads to a class of preconditioners introduced by Turkel [76], whereas $\delta = 1$, $\alpha = 0$, and $\zeta = \widetilde{c}^2$ yields a method published by Choi and Merkle [6]. Although the matrix $\mathbf{P}^{-1}(\widetilde{\mathbf{w}})$ is assumed to be nonsingular, it is obvious that a straightforward discretization of the governing equations (4.44) can be employed at most for the simulation of steady state phenomena. To overcome this fundamental restriction we follow Guillard and Viozat [14] and introduce a complete preconditioning of the governing equations in entropy form by

$$\mathbf{P}^{-1}(\widetilde{\mathbf{w}}) = \begin{pmatrix} \widetilde{\beta}^2 & 0 & 0 & 0 \\ 0 & 1 & 0 & 0 \\ 0 & 0 & 1 & 0 \\ 0 & 0 & 0 & 1 \end{pmatrix} \quad \text{with } \widetilde{\beta} = O_S(\mathbf{M}), \quad \mathbf{M} \to 0.$$

As a result we obtain

$$\mathbf{0} = \mathbf{P}(\widetilde{\mathbf{w}})\,\partial_t \widetilde{\mathbf{w}} + \sum_{\ell=1}^{2} \mathbf{P}(\widetilde{\mathbf{w}})\,\widetilde{\mathbf{G}}_\ell(\widetilde{\mathbf{w}})\,\partial_{x_\ell}\widetilde{\mathbf{w}} = \mathbf{P}(\widetilde{\mathbf{u}})\,\partial_t \widetilde{\mathbf{u}} + \sum_{\ell=1}^{2} \widetilde{\mathbf{F}}_\ell^P(\widetilde{\mathbf{u}})\,\partial_{x_\ell}\widetilde{\mathbf{u}}, \qquad (4.45)$$

where

$$\mathbf{P}(\widetilde{\mathbf{u}}) = \widetilde{\mathbf{U}}(\widetilde{\mathbf{w}})\,\mathbf{P}(\widetilde{\mathbf{w}})\,\widetilde{\mathbf{W}}(\widetilde{\mathbf{u}}) = \mathbf{I} + (\widetilde{\beta}^2 - 1)\frac{\gamma - 1}{\widetilde{c}^2} \begin{pmatrix} \frac{|\mathbf{v}|^2}{2} & -v_1 & -v_2 & 1 \\ \frac{|\mathbf{v}|v_1}{2} & -v_1^2 & -v_1 v_2 & v_1 \\ \frac{|\mathbf{v}|v_2}{2} & -v_1 v_2 & -v_2^2 & v_2 \\ \frac{|\mathbf{v}|\widetilde{H}}{2} & -\widetilde{H} v_1 & -\widetilde{H} v_2 & \widetilde{H} \end{pmatrix}$$

and $\widetilde{\mathbf{F}}_\ell^P(\widetilde{\mathbf{u}}) = \mathbf{P}(\widetilde{\mathbf{u}})\,\widetilde{\mathbf{F}}_\ell(\widetilde{\mathbf{u}})$, $\ell = 1, 2$. Note that system (4.45) is equivalent to (4.40) and (4.39) for all $\mathbf{M} > 0$.

In order to enable a flawless computation of flow fields at arbitrary speeds we combine the AUSMDV method with a preconditioned formulation of the Lax-Friedrichs scheme such that the advantageous properties of the AUSMDV flux function for transsonic, supersonic, and hypersonic fluid flow will be tied together with the asymptotic validity of the preconditioned Lax-Friedrichs method in the low Mach number regime.

Numerical flux functions of Lax-Friedrichs type usually differ from the dissipation term $\widetilde{\mathbf{D}}(\widetilde{\mathbf{z}}_R - \widetilde{\mathbf{z}}_L)$. With respect to the governing equations (4.2) Hu and Shu [30] defined

$\widetilde{\mathbf{D}} \in \mathbb{R}$ to be the largest absolute eigenvalue of the corresponding Jacobian matrix $\widetilde{\mathbf{F}}(\widetilde{\mathbf{z}};\mathbf{n})$. Similar to the formulation of Shu and Osher [67] we prefer a matrix-valued term $\widetilde{\mathbf{D}}$ which was recently proposed by Friedrich [10].
Using the abbreviations

$$\xi_1 = \lambda_3^P - \lambda_1^P \widetilde{\beta}^2, \quad \xi_2 = \lambda_4^P - \lambda_1^P \widetilde{\beta}^2, \quad \text{and} \quad \xi_3 = \frac{\lambda_4^P - \lambda_3^P}{2} \tag{4.46}$$

the matrix of the right eigenvectors of $\widetilde{\mathbf{F}}^P(\widetilde{\mathbf{u}};\mathbf{n})$ reads

$$\widetilde{\mathbf{R}}^P(\widetilde{\mathbf{u}};\mathbf{n}) = \begin{pmatrix} \frac{(\gamma-1)|\mathbf{v}|^2}{2\widetilde{p}} - \frac{\gamma}{\rho} & -\frac{(\gamma-1)v_1}{\widetilde{p}} & -\frac{(\gamma-1)v_2}{\widetilde{p}} & \frac{\gamma-1}{\widetilde{p}} \\ -\frac{v_\mathbf{t}}{\rho} & -\frac{n_2}{\rho} & -\frac{n_1}{\rho} & 0 \\ \frac{(\gamma-1)\xi_2|\mathbf{v}|^2+2\widetilde{\beta}^2\widetilde{c}^2 v_\mathbf{n}}{4\xi_3} & -\frac{(\gamma-1)\xi_2 v_1+\widetilde{\beta}^2\widetilde{c}^2 n_1}{2\xi_3} & -\frac{(\gamma-1)\xi_2 v_2+\widetilde{\beta}^2\widetilde{c}^2 n_2}{2\xi_3} & \frac{(\gamma-1)\xi_2}{2\xi_3} \\ -\frac{(\gamma-1)\xi_1|\mathbf{v}|^2+2\widetilde{\beta}^2\widetilde{c}^2 v_\mathbf{n}}{4\xi_3} & \frac{(\gamma-1)\xi_1 v_1+\widetilde{\beta}^2\widetilde{c}^2 n_1}{2\xi_3} & \frac{(\gamma-1)\xi_1 v_2+\widetilde{\beta}^2\widetilde{c}^2 n_2}{2\xi_3} & -\frac{(\gamma-1)\xi_1}{2\xi_3} \end{pmatrix}.$$

Hence the Jacobian matrix can be expressed as

$$\widetilde{\mathbf{F}}^P(\widetilde{\mathbf{u}};\mathbf{n}) = \widetilde{\mathbf{R}}^P(\widetilde{\mathbf{u}};\mathbf{n})\,\widetilde{\Lambda}^P(\widetilde{\mathbf{u}};\mathbf{n})\left(\widetilde{\mathbf{R}}^P\right)^{-1}(\widetilde{\mathbf{u}};\mathbf{n}),$$

where $\widetilde{\Lambda}^P(\widetilde{\mathbf{u}};\mathbf{n}) = \operatorname{diag}\left\{\lambda_1^P(\widetilde{\mathbf{u}};\mathbf{n}),\ldots,\lambda_4^P(\widetilde{\mathbf{u}};\mathbf{n})\right\} \in \mathbb{R}^{4\times 4}$ consists of the eigenvalues

$$\lambda_{1/2}^P(\widetilde{\mathbf{u}};\mathbf{n}) = v_\mathbf{n} \quad \text{and} \quad \lambda_{3/4}^P(\widetilde{\mathbf{u}};\mathbf{n}) = \frac{1}{2}\left(\left(1+\widetilde{\beta}^2\right)v_\mathbf{n} \pm \sqrt{((1-\widetilde{\beta}^2)v_\mathbf{n})^2 + 4\widetilde{\beta}^2\widetilde{c}^2}\right).$$

Following the proceeding of Friedrich [10] we obtain the preconditioned Lax-Friedrichs scheme in the form

$$\mathbf{H}^{LF(P)}(\widetilde{\mathbf{z}}_L,\widetilde{\mathbf{z}}_R;\mathbf{n}) = \frac{1}{2}\left(\mathbf{T}^{-1}(\mathbf{n})\left\{\widetilde{\mathbf{f}}_1(\mathbf{T}(\mathbf{n})\widetilde{\mathbf{z}}_L) + \widetilde{\mathbf{f}}_1(\mathbf{T}(\mathbf{n})\widetilde{\mathbf{z}}_R)\right\} - \widetilde{\mathbf{D}}^P(\widetilde{\mathbf{z}}_L,\widetilde{\mathbf{z}}_R;\mathbf{n})(\widetilde{\mathbf{z}}_R - \widetilde{\mathbf{z}}_L)\right), \tag{4.47}$$

where the dissipation matrix is defined to be

$$\widetilde{\mathbf{D}}^P(\widetilde{\mathbf{z}}_L,\widetilde{\mathbf{z}}_R;\mathbf{n}) = \mathbf{P}^{-1}\left(\frac{\widetilde{\mathbf{z}}_L+\widetilde{\mathbf{z}}_R}{2}\right)\widetilde{\mathbf{R}}^P\left(\frac{\widetilde{\mathbf{z}}_L+\widetilde{\mathbf{z}}_R}{2};\mathbf{n}\right)\left|\widetilde{\Lambda}^P\right|(\widetilde{\mathbf{z}}_L,\widetilde{\mathbf{z}}_R;\mathbf{n})\left(\widetilde{\mathbf{R}}^P\right)^{-1}\left(\frac{\widetilde{\mathbf{z}}_L+\widetilde{\mathbf{z}}_R}{2};\mathbf{n}\right)$$

with

$$\left|\widetilde{\Lambda}^P\right|(\widetilde{\mathbf{z}}_L,\widetilde{\mathbf{z}}_R;\mathbf{n}) = \operatorname{diag}\left\{\max_{\mathbf{z}\in\left\{\widetilde{\mathbf{z}}_L,\widetilde{\mathbf{z}}_R,\frac{\widetilde{\mathbf{z}}_L+\widetilde{\mathbf{z}}_R}{2}\right\}}\left|\lambda_1^P(\mathbf{z};\mathbf{n})\right|,\ldots,\max_{\mathbf{z}\in\left\{\widetilde{\mathbf{z}}_L,\widetilde{\mathbf{z}}_R,\frac{\widetilde{\mathbf{z}}_L+\widetilde{\mathbf{z}}_R}{2}\right\}}\left|\lambda_4^P(\mathbf{z};\mathbf{n})\right|\right\}.$$

Note that the preconditioned Lax-Friedrichs scheme represents a consistent numerical flux function with respect to the Euler equations and the difference between the

standard method and the preconditioned algorithm is exclusively contained in the dissipation term. Hence, the preconditioned method is suitable for the simulation of steady as well as unsteady flow fields.
Since the principle procedure of a discrete asymptotic analysis was extensively explained in Section 3.2, it is possible to derive the important results concerning the preconditioned numerical method in a brief manner.
In order to obtain a compact formulation of the dissipation term we introduce the following auxiliary values

$$\begin{aligned}\eta_1 =& \left(1-\mathbf{M}^2\frac{(\gamma-1)|\mathbf{v}|^2}{c^2}\right)\Delta_{ji}\rho+\mathbf{M}^2\frac{(\gamma-1)v_1}{c^2}\Delta_{ji}m_1+\mathbf{M}^2\frac{(\gamma-1)v_2}{c^2}\Delta_{ji}m_2\\ &-\frac{\gamma-1}{c^2}\Delta_{ji}(\rho E),\end{aligned} \tag{4.48}$$

$$\begin{aligned}\eta_2 =& \left(\xi_2\frac{(\gamma-1)|\mathbf{v}|^2}{2}+\mathbf{M}^2\beta^2c^2v_{\mathbf{n}}\right)\Delta_{ji}\rho-\left(\xi_2(\gamma-1)v_1+\mathbf{M}^2\beta^2c^2n_1\right)\Delta_{ji}m_1\\ &-\left(\xi_2(\gamma-1)v_2+\mathbf{M}^2\beta^2c^2n_2\right)\Delta_{ji}m_2,\end{aligned} \tag{4.49}$$

$$\begin{aligned}\eta_3 =& -\left(\xi_1\frac{(\gamma-1)|\mathbf{v}|^2}{2}+\mathbf{M}^2\beta^2c^2v_{\mathbf{n}}\right)\Delta_{ji}\rho+\left(\xi_1(\gamma-1)v_1+\mathbf{M}^2\beta^2c^2n_1\right)\Delta_{ji}m_1\\ &+\left(\xi_1(\gamma-1)v_2+\mathbf{M}^2\beta^2c^2n_2\right)\Delta_{ji}m_2,\end{aligned} \tag{4.50}$$

and

$$\eta_4 =\frac{1}{2\beta^2c^2\xi_3}, \tag{4.51}$$

where $\beta=\frac{|\widetilde{\beta}|}{\mathbf{M}}=O_S(1)$, $\mathbf{M}\to 0$, and the physical quantities φ which are occurring without an index i or j (φ_i or $\Delta_{ji}\varphi$) are defined to be the average of φ_i and φ_j, i. e. $\varphi=\frac{\varphi_i+\varphi_j}{2}$.
By means of the above mentioned values the dissipation term of the numerical mass flux reads

$$\begin{aligned}&\widetilde{\mathbf{D}}_\rho\left(\widetilde{\mathbf{u}}_i,\widetilde{\mathbf{u}}_j;\mathbf{n}\right)\Delta_{ji}\widetilde{\mathbf{u}}\\ &= \left|\lambda_1^P\right|\eta_1+\eta_4\left\{\left|\lambda_3^P\right|\eta_2+\left|\lambda_4^P\right|\eta_3+\frac{\gamma-1}{\mathbf{M}^2}\Big(\left|\lambda_3^P\right|\xi_2-\left|\lambda_4^P\right|\xi_1\Big)\Delta_{ji}(\rho E)\right\},\end{aligned} \tag{4.52}$$

where $\left|\lambda_k^P\right|$ represents the k-th diagonal term of the matrix $\left|\widetilde{\Lambda}^P\right|$ [50].

Theorem 4.3 *The discrete leading and first order pressure field satisfy*

$$p_i^{(0)}=p_j^{(0)} \;\; \textit{and} \;\; p_i^{(1)}=p_j^{(1)}$$

for all $i,j\in\mathcal{N}_h$, respectively.

Proof:
To assess the influence of the Mach number we separately explore the terms inside the numerical dissipation (4.52). It is obvious from the consideration of the eigenvalue $\lambda_1^P = v_{\mathbf{n}}$ and the equation (4.48) that $\left|\lambda_1^P\right| \eta_1 = O(1)$, $\mathbf{M} \to 0$. Furthermore, the variable ξ_3 satisfies

$$\xi_3 = -\frac{1}{2}\sqrt{\left(1 - \mathbf{M}^2\beta^2\right)^2 v_{\mathbf{n}}^2 + 4\beta^2 c^2} = \underbrace{-\frac{1}{2}\sqrt{v_{\mathbf{n}}^2 + 4\beta^2 c^2}}_{= d_{ij} < 0} + O\left(\mathbf{M}^2\right), \quad \mathbf{M} \to 0. \tag{4.53}$$

As a straightforward consequence we obtain

$$\eta_4 = \underbrace{\frac{1}{2\beta^2 c^2 d_{ij}}}_{= a_{ij} < 0} + O\left(\mathbf{M}^2\right), \quad \mathbf{M} \to 0. \tag{4.54}$$

In the case that the Mach number $\mathbf{M}$ is sufficiently small one gets $c^2 > \mathbf{M}^2 v_{\mathbf{n}}^2$ by which it follows that

$$\left(1 - \mathbf{M}^2\beta^2\right)^2 v_{\mathbf{n}}^2 + 4\beta^2 c^2 > \left(1 + \mathbf{M}^2\beta^2\right)^2 v_{\mathbf{n}}^2.$$

This equation yields $\lambda_3^P > 0$, $\lambda_4^P < 0$ and consequently

$$\left|\lambda_3^P\right| \xi_2 - \left|\lambda_4^P\right| \xi_1 = \left|\lambda_3^P\right| \lambda_4^P - \left|\lambda_4^P\right| \lambda_3^P + O\left(\mathbf{M}^2\right) = \underbrace{b_{ij}}_{< 0} + O\left(\mathbf{M}^2\right), \quad \mathbf{M} \to 0. \tag{4.55}$$

Taking account $\left|\lambda_3^P\right| \eta_2 - \left|\lambda_4^P\right| \eta_3 = O(1)$, $\mathbf{M} \to 0$, as well as $(\rho_i \mathbf{v}_i + \rho_j \mathbf{v}_j)\mathbf{n} = O(1)$, $\mathbf{M} \to 0$, in combination with (4.54), (4.55) and $\rho E = \frac{p}{\gamma - 1} + O\left(\mathbf{M}^2\right)$, $\mathbf{M} \to 0$, results in

$$\mathbf{H}_\rho^{LF(P)}\left(\widetilde{\mathbf{u}}_i, \widetilde{\mathbf{u}}_j; \mathbf{n}\right) = \frac{1}{\mathbf{M}^2} a_{ij} b_{ij} \frac{\Delta_{ji} p}{2} + O(1), \quad \mathbf{M} \to 0.$$

Introducing the asymptotic expansion (4.29) and identifying terms multiplied by the same power of the Mach number yields the perturbation equations

$$0 = \sum_{j \in N(i)} \sum_{k=1}^{2} \left(a_{ij} b_{ij}\right)^{(0)} \frac{\Delta_{ji} p^{(0)}}{2} \left|l_{ij}^k\right| + \vartheta_i \left(a_{i\infty} b_{i\infty}\right)^{(0)} \frac{\Delta_{\infty i} p^{(0)}}{2} \left|l_{\sigma_i}\right| \tag{4.56}$$

and

$$\begin{aligned} 0 = &\sum_{j \in N(i)} \sum_{k=1}^{2} \left(\left(a_{ij} b_{ij}\right)^{(0)} \frac{\Delta_{ji} p^{(1)}}{2} + \left(a_{ij} b_{ij}\right)^{(1)} \frac{\Delta_{ji} p^{(0)}}{2} \right) \left|l_{ij}^k\right| \\ &+ \vartheta_i \left(\left(a_{i\infty} b_{i\infty}\right)^{(0)} \frac{\Delta_{\infty i} p^{(1)}}{2} + \left(a_{i\infty} b_{i\infty}\right)^{(1)} \frac{\Delta_{\infty i} p^{(0)}}{2} \right) \left|l_{\sigma_i}\right|, \end{aligned} \tag{4.57}$$

where

$$(a_{ij}b_{ij})^{(0)} = \lim_{\mathbf{M}\to 0} (a_{ij}b_{ij}) > 0. \tag{4.58}$$

Corresponding to the argumentation employed in Section 3.2 (see equations (4.34) and (4.35)) the statements (4.56) and (4.58) prove that variations within the discrete pressure field are at most of order $\mathbf{M}$, i. e. the numerical method always computes a spatially homogeneous leading order pressure distribution. Thus, equation (4.57) degenerates to

$$0 = \sum_{j\in N(i)} \sum_{k=1}^{2} (a_{ij}b_{ij})^{(0)} \frac{\Delta_{ji}p^{(1)}}{2} \left|l_{ij}^{k}\right| + \vartheta_i \left(a_{i\infty}b_{i\infty}\right)^{(0)} \frac{\Delta_{\infty i}p^{(1)}}{2} \left|l_{\sigma_i}\right|. \tag{4.59}$$

Comparing (4.59) with (4.56) obviously establishes that the first order pressure field $p^{(1)}$ is likewise spatially constant in agreement with the continuous single length scale asymptotic analysis. □

As mentioned above, the final version of the numerical flux function is obtained by means of a combination of $\mathbf{H}^{AUSMDV}$ and $\mathbf{H}^{LF(P)}$. Thus, we determine

$$\mathbf{H}\left(\widetilde{\mathbf{z}}_L, \widetilde{\mathbf{z}}_R; \mathbf{n}\right) = \delta \mathbf{H}^{AUSMDV}\left(\widetilde{\mathbf{z}}_L, \widetilde{\mathbf{z}}_R; \mathbf{n}\right) + (1-\delta)\mathbf{H}^{LF(P)}\left(\widetilde{\mathbf{z}}_L, \widetilde{\mathbf{z}}_R; \mathbf{n}\right), \tag{4.60}$$

where

$$\delta = \begin{cases} 1 & , \text{ if } \widetilde{\mathrm{Ma}}_\infty > 0.1 \text{ or } \widetilde{\mathrm{Ma}}_{LR} = \frac{|\mathbf{v}_L+\mathbf{v}_R|}{\tilde{c}_L+\tilde{c}_R} > 0.1 \\ 0 & , \text{ otherwise.} \end{cases}$$

Using the function $g(\mathbf{M}) = \sum_{k=0}^{3} a_k \mathbf{M}^k$ with $a_0 = 4.997$, $a_1 = -239.86$, $a_2 = 3598.1$ and $a_3 = -15992$ the parameter $\widetilde{\beta}^2$ is defined to be

$$\widetilde{\beta}^2 = \begin{cases} 0.1\epsilon^2 & , \text{ if } \widetilde{\mathrm{Ma}}_{LR} < \epsilon, \\ 0.1\widetilde{\mathrm{Ma}}_{LR}^2 & , \text{ if } \epsilon \le \widetilde{\mathrm{Ma}}_{LR} < 0.05, \\ g\left(\widetilde{\mathrm{Ma}}_{LR}\right) & , \text{ if } 0.05 \le \widetilde{\mathrm{Ma}}_{LR} < 0.1, \\ 1 & , \text{ if } \widetilde{\mathrm{Ma}}_{LR} \ge 0.1. \end{cases}$$

Note that the threshold value $\epsilon > 0$ depends on the arithmetic accuracy of the computer and should be chosen as small as possible.

Since the validity and reliability of this method in the context of transsonic, supersonic and hypersonic flow fields was proven above we can currently focus our attention to low Mach number fluid flow. Thus, we consider exactly the same test case as used in the context of the standard finite volume scheme.

The isolines of the pressure distribution depicted in Figure 18 indicate that the derive finite volume method is convenient also for the simulation of low speed flow. Nevertheless, an evidence concerning the asymptotic correctness of the computed pressure field is demonstrably given by Figure 19. The results confirm $\mathrm{Ind}(p) = O\left(\mathbf{M}^2\right)$, $\mathbf{M} \to 0$, which coincides with the continuous as well as with the discrete asymptotic analysis.

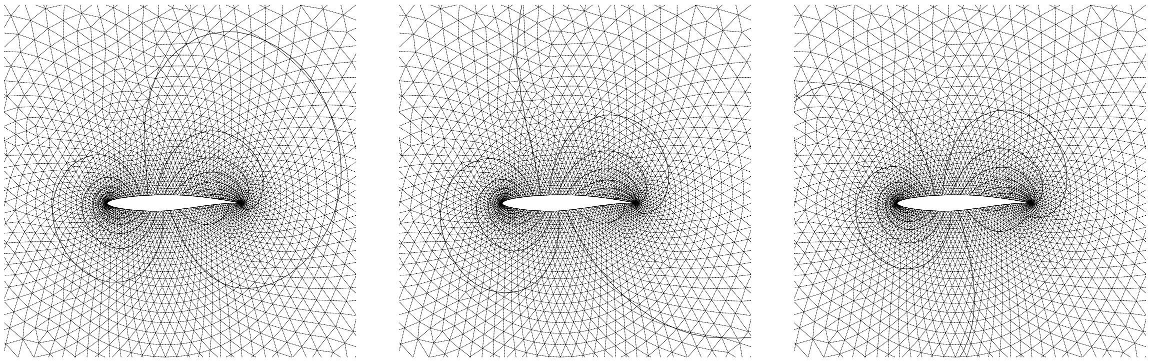

Figure 18: Isolines of the pressure distribution for varying Mach numbers (10^{-2} (left), 10^{-4} (middle), 10^{-5} (right)) for the preconditioned method (4.60)

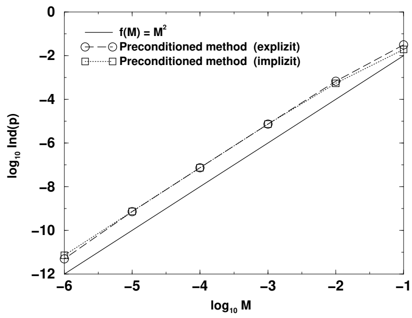

Figure 19: Pressure fluctuation $\mathrm{Ind}(p) = \dfrac{p_{\max} - p_{\min}}{p_{\max}\, \Delta \mathbf{x}_p}$ versus the Mach number for the preconditioned method (4.60)

4.3 Flux Correction Approach for one-dimensional flow

In contrast to the preconditioning technique, the flux correction approach directly includes some important simplified equations derived within the multiple scale analysis in order to achieve an accurate and stable numerical scheme in the low Mach number regime which passes over to the underlying compressible method if the reference parameter $\mathbf{M}$ is greater or equal to one. The decomposition of the pressure distribution into a high frequency and a long wave part represents a basic step inside this scheme. An adapted version of a discrete evolution algorithm [40] is used to decompose the pressure and to gain an approximation of the reference parameter based on the length scale information. This curve evolution algorithm posses several advantages compared to the classical Fourier and conjunction approaches. In order to ensure high resolution of the changing flow phenomena a time-dependent adaptation of the reference parameter $\mathbf{M}$ is employed to compute unsteady flow fields. For a detailed description of related methods we refer to [25, 50].

We consider one-dimensional fluid flow and thus, the Euler equations (3.5) writes

$$\partial_t \underbrace{\begin{pmatrix} \rho \\ m \\ \rho E \end{pmatrix}}_{\mathbf{u}=} + \partial_x \underbrace{\begin{pmatrix} m \\ mv + \frac{1}{\mathbf{M}^2} p \\ Hm \end{pmatrix}}_{\mathbf{f}(\mathbf{u})=} = \mathbf{0}. \tag{4.61}$$

With respect to the formulation we follow [27, 26, 28]. Hence, the procedure reads:

- Decompose the flux function in the form

$$\mathbf{f}(\mathbf{u}) = \mathbf{h}(\mathbf{u}) + \mathbf{a}(\mathbf{u}). \tag{4.62}$$

- Employ a modified Riemann solver to approximate the fluxes of the system

$$\partial_t \mathbf{u} + \partial_x \mathbf{h}(\mathbf{u}) = \mathbf{0}. \tag{4.63}$$

- Correct the obtained fluxes $\mathbf{a}(\mathbf{u})$ by means of the results of the asymptotic analysis in order to get an accurate approximate solution of system (4.61) independent of the Mach number.

First of all, we have to define a suitable decomposition of the flux function with respect to equation (4.62). Due to the use of a standard Riemann solver for the numerical solution of system (4.63) we require the following properties:

- System (4.63) has to be hyperbolic. The eigenvalues of the Jacobian of the flux function $\mathbf{h}$ are set to v and $v \pm c^*$ with $c^* = O(1)$, if $\mathbf{M} \to 0$.

- The flux function $\mathbf{h}$ has to reproduce $\mathbf{f}$ in the case that $\mathbf{M}$ tends to one, i. e.

$$\lim_{\mathbf{M} \to 1} \mathbf{a}(\mathbf{u}) = \mathbf{0}. \tag{4.64}$$

Due to the facts that in the limit of a vanishing Mach number the momentum equation obtains the singularity $1/\mathbf{M}^2$ as a multiplier in front of the pressure gradient and the energy fluxes have to implicitly satisfy the divergence constraint of the velocity field we expect the reasons for the singular behavior of the acoustic speeds within these two equations.

Now we present a proper choice concerning the flux function $\mathbf{h}$ and subsequently explore the validity of the above required properties.

We define a non local pressure term p_{NL} to be

$$p_{\mathrm{NL}} = \left(1 - \mathbf{M}^2\right) \frac{1}{|G|} \int_G p(x,0)\,dx. \tag{4.65}$$

Furthermore, we establish

$$H^* = \frac{\rho E + p_{\text{NL}} + \mathbf{M}^2 p}{\rho}$$

and hence, we can define the flux function $\mathbf{h}$ in the form

$$\mathbf{h}(\mathbf{u}) = (m,\ mv + p,\ H^* m)^T . \tag{4.66}$$

Straightforward calculations prove that the eigenvalues of the Jacobian of the flux function $\mathbf{h}$ are v and $v \pm c^*$, with

$$c^* = \sqrt{\frac{p + (\gamma - 1)(p_{\text{NL}} + \mathbf{M}^2 p)}{\rho}}.$$

Thus, system (4.63) is hyperbolic with signal speeds $v, v \pm c^* = O(1), \mathbf{M} \to 0$. Furthermore, we obtain

$$\mathbf{a}(\mathbf{u}) = \mathbf{f}(\mathbf{u}) - \mathbf{h}(\mathbf{u}) = \begin{pmatrix} 0 \\ -\dfrac{\mathbf{M}^2 - 1}{\mathbf{M}^2}\, p \\ -\Big((\mathbf{M}^2 - 1)pv + p_{\text{NL}} v\Big) \end{pmatrix}. \tag{4.67}$$

Taking into account the definition of the non local pressure (4.65) it is easily seen that $\mathbf{a}(\mathbf{u})$ satisfies condition (4.64). Consequently, the decomposition $\mathbf{f}(\mathbf{u}) = \mathbf{h}(\mathbf{u}) + \mathbf{a}(\mathbf{u})$ with respect to (4.66) and (4.67) is well suited.
Obviously, using a time stepping procedure for equation (4.63) and subsequently correcting the obtained fluxes by means of the asymptotic terms $\mathbf{a}(\mathbf{u})$ will inherently omit the coupling of the partial differential equations and thus, the method is at most first order in time. With regard to the simulation of unsteady flow fields it is necessary to improve the accuracy of the resulting time stepping method. Therefore, in order to develop a second order time discretization of system (4.61) we have to add some special kind of correction terms describing the influences of the asymptotic terms within the auxiliary hyperbolic system (4.63) over the time interval $[t^n, t^{n+1} = t^n + \Delta t]$.
Let $\mathbf{u}^n(x)$ denote an approximation of the solution vector $\mathbf{u}(x, t^n)$. Then

$$\begin{aligned} \mathbf{u}_{\mathbf{g}}^0(x) &= \mathbf{u}(x, t^0) \\ \mathbf{u}_{\mathbf{g}}^{n+1}(x) &= \mathbf{u}_{\mathbf{g}}^n(x) - \Delta t \Phi_{\mathbf{g}}(\mathbf{u}, \Delta t) \end{aligned} \tag{4.68}$$

with

$$\Phi_{\mathbf{g}}(\mathbf{u}, \Delta t) = -\partial_x \mathbf{g}\left(\mathbf{u}_{\mathbf{g}}^n(x) - \frac{\Delta t}{2} \partial_x \mathbf{g}\left(\mathbf{u}_{\mathbf{g}}^n(x)\right)\right)$$

represents a consistent second order time discretization according to

$$\partial_t \mathbf{u} + \partial_x \mathbf{g}(\mathbf{u}) = \mathbf{0}. \tag{4.69}$$

Due to the fact that an arbitrary second order time stepping scheme $\widetilde{\Phi}_{\mathbf{g}}$ according to (4.69) fulfills

$$\widetilde{\Phi}_{\mathbf{g}} - \Phi_{\mathbf{g}} = O(\Delta t^2),$$

it is not necessary to take account of the special discretization employed for the auxiliary system (4.63). Let us consider a second order time stepping method for the Euler equations (4.61) and the auxiliary system (4.63) represented by

$$\Phi = \left(\Phi_{(\rho)}, \Phi_{(m)}, \Phi_{(\rho E)}\right)^T$$

and $\Phi_{\mathbf{h}}$, respectively. Neglecting the space variable for simplicity, the difference between the intermediate momentum states concerning the Euler equations and the auxiliary system can be written as

$$m^{n+\frac{1}{2}} - m_h^{n+\frac{1}{2}} = \frac{\Delta t}{2} \frac{\mathbf{M}^2 - 1}{\mathbf{M}^2} \partial_x p^{n+\frac{1}{2}} + O(\Delta t^2). \tag{4.70}$$

This influence yields the asymptotic correction of the mass fluxes in the form

$$\begin{aligned}
\rho^{n+1} &= \rho^n - \Delta t \Phi_{(\rho)}(\mathbf{u}, \Delta t) + O(\Delta t^3) \\
&\overset{(4.70)}{=} \rho^n - \Delta t \partial_x \left(m_{\mathbf{h}}^{n+\frac{1}{2}} + \frac{\Delta t}{2} \frac{\mathbf{M}^2 - 1}{\mathbf{M}^2} \partial_x p^{n+\frac{1}{2}} \right) + O(\Delta t^3) \\
&= \rho^n - \Delta t \Phi_{\mathbf{h},(\rho)}(\mathbf{u}, \Delta t) - \Delta t \Phi_{\mathbf{a},(\rho)}(\mathbf{u}, \Delta t) + O(\Delta t^3)
\end{aligned}$$

with

$$\Phi_{\mathbf{a},(\rho)}(\mathbf{u}, \Delta t) = \frac{\Delta t}{2} \frac{\mathbf{M}^2 - 1}{\mathbf{M}^2} \partial_x^2 p^{n+\frac{1}{2}}. \tag{4.71}$$

The same methodology with respect to the intermediate velocity distribution using $\rho^{n+\frac{1}{2}} = \rho_{\mathbf{h}}^{n+\frac{1}{2}}$ gives

$$v^{n+\frac{1}{2}} = v_{\mathbf{h}}^{n+\frac{1}{2}} + \frac{\Delta t}{2\rho^{n+\frac{1}{2}}} \frac{\mathbf{M}^2 - 1}{\mathbf{M}^2} \partial_x p^{n+\frac{1}{2}} + O(\Delta t^2).$$

Consequently, the entire momentum flux including the second order asymptotic correction terms reads

$$m^{n+1} = m^n - \Delta t \Phi_{\mathbf{h},(m)}(\mathbf{u}, \Delta t) - \Delta t \Phi_{\mathbf{a},(m)}(\mathbf{u}, \Delta t) + O(\Delta t^3)$$

where

$$\Phi_{\mathbf{a},(m)}(\mathbf{u}, \Delta t) = \frac{1 - \mathbf{M}^2}{\mathbf{M}^2} \partial_x p^{n+\frac{1}{2}} + \partial_x (p - p_{\mathbf{h}})^{n+\frac{1}{2}} + \Delta t \frac{\mathbf{M}^2 - 1}{\mathbf{M}^2} \partial_x \left(v_{\mathbf{h}}^{n+\frac{1}{2}} \partial_x p^{n+\frac{1}{2}} \right). \tag{4.72}$$

Analogously, we achieve the energy flux in the form

$$(\rho E)^{n+1} = (\rho E)^n - \Delta t \Phi_{\mathbf{h},(\rho E)}(\mathbf{u}, \Delta t) - \Delta t \Phi_{\mathbf{a},(\rho E)}(\mathbf{u}, \Delta t) + O(\Delta t^3) \tag{4.73}$$

where

$$\begin{aligned}
\Phi_{\mathbf{a},(\rho E)}(\mathbf{u}, \Delta t) \quad = \quad & -(\mathbf{M}^2 - 1)\partial_x (pv)^{n+\frac{1}{2}} - \partial_x (p_{\mathrm{NL}} v)^{n+\frac{1}{2}} + \mathbf{M}^2 \partial_x \Big((p^{n+\frac{1}{2}} - p_{\mathbf{h}}^{n+\frac{1}{2}}) v^{n+\frac{1}{2}} \Big) \\
& + \frac{\Delta t}{2} \frac{\mathbf{M}^2 - 1}{\mathbf{M}^2} \partial_x (H_{\mathbf{h}}^{*,n+\frac{1}{2}} \partial_x p^{n+\frac{1}{2}}) \\
& + \frac{\Delta t}{2} \partial_x \Big(\big((\mathbf{M}^2 - 1)\partial_x (pv)^{n+\frac{1}{2}} + \partial_x (p_{\mathrm{NL}} v)^{n+\frac{1}{2}} \big) v^{n+\frac{1}{2}} \Big).
\end{aligned} \tag{4.74}$$

Two facts are remarkable. First, the additional terms representing the differences between $\Phi_{\mathbf{a}}$ and a straightforward discretization of the asymptotic fluxes $\mathbf{a}(\mathbf{u})$ are of order $O(\Delta t^2)$ and hence negligible in the case of a first order time stepping procedure. Second, the above mentioned additional terms can be substituted by an arbitrary first order approximation without affecting the order of accuracy. For example, one can evaluate the pressure derivative within equation (4.70) at any time level $t^m \in [t^n, t^{n+1}]$.

4.3.1 Evolution of the spatial homogeneous leading order pressure

Concerning the results of the asymptotic single as well as multiple scale analysis the evolution of the spatial homogeneous leading order pressure $p^{(0)}$ is due to compression from the boundary ∂G or expansion of the reacting gas itself. Therefore, we usually employ

$$p^{(0),n+1} = p^{(0),n} - \Delta t \gamma p^{(0),n} \left(v_r^n - v_\ell^n \right), \tag{4.75}$$

where v_r and v_ℓ represent the velocity at the right and left boundary of the computational domain, respectively. Note, that the leading order pressure is constant in space and time if periodic boundary conditions are considered.

4.3.2 Evolution of the acoustic first order pressure

The evolution of the acoustic pressure $p^{(1)}$ is governed by the system of linearized acoustics which can be written in the form

$$\begin{aligned}
\partial_t \overline{m} \quad &+ \quad \frac{1}{\mathbf{M}} \partial_x p^{(1)} \quad &= \quad 0 \\
\partial_t p^{(1)} \quad &+ \quad \frac{1}{\mathbf{M}} \partial_x \left(\overline{c}\, \overline{m} \right) \quad &= \quad 0
\end{aligned} \tag{4.76}$$

where $\overline{c} = \sqrt{\gamma \frac{p^{(0)}}{\overline{\rho}}}$. In higher spatial dimensions one has to introduce a specific assumption for the underlying density distribution to achieve system (4.76), see [36]. The system (4.76) is hyperbolic with characteristic signal speeds $\pm \frac{\overline{c}}{\mathbf{M}} = O\left(\frac{1}{\mathbf{M}}\right)$. Since the time step size within the explicit discretization of the auxiliary system satisfies

$\Delta t = O(\Delta x)$ it is necessary to employ a suitable discretization technique for the solution of system (4.76) to overcome the restrictive Courant-Friedrichs-Lewy condition [8] for an explicit forward Euler time discretization. Implicit time stepping schemes have the advantage that the numerical domain of dependence always covers the physical one and hence, these methods inherently fulfill the CFL-condition. Due to the fortunate property that the Jacobian of the flux function within the system (4.76) is very simple we decided to employ an implicit discretization. The linear system arising from the linearization of the flux function is solved by means of the Bi-CGSTAB method [78] preconditioned by an incomplete LU factorization technique [47, 49]. The initialization of the long wave momentum and density distribution is performed by the decomposition algorithm described below.

4.3.3 Energy-Poisson-Equation

Existing methods developed for incompressible flow fields are treating the pressure as a main dependent variable. One should expect from the equations considered above that we retain density, momentum, and total energy as the working variables. Indeed, in the purely compressible case ($\mathbf{M} \geq 1$) the conserved variable are chosen since they represent a common, widely used, and convenient choice in the context of transonic and supersonic flow fields. Due to the fact that we want to develop a numerical scheme which should be endowed with a great versatility it is advantageous to establish the pressure as a dependent variable in the low Mach number regime.
In the following we briefly describe the establishment of the pressure as a main variable in the low Mach number regime ($\mathbf{M} < 1$). Introducing the equation of state written as

$$(\rho E)^{n+1} = \frac{p^{(0),n+1}}{\gamma - 1} + \frac{\mathbf{M}p^{(1),n+1}}{\gamma - 1} + \frac{\mathbf{M}^2 p^{(2),n+1}}{\gamma - 1} + \frac{\mathbf{M}^2}{2}\rho^{n+1}\left(v^{n+1}\right)^2$$

into the energy equation (4.73) and omitting terms of order $O(\Delta t^3)$ yield

$$\begin{aligned} \frac{\mathbf{M}^2}{\gamma - 1} p^{(2),n+1} \quad &= \quad (\rho E)^n - \frac{p^{(0),n+1}}{\gamma - 1} - \frac{\mathbf{M}p^{(1),n+1}}{\gamma - 1} - \frac{\mathbf{M}^2}{2}\rho^{n+1}\left(v^{n+1}\right)^2 \\ &\quad -\Delta t \Phi_{\mathbf{h},(\rho E)}\left(\mathbf{u}, \Delta t\right) - \Delta t \Phi_{\mathbf{a},(\rho E)}\left(\mathbf{u}, \Delta t\right). \end{aligned}$$

Remember that the leading order pressure $p^{(0),n+1}$ as well as the acoustic pressure $p^{(1),n+1}$ are previously computed by means of the evaluation of the boundary integral (4.75) and the system of linearized acoustics (4.76), respectively. Thereafter, we employ an implicit discretization of the asymptotic part (4.74) in the form

$$\begin{aligned} &\Phi_{\mathbf{a},(\rho E)}\left(\mathbf{u}, \Delta t\right) \\ &\quad = \frac{\Delta t}{2}\frac{\mathbf{M}^2 - 1}{\mathbf{M}^2}\partial_x\left(H_{\mathbf{h}}^{*,n+\frac{1}{2}}\partial_x p^{n+1}\right) + \frac{\Delta t}{2}\partial_x\left(\left((\mathbf{M}^2 - 1)\partial_x(pv)^{n+1} + \partial_x(p_{\mathrm{NL}}v)^{n+1}\right)v^{n+1}\right) \\ &\qquad -(\mathbf{M}^2 - 1)\partial_x(pv)^{n+\frac{1}{2}} - \partial_x(p_{\mathrm{NL}}v)^{n+\frac{1}{2}} + \mathbf{M}^2\partial_x\left((p^{n+\frac{1}{2}} - p_{\mathbf{h}}^{n+\frac{1}{2}})v^{n+1}\right). \qquad (4.77) \end{aligned}$$

Using the pressure decomposition in the asymptotic flux function (4.77) and assuming that the pressure terms $p^{n+\frac{1}{2}}$ and $p_{\mathbf{h}}^{n+\frac{1}{2}}$ as well as the enthalpy form $H_{\mathbf{h}}^{*,n+\frac{1}{2}}$ are available we can discretize the derivatives within the asymptotic fluxes by means of central differences to achieve a linear system of equations

$$\mathbf{A}\mathbf{p}^{(2)} = \mathbf{b},\ \mathbf{p}^{(2)} = \begin{pmatrix} p_1^{(2),n+1} \\ \vdots \\ p_n^{(2),n+1} \end{pmatrix} \tag{4.78}$$

for the calculation of the second order pressure. It is remarkable that the matrix and the right hand side of equation (4.78) contain density and velocity contributions at the time level t^{n+1}. Due to this fact we employ a fix-point iteration where the asymptotic flux corrections $\Phi_{\mathbf{a}}$ are computed simultaneously. Therefore, we take $v_{\mathbf{h}}^{n+1}$ and $\rho_{\mathbf{h}}^{n+1}$ provided by the discretization of the auxiliary system as the initial guess for the velocity and density (i.e. $v^{n+1,0} = v_{\mathbf{h}}^{n+1}$, $\rho^{n+1,0} = \rho_{\mathbf{h}}^{n+1}$), respectively. Now, the matrix and the right hand side are fixed and one can solve the system (4.78) to obtain $p^{(2),n+1,0}$. Using the variables $\rho^{n+1,0}$, $v^{n+1,0}$, and $p^{(2),n+1,0}$ we can evaluate the asymptotic fluxes completely by means of a Crank-Nicolson approach. Clearly, a prescription for the computation of $p^{n+\frac{1}{2}}$, $p_{\mathbf{h}}^{n+\frac{1}{2}}$, and $H_{\mathbf{h}}^{*,n+\frac{1}{2}}$ is required to close the system. The pressure $p_{\mathbf{h}}^{n+\frac{1}{2}}$ and the enthalpy form $H_{\mathbf{h}}^{*,n+\frac{1}{2}}$ are given by the discretization of the auxiliary system (4.63) using $\widetilde{\Delta t} = \frac{\Delta t}{2}$. In order to compute the pressure $p^{n+\frac{1}{2}}$ we use the same procedure as mentioned above concerning the time interval $[t^n, t^{n+\frac{1}{2}} = t^n + \widetilde{\Delta t}]$ where the approximation

$$\begin{aligned}
&\Phi_{\mathbf{a},(\rho E)}(\mathbf{u}, \Delta t) \\
&\quad = -(\mathbf{M}^2 - 1)\partial_x(pv)^{n+\frac{1}{2}} - \partial_x(p_{\mathrm{NL}}v)^{n+\frac{1}{2}} + \mathbf{M}^2\partial_x\left((p^{n+\frac{1}{2}} - p_{\mathbf{h}}^{n+\frac{1}{2}})v^{n+\frac{1}{2}}\right) \\
&\qquad + \widetilde{\Delta t}\frac{\mathbf{M}^2 - 1}{\mathbf{M}^2}\partial_x(H_{\mathbf{h}}^{*,n+\frac{1}{2}}\partial_x p^{n+\frac{1}{2}}) + \widetilde{\Delta t}\partial_x\left(\left((\mathbf{M}^2 - 1)\partial_x(pv)^{n+\frac{1}{2}} + \partial_x(p_{\mathrm{NL}}v)^{n+\frac{1}{2}}\right)v^{n+\frac{1}{2}}\right)
\end{aligned}$$

is employed and the Crank-Nicolson time stepping scheme for the asymptotic fluxes is replaced by a backward Euler approach.
Obviously, the restriction to consider one-dimensional flow fields was only established for simplicity. All the results obtained above can directly be extended to higher spatial dimensions with the caveat that the nontrivial small scale long scale coupling may occur as discussed in the context of system (4.76).

4.3.4 Spatial discretization

A standard finite volume approach is used to discretize the auxiliary hyperbolic system (4.63). Thus, the computational domain $G \subset \mathbb{R}$ is subdivided into control volumes $\sigma_1, \ldots, \sigma_n$ and the evolution of the cell average of each control volume is calculated due to the numerical fluxes at the boundary of σ_i.

We modified the Roe–Riemann solver with entropy fixing to calculate the numerical fluxes. To achieve a scheme of high order in space and time we use linear reconstruction of the characteristic variables in spatial directions as well as a MUSCL approach in time. In the limit $\mathbf{M} \to 1$ the modifications cancel each other and the usual Roe-Riemann solver is recovered. A detailed description of this Godunov-type algorithm is given in [75]. Similarly, further numerical flux functions can be modified. The variation of the AUSMDV is described in [50].
With respect to the numerical approximation of the Euler equations we finally have to determine the discretization of the asymptotic fluxes. The approximation is achieved in a simple finite difference manner where each physical quantity $\varphi_{i+\frac{1}{2}}$ at the interface between two adjacent boxes σ_i and σ_{i+1} is computed as a mean value of the corresponding cell averages. Similarly, we approximate the derivatives $(\partial_x \varphi)_{i+\frac{1}{2}}$ in the form of central differences.

4.3.5 Identification of an Asymptotic Regime

The identification of an asymptotic or weakly compressible regime is closely related to the determination of the reference parameter $\mathbf{M} \in (0,1]$ as well as the decomposition of the primitive variables $\hat{\rho}, \hat{v}, \hat{p}$ needed in the ansatz of the multiple scale analysis. We translate the analytical requirements into the discrete context.
The density $\hat{\rho}$ and the velocity $\hat{v}$ can be written in the form

$$\hat{\rho} = \overline{\rho} + \rho' \qquad \text{and} \qquad \hat{v} = \overline{v} + v',$$

where the superscript $'$ denotes short wave phenomena and the overbar denotes the long wave parts, respectively.
In order to develop a specific extension of an existing numerical method by means of the results of the asymptotic multiple scale analysis it is appropriate to decompose the pressure in the form

$$\hat{p} = \hat{p}^{(0)} + \mathbf{M}\hat{p}^{(1)} + \mathbf{M}^2\hat{p}^{(2)}. \tag{4.79}$$

Note that no truncation error of order $o(\mathbf{M}^2)$ appears in equation (4.79). The splitting is exact in contrast to the expansion introduced in the asymptotic analysis. Hence, we do not assume that the pressure terms $\hat{p}^{(0)}$, $\hat{p}^{(1)}$, and $\hat{p}^{(2)}$ are equal to those employed in the mathematical theory, but we require that the pressure terms have the same qualitative behavior.
With regard to the asymptotic analysis we demand a spatially homogenous leading order pressure $\hat{p}^{(0)}$, if the reference parameter is sufficiently small. Moreover, the first order pressure $\hat{p}^{(1)}$ has to represent exclusively long wave phenomena.
Contrarily to the theoretical analysis, we also are not interested in estimates of each pressure component $\hat{p}^{(i)}$ in the limit of a vanishing Mach number, but in those which are valid for all values of $\mathbf{M}$. Therefore, we establish the following weaker assumptions

$$\hat{p}^{(i)} \leq C\hat{p}_{ref}, \; i = \{0, 1, 2\}, \tag{4.80}$$

which have to be fulfilled by the decomposition. The constant C can be chosen freely. With regard to the splitting of the pressure in equation (4.79) it is obvious that the numerical algorithm to decompose the pressure has to be defined in accordance with the calculation of the reference parameter $\mathbf{M}$. If one cannot determine a pressure decomposition satisfying condition (4.80), then the reference parameter is set equal to one. The considered regime is now purely compressible and the assumptions of the multiple scale asymptotic are no longer valid. In the case of a vanishing reference parameter we reach the purely incompressible regime which has been discussed in detail in [64]. If we define

$$\hat{p}^{(0)}(t) := \frac{1}{|G|} \int\limits_G \hat{p}(x,t)dx,$$

then all requirements to the leading order pressure $\hat{p}^{(0)}$ hold for all $\mathbf{M} \in (0,1]$. Furthermore it is possible to rewrite the pressure decomposition (4.79) as

$$\phi = \overline{\phi} + \phi',$$

with $\phi := \hat{p} - \hat{p}^{(0)}$, $\overline{\phi} := \hat{p}^{(1)}$ and $\phi' := \mathbf{M}^2\hat{p}^{(2)}$. Now we can describe the purpose of the decomposition in the following way:

> *Let I denote the index set of the discretization. Decompose every given signal $(f_i)_{i\in I}$ of a function f in the form*
>
> $$f_i = \overline{f}_i + f_i', \quad \forall i \in I,$$
>
> *where $(\overline{f}_i)_{i\in I}$ represents exclusively long wave phenomena and $(f_i')_{i\in I}$ contains the remaining long and short wave parts. Furthermore $(f_i')_{i\in I}$ has to be small compared to $(\overline{f}_i)_{i\in I}$ with regard to the maximum norm, i. e.*
>
> $$\|(\overline{f}_i)_{i\in I}\|_\infty \gg \|(f_i')_{i\in I}\|_\infty.$$

Due to their weak numerical performance average operators which are based on convolutions with a box function or a Gaussian kernel are left out of consideration, even though it is possible to fulfill all requirements of the decomposition using suitable a-priori estimates to calculate $\mathbf{M}$. We also disregard filter algorithms based on Fourier transformations of the signal. These would require certain manipulations of high frequencies associated with aliasing errors and non-periodicity of the analyzed signals. Grid effects on the resulting signal components are ambiguous and hard to control, especially on unstructured meshes. Besides, Fourier decomposition is a global operation on the domain $\hat{G}$.

Wavelets have local properties in space and time, but unfortunately the reference parameter $\mathbf{M}$ must be precisely determined for small values, which is impossible by means of a single wavelet analysis. Sampling the high frequency parts of the wavelet analysis

again it is possible to determine all frequencies at the cost of loosing the multiple scale properties and the order of the algorithm.
A survey of scale-space evolution algorithms based on parabolic differential equations is given in [83].
We employ a decomposition operator which is derived from a new evolution algorithm of polygonal curves that is especially designed to fit the discrete nature of curves [40]. In the area of discrete data analysis polygonal curves are simplified to extract the important visual parts neither changing the coarse structure of the borderline nor dislocating the relevant features.
During each evolution step a certain number of successive edges are replaced by a straight line connecting the endpoints of such a set of edges. The key of success of this very simple algorithm is hidden in the order of these replacements. In each step of the evolution a relevance measure assigns a cost value to each pair of edges. This value represents the significance of the contour compared to all others. If the cost value is small, i.e. the structure which is build up by the pair of edges is inessential, then it will be replaced as mentioned above.
The sequence of replacements forced by the relevance measure produces a hierarchy of structures, so that two different phases are seen during the evolution. In the first phase artifical noise is eliminated without changing the shape of the object in a significant way. Successive simplifications of the shape take place only in the second phase of the evolution.
Transfered to our aim a suitable relevance measure has to be defined to classify those points of a discrete distribution $(f_i)_{i \in I}$ which are not represented by $\overline{f}$. In a second step these points have to be replaced to give $\overline{f}$ some kind of discrete smoothness.
First of all, we must derive an appropriate definition to distinguish long wave and short wave phenomena in our current context. In contrast to the Fourier ansatz we will call any function to be of long wave type, if the distance between its inflection points is sufficiently large. By means of this definition the sinusoidal function belongs to the same class as an arbitrary function having equivalent minimal distances between its turning points. In general, inflection points are frequent in areas with short wave structures, whereas in areas with long wave structures only few inflection points can be found. We will employ this property of the wavelength to define a cost function and finally derive the relevance measure.

4.3.5.1 Discrete evolution algorithm

Let $(\sigma_i)_{i \in I}$ be the given disjunct decomposition of the domain G into control volumes, boxes for short. Thereby, I represents an index set with $n := \#(I)$. We consider the cell averages $(f_i)_{i \in I}$ of any function f located at the barycenters of the boxes. Applying a simple recovery procedure by a linear function of every cell average value on adjacent boxes directly leads to a piecewise linear function comparable to the polygonal contours investigated in [41].
A discrete curve evolution of a function f produces a sequence of functions $f = f^0, \dots, f^m$ and a sequence of index sets $I = I^0, \dots, I^m$ with $\#I^{l+1} < \#I^l$ and $\#I^m \leq 2$.

In this methodology the index set I^l denotes those points which are still unchanged at the beginning of the $l-$th evolution step. To determine those points f_i^l which are equal to the function $f = f^0$ at the beginning of the evolution, for every point f_i^l, $i \in I^l$, a cost value $k(i, I^l) \in \mathbb{R}^+$ is allocated via the reference measure. Let

$$k_{min}(I^l) = \min\{k(i, I^l) : i \in I^l\}.$$

The set $I_{min}(I^l)$ denotes the set of points with minimal costs at the $l-$th evolution step,

$$I_{min}(I^l) = \{i \in I^l : k(i, I^l) = k_{min}(I^l)\}.$$

Now the evolution algorithm removes the index set $I_{min}(I^l)$ from I^l,

$$I^{l+1} = I^l \setminus I_{min}(I^l).$$

We noticed that the relevance measure represents the significance of each individual structure compared to all others and therefore controls the sequence of the evolution steps. In our case the relevance measure should be characterized by the wavelength of the function. The wavelength itself was fixed by the distance of the inflection points from each other. So the cost function at a cell average f_i should primarily be a function of the sum of the distances from its neighboring points of inflection. We subdivide the domain G into overlapping concave and convex sub-domains $\sigma_j, j \in J$, using the distribution of the sign of the turning angle α_i. Each sub-domain covers points with the same sign of the turning angle including those two vertices left and right where the sign changes by definition. In the discrete context the sum of the distances to the neighboring inflection points is equal to the length of the concave or convex sub-domains $|\sigma_j|$ projected onto the x-axis. In order to emphazise that the box σ_i associated with the cell average f_i is located in the interior of the sub-domain σ_j we introduce the notation σ_j^i, $i \in \sigma_j^i$ for short. Note that f_i can be a member of up to three different sub-domains σ_j. Because the number of sub-domains changes during the evolution, we also introduce a sequence of index sets $J = J^0, \ldots, J^m$ of sub-domains σ_j. Now, define the cost function $k(i, I^l) \in \mathbb{R}$ to be

$$k(i, I^l) := \big|\min_{i \in \sigma_j^i} |\sigma_j^i| - \min_{j \in J^l} |\sigma_j|\big| \cdot |\alpha_i|, \tag{4.81}$$

for all $i \in I^l$. Obviously, the cost function represents a non-negative function which is equal to zero for all points of the smallest sub-domain. Hence, in addition to the points with collinear arranged function values all points of the smallest sub-domain are removed during the following evolution step.
If we interpret the minimal distance of two neighboring sub-domains σ_j as the minimal wavelength of the function f^l

$$\lambda_{min}(f^l) := \min_{j \in J^l}\big(|\sigma_j| + |\sigma_{j+1}| - |\sigma_j \cap \sigma_{j+1}|\big)$$

with $\sigma_j := \emptyset,\ \forall j \notin J^l$, then the inequality

$$\lambda_{min}(f^l) \leq \lambda_{min}(f^{l+1})$$

does not hold for all $l \in \{0, \ldots, (m-1)\}$, in general. Nevertheless, for the stopping criterion, it follows

$$\lambda_{min}(f^0) \leq \lambda_{min}(f^m) = |G|.$$

In the case $\lambda_{min}(f^0) \neq |G|$ the inequality is sharp. Thus, the minimal wavelength increases during the evolution although it is theoretically possible that the progress is not monotone.
Now we can easily define an indicator $\mathbf{M}_l$ based on the length scale information which will be used to determine the reference parameter $\mathbf{M}$ in section 4.3.6,

$$\mathbf{M}_l(f^l) := \min\left\{\frac{1}{\lambda_{min}(f^l)}, 1\right\}. \tag{4.82}$$

Let us briefly summerize the steps of the algorithm:

1. Set $M_l = 1,\ l = 0,\ \overline{f}_i = f_i,\ f_i' = 0$, for all $i \in I = I^0$.
2. Subdivide G into overlapping concave and convex sub-domains σ_j with respect to the function $\overline{f}_i,\ \forall i \in I^0$.
3. Compute $\mathbf{M}_l$ by means of equation (4.82) and check the validity of the estimates in equation (4.80) as well as $\#I^l > 2$. If one of these conditions is not satisfied the evolution is stopped.
4. Assign the relevance measure $k(i, I^l)$ to each box $\sigma_i,\ i \in I^l$, using the cost function (4.81).
5. Compute $I_{min}(I^l) = \{i \in I^l : k(i, I^l) = 0\}$.
6. Reduce the index set of the maintained function values, $I^{l+1} = I^l \setminus I_{min}(I^l)$.
7. Compute $\overline{f}_i,\ i \in I^0 \setminus I^{l+1}$ taking the maintained points $f_i,\ i \in I^{l+1}$ into account.
8. Compute $f_i' = f_i - \overline{f}_i,\ i \in I^0 \setminus I^{l+1}$.
9. Increase the index of the evolution, $l = l + 1$.
10. Go to 2.

We want to add some remarks regarding the smoothness of the discrete function $\overline{f}$. The use of a simple linear interpolation in order to define discrete values for the smooth function $\overline{f}$ at those points which are actually removed does not lead to a suitable recovery procedure since it is possible that all points in larger parts of the domain

have been removed. Cubic splines represent a better choice, but one has to be quite optimistic that no additional inflection points are generated within this procedure. We decide to employ the following ansatz. First of all we add some of the removed points in a suitable way such that no additional inflection points are introduced and thereafter we apply one of the recovery techniques mentioned above.
The resulting scheme yields good results already in the case that the recovery step is given in the form of a linear interpolation as you can see in Section 4.4.

4.3.6 Process of non–dimensionalization and time-dependent calculation of the reference parameter

In order to gain a suitable non-dimensionalization of the physical quantities one has to calculate the required reference values in a proper manner from the flow field given. Usually, no differences are made between the modeling of a compressible or incompressible fluid flow within this process. The reference values with respect to the length $\hat{x}_{ref}$, the density $\hat{\rho}_{ref}$ and the velocity $\hat{v}_{ref}$ are determined once at the beginning of the computation and the other reference values are calculated in correspondence to them. These models are based on the assumption that the overall character of the flow field will not change during the time of computation. Therefore, in those cases it is justified to fix the reference values at the beginning. However, in order to compute fluid flows which may change their overall character from incompressible to compressible or vice versa, it is necessary to implement a time-dependent process of non-dimensionalization. As mentioned in Section 3 we establish an additional pressure reference. Consequently the Mach number $\mathbf{M}$ appears in the Euler equations which is assumed to be a measure of the compressibility of the flow as well as a measure of the wave length of the acoustic waves, as stated in Section 4.3.5. We assume that a nearly incompressible flow field is characterized by the following two properties on the dimensional quantities. First, we expect that the divergence of the velocity is very small, and second, the flow field shows only tiny fluctuations within the pressure distribution.
The time dependent reference value for the density as well as the pressure is determined by means of averaging each quantity over the whole domain G,

$$\hat{\rho}_{ref} = \hat{\rho}_{ref}(t) = \frac{1}{|G|}\int\limits_{G} \hat{\rho}(x,t)dx \quad \text{and} \quad \hat{p}_{ref} = \hat{p}_{ref}(t) = \frac{1}{|G|}\int\limits_{G} \hat{p}(x,t)dx,$$

respectively. If we also set the velocity reference to the average of the velocity over the domain G, none of the above defined reference values can be employed to decide whether the flow is incompressible or compressible. Thus, for the present we determine the reference parameter $\mathbf{M}$, so that it can be employed to weight the influence of the asymptotic analysis according to the asymptotic fluxes $\Phi_{\mathbf{a}}$ in Section 3. Then the reference value for the velocity is calculated using equation (3.7).
We define three indicators to measure the different properties of weakly compressible fluid flows. One of them is coupled with the pressure distribution as stated in Section

4.3.5. This length scale indicator $\mathbf{M}_l$ was defined in the last Section, equation (4.82). The other two characterize the velocity flow field,

$$\mathbf{M}_v = C_v \frac{\max_{x\in G}|\hat{v}|}{\sqrt{\hat{p}_{ref}/\hat{\rho}_{ref}}} \quad and \quad \mathbf{M}_{div} = C_{div}\sqrt{\frac{\max_{x\in G}|\partial_x \hat{v}|}{\sqrt{\hat{p}_{ref}/\hat{\rho}_{ref}}}}.$$

Now, we are able to formally define the reference parameter $\mathbf{M}$. In order to ensure that a standard Godunov type solver is used in the case that one indicator is greater or equal than a critical value α, $0 < \alpha \leq 1$, we define a function g,

$$g(\tilde{\mathbf{M}}) = 1 + \frac{\frac{1}{\alpha} - 1}{\alpha^2}\tilde{\mathbf{M}}^2$$

with

$$\tilde{\mathbf{M}} = \min\left\{\alpha, \max(\mathbf{M}_v, \mathbf{M}_{div}, \mathbf{M}_l)\right\}.$$

The reference parameter is then given by

$$\mathbf{M} = g(\tilde{\mathbf{M}})\tilde{\mathbf{M}}, \quad \mathbf{M} \in [0,1],$$

whereby equation (3.7) now yields the velocity reference in the form

$$\hat{v}_{ref} = \mathbf{M}\sqrt{\frac{\hat{p}_{ref}}{\hat{\rho}_{ref}}}.$$

In Figure 20 the effect of the function g with different values of α is visualized.

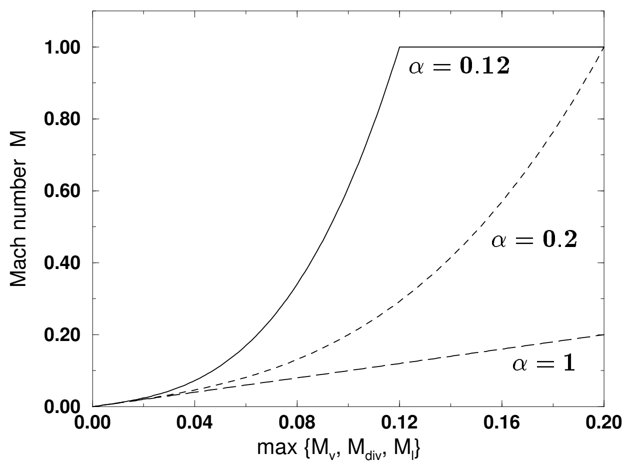

Figure 20: Effect of the function g to the reference parameter

Finally, to conclude the process of the non-dimensionalization the characteristic time scale is given by $\hat{t}_{ref} = \hat{x}_{ref}/\hat{v}_{ref}$. Due to the indicators $\mathbf{M}_v$ and $\mathbf{M}_{div}$ it is guaranteed that the dimensionless velocity field is limited,

$$\max_{x \in G} |v| = \frac{\max_{x \in G} |\hat{v}|}{\hat{v}_{ref}} = \sqrt{\gamma}\frac{\mathbf{M}_v}{\mathbf{M}},$$

and that the divergence free condition in the limit of a vanishing Mach number is fulfilled,

$$\max_{x \in G} |\partial_x \hat{v}| = \frac{\max_{x \in G} |\partial_x v|}{\hat{v}_{ref}} = \sqrt{\gamma}\frac{\mathbf{M}_{div}^2}{\mathbf{M}}.$$

As seen before, a time-dependent adaptation can easily be achieved by a simple rescaling of each physical quantity after each time step. Since the decomposition of the physical quantities has to be resolved during every time step the computation of the indicators as well as of the average values is not very expensive in comparison to the costs of the decomposition. But it is possible to decrease the computational effort and neglect the rescaling of density and pressure, if their average values do not rapidly change in time. Then only the velocity field has to be rescaled after each time step to employ the influences of a varying reference parameter $\mathbf{M}$ to the flow field.

4.4 Numerical results

In order to use the decomposition algorithm described in Section 4.3.5.1 we restrict ourselves to one dimensional test cases to demonstrate the performance and applicability of the numerical scheme.
Therefore, we study an example of a nearly incompressible flow field and one which changes its overall character from weakly compressible to compressible. In both cases the critical value for changing to the compressible scheme is set to be $\alpha = 0.12$.
Let us consider a long wave acoustic flow field of an ideal gas. Its density profile shows some short wave fluctuations which will be moved within the acoustic field. We prescribe periodic boundary conditions whereby the computational domain $\hat{G} = [-51\ m, 51\ m]$ is equidistantly subdivided into 1020 cells. The initial conditions are given by

$$\begin{aligned}
\hat{\rho}(x,0) &= \Big(1 + 2\mathbf{M}\big(1+\cos(2\mathbf{M}\pi x)\big) + \Psi(x)\frac{1}{2}\sin(80\mathbf{M}\pi x)\Big)\frac{kg}{m^3},\\
\hat{v}(x,0) &= \sqrt{\gamma}\Big(1+\cos(2\mathbf{M}\pi x)\Big)\frac{m}{s},\\
\hat{p}(x,0) &= \frac{1}{4\mathbf{M}^2}\Big(1 + 2\gamma\mathbf{M}(1+\cos(2\pi\mathbf{M}x))\Big)\frac{N}{m^2}
\end{aligned}$$

and

$$\Psi(x) = \begin{cases} \dfrac{1-\cos(10\mathbf{M}\pi x)}{2} & ; 0 \le x \le \dfrac{2}{10\mathbf{M}} \\ 0 & ; \text{otherwise.} \end{cases}$$

The parameter $\mathbf{M}$ and the reference of the length scale are set to be $\mathbf{M} = \frac{1}{102}$ and $\hat{x}_{ref} = 1\ m$, respectively.

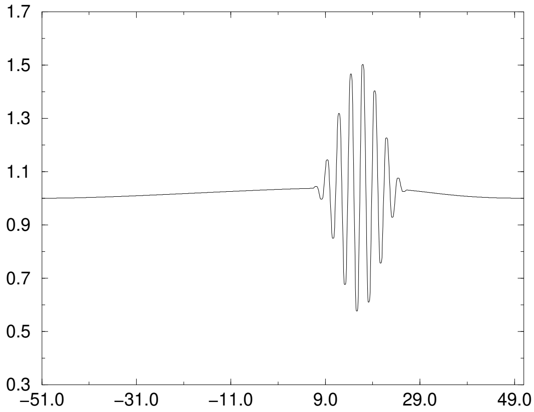

Figure 21: Density distribution at time $t = 5,071\ s$

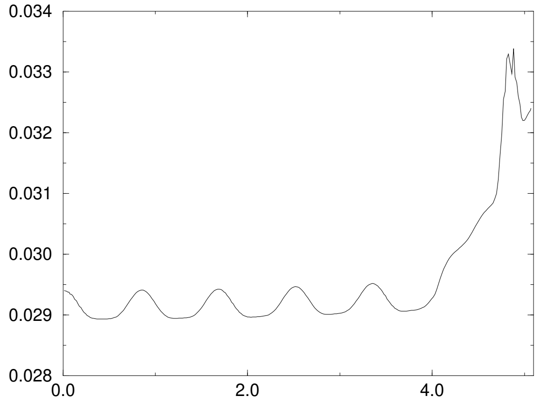

Figure 22: Time dependent adaptation of $\mathbf{M}$

In Figure 21 the density profile at the end of the computation ($T = 5,071$) is plotted. The amplitudes of the short wave density perturbation are almost preserved.
The time-dependent adaptation of the reference parameter $\mathbf{M}$ is presented in Figure 22. The small oscillations of the reference parameter in Figure 22 are based on the fact that the acoustic wave moves faster than the density perturbation and therefore the small fluctuations change their relative position to the extrema of the acoustic wave. At the beginning of the computation the indicator $\mathbf{M}_v$ controlled the progress of the reference parameter. Then, for $t > 4.0s$, the acoustic wave slowly steepened and at the end the indicator $\mathbf{M}_{div}$ took over.
This first example is also been used to demonstrate the numerical accuracy of the decomposition algorithm and to show all the advantages of the used decomposition over the other filters mentioned in Section 4.3.5 in an impressive way. The decomposition is almost completely restricted to the domain where the short wave oszillations of the density distribution are found. In the other parts of G the filtered function and the original one are almost the same neglecting numerical noise of the size $(\Delta x)^2$. No shape rounding effects have taken place.
Now a wave steepening into a shock is considered and thus the passing of a weakly compressible flow field into a compressible one is investigated. We use an equidistant discretization of the domain $\hat{G} = [-22\ m, 44\ m]$ into 330 boxes with boundary conditions set to be periodic. The initial conditions are

$$\hat{\rho}(x,0) = \Big(0.955 + \frac{1}{11}\Big(1 - \cos(\frac{\pi x}{11})\Big)\Big)\frac{kg}{m^3},$$
$$\hat{v}(x,0) = \frac{\sqrt{\gamma}}{11}\Big(1 - \cos(\frac{\pi x}{11})\Big)\frac{m}{s},$$
$$\hat{p}(x,0) = \Big(2\gamma + \frac{\gamma}{11}\Big(1 - \cos(\frac{\pi x}{11})\Big)\Big)\frac{N}{m^2},$$

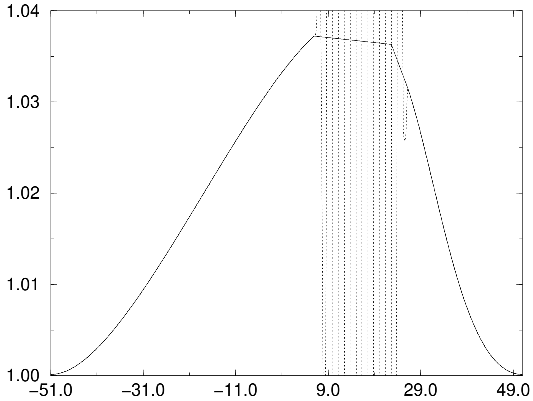

Figure 23: Filtered long wave signal

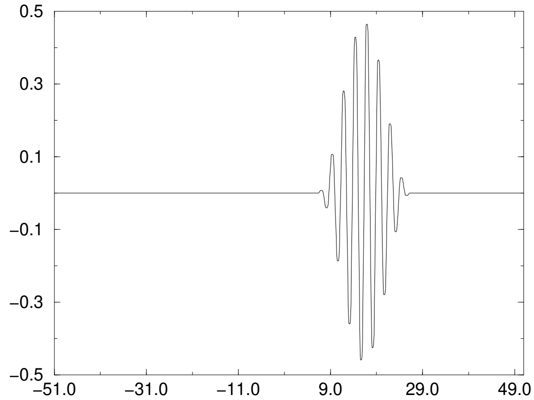

Figure 24: Short wave oszillations

for $x \leq 0$ and

$$\begin{aligned}
\hat{\rho}(x,0) &= 0.955\ \frac{kg}{m^3},\\
\hat{v}(x,0) &= 0\ \frac{m}{s},\\
\hat{p}(x,0) &= 2\gamma\ \frac{N}{m^2},
\end{aligned}$$

otherwise. Again the reference length is set to be $\hat{x}_{ref} = 1\ m$. Figure 25 shows the density distribution with and without adaptation of the reference parameter at the end of the computation at time $t = 33\ s$. Besides, the progress of the parameter $\mathbf{M}$ is given in Figure 26. The comparison between the results obtained with and without adaptation

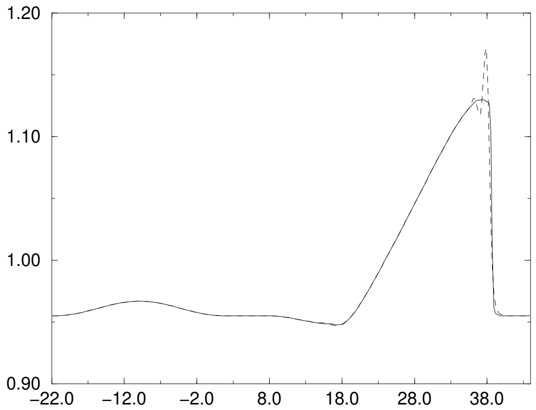

Figure 25: Density distribution at time $t = 33\ s$

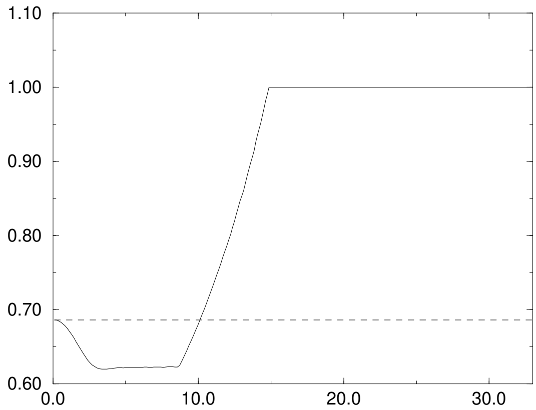

Figure 26: Progress of the reference parameter

indicates the necessity of an adaptation of the reference parameter $\mathbf{M}$ in the case of passing from weakly compressible to compressible flow fields. Although the solutions coincide in the regions where the distribution of the density is smooth, the shock was accurately resolved only by the adapted approach. This is not surprising, because it was necessary to use central differences to discretize the asymptotic corrections $\Phi_{\mathbf{a}}$ in equations (4.71), (4.72) and (4.74) in a sensible way to achieve a scheme of high order.

5 Conclusion

An introduction concerning the properties and performance of asymptotic expansions is given. At first, simple model problems are considered to emphasize the applicabilities and limitations of different types of expansions. Thereafter, a detailed low Mach number analysis of the Euler equations of gas dynamics by means of a single as well as multiple scale asymptotic expansion is presented. The results are afterwards employed to extend the applicability of standard finite volume discretizations from the compressible to the low Mach number regime in the form of a preconditioning technique as well as a flux correction approach. The validity of these approaches is established by means of numerical experiments as well as a discrete asymptotic analysis.

Acknowledgment

The author is grateful to Prof. Dr. Th. Sonar for years of fruitful collaboration in the field of finite volume methods. The author furthermore would like to express his thanks to Dr. N. Botta, Dr. L. Hoffmann, Prof. Dr. R. Klein, Prof. Dr. C.-D. Munz and Dr. S. Roller for numerous valuable discussions. Moreover, the author is indebted to Prof. J. C. Misra from the Indian Institute of Technology for his invitation and support. The work was financially supported by Deutsche Forschungsgemeinschaft (DFG) within the project So 363/3-1.

References

[1] J. D. Anderson. *Hypersonic and high temperature gas dynamics*. MacGraw-Hill, Series in aeronautical and aerospace engineering, Singapore, 1989.

[2] K. Asano. On the Incompressible Limit of the Compressible Euler Equations. *Japan J. Appl. Math.*, 4: 455–488, 1987.

[3] O. Axelsson. *Iterative Solution Methods*. Cambridge University Press, Cambridge, 1996.

[4] T. J. Barth, D. C. Jesperson. The Design and Application of Upwind Schemes on Unstructured Meshes. *AIAA paper*, 89–0366, 1989.

[5] W. R. Briley, H. McDonald, S. J. Shamroth. A Low Mach Number Euler Formulation and Application to Time-Iterative LBI Schemes. *AIAA J.*, 21 (10): 1467–1469, 1983.

[6] D. Choi, C. L. Merkle. The Application of Preconditioning in Viscous Flows. *J. Comput. Phys.*, 105: 207–223, 1993.

[7] A. J. Chorin. A Numerical Method for Solving Incompressible Viscous Flow Problems. *J. Comput. Phys.*, 2: 12–26, 1967.

[8] R. Courant, K. O. Friedrichs, H. Lewy. "Uber die partiellen Differentialgleichungen der mathematischen Physik. *Math. Annalen*, 100: 32–74, 1928.

[9] O. Friedrich. Weighted Essential Non-Oscillatory Schemes for the Interpolation of Mean Values on Unstructured Grids. *J. Comput. Phys.*, 144: 194–212, 1998.

[10] O. Friedrich. *Gewichtete wesentlich nicht-oszillierende Verfahren auf unstrukturierten Gittern.* Dissertation, Fachbereich Mathematik, Schwerpunkt Differentialgleichungen und Dynamische Systeme, Universität Hamburg, 1999.

[11] O. Friedrich, D. Hempel, A. Meister, Th. Sonar. Adaptive Computation of Unsteady Flow Fields with the DLR-$\mathcal{T}$-Code. in: 77th AGARD Fluid Dynamics Panel Meeting and Symposium on Progress and Challenges in CFD Methods and Algorithms, AGARD-CP-578, Sevilla, 1995.

[12] E. Godlewski, P.-A. Raviart. *Numerical Approximation of Hyperbolic Systems of Conservation Laws*, volume 118 of *Applied Mathematical Sciences.* Springer, New York, Berlin, Heidelberg, 1996.

[13] S. K. Godunov. A Finite Difference Method for the Numerical Computation of Discontinuous Solutions of the Equations of Fluid Dynamics. *Mat. Sb.*, 47: 357–393, 1959.

[14] H. Guillard, C. Viozat. On the Behaviour of Upwind Schemes in the Low Mach Number Limit. *Computers and Fluids*, Vol. 28: 63–86, 1999.

[15] W. Hackbusch. *Iterative Lösung großer schwachbesetzter Gleichungssysteme.* Teubner, Stuttgart, 2., überarb. und erw. edition , 1993.

[16] D. Hänel, R. Schwane. An implicit flux-vector splitting scheme for the computation of viscous hypersonic flow. *AIAA Paper*, 89–0274, 1989.

[17] D. Hänel, R. Schwane, G. Seider. On the accuracy of upwind schemes for the solution of the navier-stokes equations. *AIAA Paper*, 87–1105, 1987.

[18] V. Hannemann. *Numerische Simulation von Stoß-Stoß-Wechselwirkungen unter Berücksichtigung von chemischen und thermischen Nichtgleichgewichtseffekten.* Dissertation, Universität Göttingen, 1996.

[19] V. Hannemann, D. Hempel, Th. Sonar. Dynamic Adaptivity and Residual Control in Unsteady Compressible Flow Computation. *Mathematical and Computer Modelling*, 20: 201–213, 1994.

[20] G. Hauke, T. J. R. Hughes. A Comparative Study of Different Sets of Variables for Solving Compressible and Incompressible Flows. *Comput. Methods Appl. Mech. Engrg*, 153: 1–44, 1998.

[21] B. Heinrich. *Finite Difference Methods on Irregular Networks.* Birkhäuser Verlag, Basel, 1987.

[22] D. Hietel, A. Meister, Th. Sonar. On the comparison of four different implementations of an third-order ENO scheme of box type for the computation of compressible flow. *Numerical Algorithms*, 13: 77–105, 1996.

[23] C. Hirsch. *Numerical computation of internal and external flows*, volume 1. Wiley & Sons, Chicester, New York, 1988.

[24] C. Hirsch. *Numerical computation of internal and external flows*, volume 2. Wiley & Sons, Chicester, New York, 1988.

[25] L. Hoffmann. *Ein zeitlich selbstadaptives numerisches Verfahren zur Berechnung von Strömungen aller Mach-Zahlen basierend auf Mehrskalenasymptotik und diskreter Datenanalyse.* Dissertation, Fachbereich Mathematik, Schwerpunkt Differentialgleichungen und Dynamische Systeme, Universität Hamburg, 2000.

[26] L. Hoffmann, A. Meister. A Numerical Scheme for Low Mach Number Flow based on Asymptotic Analysis with Time-Dependent Adaptation of the Asymptotic Sequence. In *Proceedings of the Fourth ECCOMAS Computational Fluid Dynamics Conference*, (Eds.) C. Hirsch, et. al. Pandolfi, M., volume 1, Part 1, pp. 567–572, Athens, 1998.

[27] L. Hoffmann, A. Meister. The Extension of a Compressible Flow Solver to the Low Mach Number Regime. In *Proceedings of the 3nd Seminar on Euler and Navier-Stokes Equations*, Prague, 1998.

[28] L. Hoffmann, A. Meister. A Compressible Low Mach Number Scheme based on Image Processing and Asymptotic Analysis. *Computational Fluid Dynamics Journal*, Vol. 9: 399–410, 2001.

[29] M. H. Holmes. *Introduction to Perturbation Methods*, volume 20 of *Texts in Applied Mathematics.* Springer, New York, Berlin, Heidelberg, 1995.

[30] C. Hu, C.-W. Shu. Weighted Essentially Non-oscillatory Schemes on Triangular Meshes. *J. Comput. Phys.*, 150: 97–127, 1999.

[31] A. Jameson. Computational Transonics. *Comm. Pure Appl. Math.*, 41: 507–549, 1988.

[32] A. Jeffrey, T. Kawahara. *Asymptotic Methods in Nonlinear Wave Theory.* Pitman Advanced Publishing Program, Boston, London, Melbourne, Applicable Mathematical Sciences edition , 1982.

[33] J. KEVORKIAN, J. D. COLE. *Multiple Scale and Singular Perturbation Methods*, volume 114 of *Applied Mathematical Sciences*. Springer, New York, Berlin, Heidelberg, 1996.

[34] S. KLAINERMAN, A. MAJDA. Singular limits of quasilinear hyperbolic system with large parameters and the incompressible limit of compressible fluids. *Comm. Pure Appl. Math.*, 34: 481–524, 1981.

[35] S. KLAINERMAN, A. MAJDA. Compressible and incompressible fluids. *Comm. Pure Appl. Math.*, 35: 629–651, 1982.

[36] R. KLEIN. Semi-Implicit Extension of a Godunov-Type Scheme Based on Low Mach Number Asymptotics I: One-Dimensional Flow. *J. Comput. Phys.*, 121: 213–237, 1995.

[37] R. KLEIN, N. BOTTA, T. SCHNEIDER, C.D. MUNZ, S. ROLLER, A. MEISTER, L. HOFFMANN, TH. SONAR. Asymptotic adaptive methods for multi-scale problems in fluid mechanics. *Journal of Engineering Mathematics*, Vol. 9 (1/4) (2): 261–343, 2001.

[38] N. KROLL, R.K. JAIN. Solution of Two-Dimensional Euler Equations — Experience with a Finite Volume Code. Deutsche Forschungs- und Versuchsanstalt für Luft- und Raumfahrt DFVLR, Forschungsbericht FB 87-41, Köln, 1987.

[39] D. KRÖNER. *Numerical Schemes for Conservation Laws.* Teubner, Stuttgart, 1997.

[40] J. L. LATECKI, R. LAKÄMPER. Polygon Evolution by Vertex Deletion. In *2nd Int. Conf. on Scale-Space Theories in Computer Vision*, pp. 398–409, Corfu, Greece, 1999. Springer-Verlag.

[41] L. J. LATECKI, R. LAKÄMPER. Convexity Rule for Shape Decomposition Based on Discrete Contour Evolution. *Comput. Vision Image Understanding*, 73 (3): 441–454, 1999.

[42] R. J. LEVEQUE. *Numerical Methods for Conservation Laws.* Birkhäuser, Basel, 1990.

[43] M.-S. LIOU, C.J. STEFFEN. A New Flux Splitting Scheme. NASA Technical Memorandum 104404, Cleveland, Ohio, May 1991. also in J. Comput. Phys. **107**, 23–39, 1993.

[44] A. MEISTER. Ein Beitrag zum DLR-$\mathcal{T}$-Code: Ein explizites und implizites Finite-Volumen-Verfahren zur Berechnung instationärer Strömungen auf unstrukturierten Gittern. DLR-IB 221 - 94 A 36, Göttingen, 1994.

[45] A. Meister. Development of an Implicit Finite Volume Scheme for the Computation of Unsteady Flow Fields on Unstructured Moving Grids. In *Numerical Methods for Fluid Dynamics V*, pp. 481–488, Oxford, 1995. Clarendon Press. Ed. K.W. Morton and M.J. Baines.

[46] A. Meister. *Zur zeitgenauen numerischen Simulation reibungsbehafteter, kompressibler, turbulenter Strömungsfelder mit einer impliziten Finite-Volumen-Methode vom Box-Typ.* Dissertation, Technische Hochschule Darmstadt, 1996.

[47] A. Meister. Comparison of Different Krylov Subspace Methods Embedded in an Implicit Finite Volume Scheme for the Computation of Viscous and Inviscid Flow Fields on Unstructured Grids. *J. Comput. Phys.*, 140: 311–345, 1998.

[48] A. Meister. Asymptotic Single and Multiple Scale Expansions in the Low Mach Number Limit. *SIAM J. Appl. Math.*, Vol. 60 (1): 256–271, 1999.

[49] A. Meister. *Numerik linearer Gleichungssysteme, Eine Einführung in moderne Verfahren.* Vieweg, Wiesbaden, 1999.

[50] A. Meister. Analyse und Anwendung Asymptotik-basierter numerischer Verfahren zur Simulation reibungsbehafteter Strömungen in allen Mach-Zahlbereichen, 2001. Habilitationsschrift, Universität Hamburg.

[51] A. Meister, M. Oevermann. Computation of Laminar and Turbulent Compressible Flow Fields on Unstructured Grids with an Implicit Finite Volume Scheme. In *Proceedings of the 2nd Seminar on Euler and Navier-Stokes Equations*, Prague, 1996.

[52] A. Meister, M. Oevermann. An Implicit Finite Volume Approach of the $k-\epsilon$ Turbulence Model on Unstructured Grids. *Z. Angew. Math. Mech.*, 78 (11): 743–757, 1998.

[53] A. Meister, Th. Sonar. Asymptotische Entwicklungen und ihre Anwendungen in technischen Problemstellungen. Vorlesungsausarbeitung, Universität Hamburg, 1997.

[54] A. Meister, Th. Sonar. Finite-volume schemes for compressible fluid flow. *Surv. Math. Ind.*, 8: 1–36, 1998.

[55] A. Meister, C. Vömel. Efficient Preconditioning of Linear Systems arising from the Discretization of Hyperbolic Conservation Laws. *Advances in Computational Mathematics*, Vol.14 (1): 49–73, 2001.

[56] C. L. Merkle, Y.-H. Choi. Computation of Low-Speed Compressible Flows with Heat Addition. *AIAA J.*, 25 (6): 831–838, 1987.

[57] M. Oevermann. *Ein Finite-Volumen-Verfahren auf unstrukturierten Dreiecksgittern zur Berechnung turbulenter Diffusionsflammen in kompressiblen Strömungsfeldern.* Dissertation, RWTH Aachen, 1997.

[58] S. Osher, F. Solomon. Upwind Schemes for Hyperbolic Systems of Conservation Laws. *Math. Comput.*, 38: 339–377, 1982.

[59] H. Poincaré. *Acta Math.*, 8: 295–344, 1886.

[60] J. J. Quirk. A Contribution to the Great Riemann Solver Debate. ICASE Report 92–64, Hampton, Virginia, 1992.

[61] (Eds.) A. Rizzi, H. Viviand. *Numerical Methods for the Computation of Inviscid Transonic Flows with Shock Waves*, number 3 in Notes on Numerical Fluid Mechanics, Braunschweig, Wiesbaden, 1981. Vieweg.

[62] P. L. Roe. Approximate Riemann Solvers, Parameter Vectors, and Difference Schemes. *J. Comput. Phys.*, 43: 357–372, 1981.

[63] Y. Saad. *Iterative Methods for Sparse Linear Systems.* PWS Publishing Company, Boston, 1996.

[64] T. Schneider, N. Botta, K. J. Geratz, R. Klein. Semi-Implicit Extension of a Godunov-Type Compressible Solver Based on Low Mach Number Asymptotics II: Multi-Dimesional, Variable Density Zero Mach Number Flow. *J. Comput. Phys.*, 155: 248–286, 1999.

[65] W. Schneider. *Mathematische Methoden der Strömungsmechanik.* Vieweg, Braunschweig, 1987.

[66] J. Sesterhenn. *Zur numerischen Berechnung kompressibler Strömungen bei kleinen Mach-Zahlen.* PhD thesis, Swiss Federal Institute of Technology, Diss. ETH No. 11334, 1995.

[67] C.-W. Shu, S. Osher. Efficient Implementation of Essentially Nonoscillatory Shock-Capturing Schemes. *J. Comput. Phys.*, 77: 439–471, 1988.

[68] Th. Sonar. *Mehrdimensionale ENO-Verfahren.* Teubner Verlag, Stuttgart, 1997.

[69] Th. Sonar. On the Construction of Essentially Non-Oscillatory Finite Volume Approximations to Hyperbolic Conservation Laws on General Trinagulations: Polynomial Recovery, Accuracy, and Stencil Selection. *Comp. Meth. Appl. Mech. Eng.*, 140: 157–181, 1997.

[70] E. Stanewsky. private communication. 1999.

[71] E. Stanewsky, J. J. Thibert. Airfoil SKF 1.1 with maneuver flap. AGARD AR 138, A5-1 - A5-29, 1979.

[72] J. L. Steger, R. F. Warming. Flux Vector Splitting of the Inviscid Gasdynamic Equations with Application to Finite-Differnce Mehtods. *J. Comput. Phys.*, 40: 263–293, 1981.

[73] Th. Stieltjes. *Ann. de l'Éc. Norm. Sup.*, 3 (3): 201–258, 1886.

[74] I. Thomas. Zur Lösung der zweidimensionalen Euler - Gleichungen: Elliptische Netzgenerierung und Finite - Volumen - Verfahren. Diplomarbeit, Hamburg, 1998.

[75] E. F. Toro. *Riemann Solvers and Numerical Methods for Fluid Dynamics.* Springer, Berlin, Heidelberg, New York, 1997.

[76] E. Turkel. Preconditioned Methods for Solving the Incompressible and Low Speed Compressible Equations. *J. Comput. Phys.*, 72: 277–298, 1987.

[77] S. Ukai. The incompressible limit and the initial layer of the compressible Euler equations. *J. Math. Kyoto Univ.*, 26: 323–331, 1986.

[78] H. A. van der Vorst. BI-CGSTAB: A fast and smoothly converging variant of BI-CG for the solution of nonsymmetric linear systems. *SIAM J. Sci. Stat. Comput.*, 13: 631–644, 1992.

[79] B. van Leer. Flux-vector splitting for the Euler equations. In *Eighth International Conference on Numerical Methods in Fluid Dynamics*, (Ed.) E. Krause, number 170 in Lecture Notes in Physics, pp. 507–512, Berlin, 1982. Springer Verlag.

[80] G. Volpe. Performance of Compressible Flow Codes at Low Mach Numbers. *AIAA J.*, 31 (1): 49–56, 1993.

[81] Y. Wada, M.-S. Liou. A Flux Splitting Scheme with High-Resolution and Robustness for Discontinuities. *AIAA Paper*, 94–0083, 1994.

[82] W. Waidmann, F. Alff, M. Böhm, U. Brummund, W. Clauss, M. Oschwald. Supersonic Combustion of Hydrogen/Air in a SCRAMJET Combustion Chamber. *45th Conference of the International Astronautical Federation*, IAF-94-S.4.429, 1994.

[83] J. Weickert. A Review of Nonlinear Diffusion Filtering. *Scale-Space Theory in Computer Visions, Lecture Notes in Comp. Sciences*, 1252: 3–28, 1997.